DIN
GMA

Quaderni di ricerca

Dodicesima giornata di studio Ettore Funaioli

20 luglio 2018

A cura di
Vincenzo Parenti Castelli e Alessandro Rivola

SOCIETÀ EDITRICE ESCULAPIO

AlmaDL
University of Bologna Digital Library

Quaderni del **DIN – GMA**

Atti di giornate di studio – 12

A cura di:
Vincenzo Parenti Castelli e Alessandro Rivola

Coordinatore di redazione: Alberto Martini

DIN
Dipartimento di Ingegneria Industriale
http://www.ingegneriaindustriale.unibo.it

GMA
Gruppo Italiano di Meccanica Applicata
http://www.meccanicaapplicata.it/

Accademia delle Scienze dell'Istituto di Bologna
http://www.accademiascienzebologna.it/it

Dodicesima giornata di studio Ettore Funaioli

20 luglio 2018

A cura di:
Vincenzo Parenti Castelli e Alessandro Rivola

Proprietà letteraria riservata
© Copyright 2019 degli autori Tutti i diritti riservati

Dodicesima giornata di studio Ettore Funaioli – 20 luglio 2018
A cura di Vincenzo Parenti Castelli e Alessandro Rivola
Bologna: 2019

ISSN 2532-7046
ISBN 978-88-9385-140-4

Versione elettronica disponibile alla pagina

http://amsacta.unibo.it/id/eprint/6183

Stampa a richiesta eseguita da:

SOCIETÀ EDITRICE ESCULAPIO

40131 Bologna – Via U. Terracini 30 – Tel. 051- 6340113 – Fax 051- 6341136
www.editrice-esculapio.com

INDICE

LAVORI ESTESI 1

Giuseppe Catania, Stefano Amadori
Vibration control by a passive damping approach based on the multilayer coating technology 3

Alessandro Zanarini
An old mechanism to improve wind energy harvesting..... 15

SOMMARI 37

Riccardo Pelaccia, Barbara Reggiani, Ivan Todaro, Giuseppe Valli, Lorenzo Donati, Rosario Squatrito, Alessandro Fortunato, Luca Tomesani
SLM of extrusion dies with liquid nitrogen cooling 39

Andrea Tosini, Emiliano Mucchi, Giorgio Dalpiaz
Verifica sperimentale di metodologie di test tailoring con eccitazione stocastica monoassiale e multiassiale..... 41

Emanuele Pesaresi, Marco Troncossi
Test accelerati di qualifica a vibrazione: sviluppo di nuovi software di mission synthesis..... 43

Julian Marcell Enzveiler Marques, Denis Benasciutti, Roberto Tovo
Uncertainties on fatigue damage under random loadings through spectral methods..... 45

Jacopo Cavalaglio Camargo Molano, Marco Cocconcelli, Riccardo Rubini, Massimo Gibertini
Modello di un segnale di guasto su cuscinetti in azionamenti a carrelli indipendenti 47

Gianluca D'Elia, Giorgio Dalpiaz, Emiliano Mucchi
On the diagnostics of two degrees of freedom planetary gearboxes..... 49

Luca Capelli, Marco Cocconcelli, Riccardo Rubini
Riconoscimento di infestazione da *sitophilus oryzae* tramite l'analisi dei suoni rilevati..... 51

Michele Conconi, Nicola Sancisi, Vincenzo Parenti-Castelli
Use of the principle of virtual work to explain the human joint motion: application to the knee 53

Alberto Sensini, Maria Letizia Focarete, Chiara Gualandi, Juri Belcari, Andrea Zucchelli, Alexander Kao, Gianluca Tozzi, Liam Boyle, Gwendolen Reilly, Luca Cristofolini
Hierarchical multiscale resorbable nanofibrous scaffolds for tendon tissue regeneration ... 55

Marco Palanca, Saulo Martelli, Egon Perilli, Luca Cristofolini
Body anthropometry and local bone microarchitecture may improve determining hip fracture risk beyond DXA 57

Ivo Campione, Jessica Rossi, Augusto Bianchini, Giangiacomo Minak, Marco Troncossi
Laboratorio di Formazione e Ricerca TAILOR:
Technology and Automation for Industry LabORatory 59

Alessandro Rivola, Nicola Golfari
Triangoli e quadrilateri pieghevoli 61

Giovanni Mottola, Marco Carricato
Dynamically feasible trajectories for a delta-like cable-suspended robot 63

Eugenio Dragoni, Valerio Armando Ciace
Lightweight volume filling with trabecular structures evolved
from regular tessellation of 3D space 65

Andrea Sorrentino, Davide Castagnetti, Andrea Spaggiari, Eugenio Dragoni
Shape optimization of the fillet under a bolt's head 67

Luigi Leopardi, Roberto Lugli, Antonio Strozzi
Un paradosso in travi curve: dalla accademia alla applicazione 69

Margherita Peruzzini, Fabio Grandi, Luca Zanni, Juliana Schmidt, Marcello Pellicciari, Angelo Oreste Andrisano
Virtual simulation technologies for human-centred design of tractors 71

Chen Yi, Lorenzo Agostini, Marco Fontana, Rocco Vertechy
Fatigue life characterization of dielectric elastomer transducers made of styrenic rubber .. 73

Marco Polastri, Emiliano Mucchi, Giorgio Dalpiaz
Sviluppo di una trasmissione pto ibrida elettrica di trattore mediante modellazione multifisica in ambiente Imagine.Lab Amesim 75

Luke Mizzi, Andrea Spaggiari
A Finite Element Study on Actuators made from Shape Memory
Alloy/Matrix composites 77

Angelo Oreste Andrisano, Giovanni Berselli, Pietro Bilancia, Marcello Pellicciari
Design and virtual prototyping of a variable stiffness joint via shape optimization in a CAD/CAE environment 79

PREFAZIONE

Questo volume raccoglie le 23 memorie presentate alla dodicesima "Giornata di studio Ettore Funaioli", svoltasi il 20 luglio 2018. Alcune memorie sono riportate in esteso mentre di altre ne viene riportato il solo sommario. Ai partecipanti, e in particolare agli autori delle memorie qui raccolte, va il sentito ringraziamento degli organizzatori della Giornata: a loro si deve il continuo successo della manifestazione, chiaramente legato anche al ricordo del Prof. Ettore Funaioli, che ricordiamo sempre con grande stima e gratitudine per l'appassionato insegnamento scientifico e la profonda umanità.

La folta adesione a queste Giornate di Studio conferma anche l'apprezzamento dei partecipanti per l'occasione che esse offrono di ritrovarsi amichevolmente fra colleghi, per scambiarsi idee e opinioni sulle ricerche in corso e sui problemi generali della nostra comunità scientifica.

È motivo di grande soddisfazione per tutti, e sicuramente ragione di orgoglio per i nostri Maestri, constatare l'elevata qualità scientifica dei lavori presentati e il costante impegno dei Ricercatori di Meccanica che hanno partecipato alla manifestazione.

Questa Giornata di studio si è svolta con il patrocinio dell'Accademia delle Scienze dell'Istituto di Bologna e del GMA – Gruppo di Meccanica Applicata. Di ciò ringraziamo vivamente il Presidente dell'Accademia delle Scienze, Prof. Walter Tega, e il Presidente del GMA, Prof. Terenziano Raparelli.

La Giornata ha potuto svolgersi anche grazie alla collaborazione della Scuola di Ingegneria e Architettura e del DIN – Dipartimento di Ingegneria Industriale dell'Alma Mater Studiorum – Università di Bologna. Ringraziamo il Presidente della Scuola di Ingegneria e Architettura, Prof. Ezio Mesini, e il Direttore del DIN, Prof. Antonio Peretto, che hanno consentito queste collaborazioni e hanno voluto aprire la Giornata porgendo il loro saluto ai partecipanti.

Bologna, 12 giugno 2019

Vincenzo Parenti Castelli – Alessandro Rivola

LAVORI ESTESI

VIBRATION CONTROL BY A PASSIVE DAMPING APPROACH BASED ON THE MULTILAYER COATING TECHNOLOGY

Giuseppe Catania
Department of Industrial Engineering, CIRI Mam,
University of Bologna, Italy
E-mail: giuseppe.catania@ unibo.it

Stefano Amadori
CIRI Mam,
University of Bologna, Italy
E-mail: stefano.amadori4@unibo.it

Abstract. *In this work innovative coating solutions are presented and their damping behaviour experimentally is investigated by means of dynamic measurements on specimens in the form of coated slender beams. The effectiveness of the different solutions is compared by means of a damping estimator and the results are discussed. A multilayer beam model, taking into account of the dissipative actions at the interface between the layers by means of a complex interlaminar impedance, is also presented. Some model application examples and some prototype solutions based on organic polymers are shown.*

Keywords: *coating technology, damping, multilayer beam, organic polymers*

1. INTRODUCTION

Composite components that combine high damping with high stiffness and resistance properties can be obtained by means of the multilayer coating technology [1-6]. The adoption of relatively thick coating layers made of high damping materials generally requires strong modifications of both the geometrical and the mechanical properties of the component. Nevertheless, by controlling the coating materials, architecture and production technique, the component geometry, stiffness and strength properties can be tuned according to the designer specifications. Since high energy dissipation by viscous internal actions requires the adoption of a coating volume being not negligible with respect to the volume of the uncoated component, high thickness coating layers should be adopted as well. Nevertheless, a multilayered thin coating architecture can be designed by maximizing the work of the dissipative actions at the interface between the coating layers, so that better results in term of damping behaviour can be obtained with a coated thin multilayer component with respect to a single-layered coating solution of the same thickness.

In this work the effectiveness of different coating solutions is estimated by means of numerical simulations and of experimental measurements on test specimens in the form of thin multi-layered slender beams. To simulate the response of composite beam specimens an extended multi-layer beam model based on zig-zag beam theory is presented [7-8]. The model takes into account of both the dissipative actions at the layer interface and the effects of distributed viscous ground-coupled-constraints.

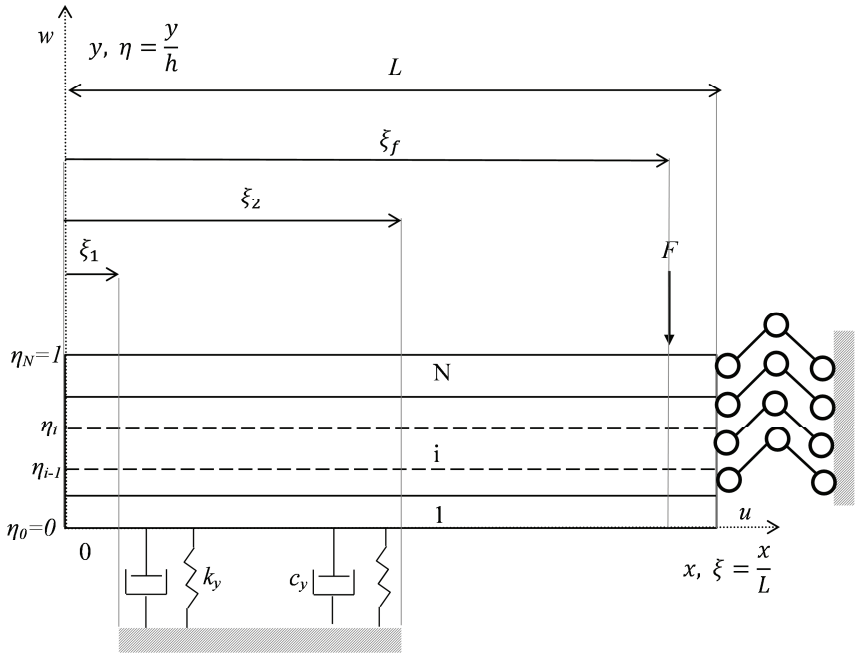

Figure 1. Multilayer beam experimental specimen.

2. MULTILAYER BEAM MODEL

Models of composite beams and plates were developed in the past by many researchers [9-12], but no effort was dedicated on locally modeling the system internal dissipative actions and on validating the model by experimental tests. Modified Bernoulli-Euler, Timoshenko beam and high-order beam theories, taking into account of different stress strain relationship related to the different layers, e.g. layer-wise theories, were proposed in the past [11]. In some layer-wise beam theories the number of kinematic variables and the computational load may increase with the number of layers. Zig zag theories make it possible to deal with a low number of state space variables, strictly not depending on the number of layers [9,12].

The model presented is an extended multilayer beam model based on zig zag multilayer beam theories [7,8]. The dissipative actions are modelled by relaxing the kinematical displacement continuity at the layer interface and by introducing complex elasto-hysteretic dynamical interface coupling. The effects on the dissipative properties of standard distributed viscous constraints are also taken into account.

The constitutive equations of the *i-th* layer are (Fig.1):

$$\begin{aligned} \sigma(\xi,\eta,t) &= E_i \cdot \varepsilon(\xi,\eta,t) \\ \tau(\xi,\eta,t) &= G_i \cdot \gamma(\xi,\eta,t) \end{aligned} \quad , \quad \eta \in [\eta_{i-1},\eta_i], \quad i = 1,\ldots,N \tag{1}$$

Small displacement and deformation field is assumed so that transverse displacement $\bar{w}$ is assumed as being stationary with respect to η. Transverse and longitudinal displacement $\bar{w}$, $\bar{u}$ are assumed as:

$$\begin{aligned} &\bar{u}(\xi,\eta,t) = h \cdot u(\xi,\eta,t), \quad \bar{w}(\xi,t) = L \cdot w(\xi,t) \\ &u(\xi,\eta,t) = u_0 + a \cdot \eta + g \cdot \eta^2 + c \cdot \eta^3 + d_i \cdot \eta + l_i, \quad i = 1,\ldots,N \end{aligned} \tag{2}$$

$2N$+3 state variables result:

$$\begin{aligned} &d_i = d_i(\xi,t) \quad , \quad l_i = l_i(\xi,t) \quad ; \quad i=2,\ldots,\mathrm{N} \\ &w = w(\xi,t), \; u_0 = u_0(\xi,t), \; a = a(\xi,t), \; g = g(\xi,t), \; c = c(\xi,t) \end{aligned} \tag{3}$$

N+1 equilibrium conditions are imposed at the layer interfaces:

$$\begin{aligned} &\tau(\eta = 0) = G_1 \cdot \gamma(0) = 0 \,, \quad \tau(\eta = 1) = G_N \cdot \gamma(1) = 0 \\ &\tau(\eta = \eta_i) = G_i \cdot \gamma\left((\eta_i)^-\right) = G_{i+1} \cdot \gamma\left((\eta_i)^+\right) \end{aligned} \quad , \quad i = 1,\ldots,N-1 \tag{4}$$

At the interface between layers an elasto-hysteretic constitutive relationship is assumed and a complex impedance is introduced, resulting in N-1 dynamic slipping elasto-hysteretic coupling condition:

$$\begin{aligned} &\tau(\eta_i) = \Theta_i \cdot \left[\bar{u}\left((\eta_i)^+\right) - \bar{u}\left((\eta_i)^-\right)\right] \\ &\Theta_i = s_i + j \cdot \varphi_i \,, \quad \Theta_i^{-1} = \frac{s_i - j \cdot \varphi_i}{\left|\Theta_i\right|^2} \end{aligned} \quad , \quad i = 1,\ldots,N-1 \tag{5}$$

It is assumed that longitudinal displacement $\bar{u}$ can show slip discontinuity at the interfaces between different layers:

$$\Delta\bar{u}(\eta_i) = \bar{u}\left((\eta_i)^+\right) - \bar{u}\left((\eta_i)^-\right) \tag{6}$$

By means of the application of the N+1 equilibrium conditions and the N-1 interface slip equations the $2N$+3 state variables are reduced to only three independent state variables, w, a, d [7,8]. This result is not dependent on the number of layers of the beam model considered. A 3 state variable vector is introduced

$$\mathbf{V}(\xi,t) = \left\{u_0(\xi,t) \quad w(\xi,t) \quad c(\xi,t)\right\}^T = \mathbf{Z}(\xi) \cdot \boldsymbol{\delta}(t) \tag{7}$$

and $\mathbf{Z}$ can be modeled by means of a discrete set of known harmonic functions:

$$\mathbf{Z}(\xi)=\begin{bmatrix}\mathbf{Z}_u(\xi) & \mathbf{0} & \mathbf{0}\\ \mathbf{0} & \mathbf{Z}_w(\xi) & \mathbf{0}\\ \mathbf{0} & \mathbf{0} & \mathbf{Z}_c(\xi)\end{bmatrix} \tag{8}$$

$$\begin{aligned}
&\mathbf{Z}_u=\sqrt{2}\cdot\left[\frac{1}{\sqrt{2}}\quad \sin(\pi\cdot\xi)\quad \cos(\pi\cdot\xi)\quad \ldots\quad \sin(n_u\cdot\pi\cdot\xi)\quad \cos(n_u\cdot\pi\cdot\xi)\right]\\
&\mathbf{Z}_w=\sqrt{2}\cdot\left[\frac{1}{\sqrt{2}}\quad \sqrt{12}\cdot(\xi-0.5)\quad \sin(\pi\cdot\xi)\quad \cos(\pi\cdot\xi)\quad \ldots\quad \sin(n_w\cdot\pi\cdot\xi)\quad \cos(n_w\cdot\pi\cdot\xi)\right]\\
&\mathbf{Z}_c=\sqrt{2}\cdot\left[\sin(\pi\cdot\xi)\quad \cos(\pi\cdot\xi)\quad \ldots\quad \sin(n_c\cdot\pi\cdot\xi)\quad \cos(n_c\cdot\pi\cdot\xi)\right]\\
&\boldsymbol{\delta}=\left[\delta_1\quad \ldots\quad \delta_n\right]^T,\ n=2\times(n_u+n_w+n_c)+3
\end{aligned} \tag{9}$$

The equations of motion can be obtained by applying the system total potential energy (Π) stationarity condition. The contribution of the work U of the internal elasto-hysteretic actions, W_{in} of the inertial actions, W_{ex} of the external forces, and $\Delta\Pi_{vis}$, $\Delta\Pi_{el}$ of the distributed viscous and the elastic constraints is taken into account:

$$\Pi(\mathbf{V})=U+W_{in}+W_{ex}+\Delta\Pi\rightarrow\min\ ,\quad \frac{\partial\Pi}{\partial\mathbf{V}}=\mathbf{0}\ ,\quad \Delta\Pi=\Delta\Pi_{el}+\Delta\Pi_{vis} \tag{10}$$

The resulting equation of motion is:

$$\mathbf{M}\cdot\ddot{\boldsymbol{\delta}}+\mathbf{C}\cdot\dot{\boldsymbol{\delta}}+(\mathbf{K}+\boldsymbol{\Delta}\mathbf{K})\cdot\boldsymbol{\delta}=\mathbf{F} \tag{11}$$

where **M**, **C**, **K**, **ΔK** are complex, symmetric, matrices. Detailed calculations for the equations of **M**, **C**, **K**, **ΔK** can be found in the author's previous work [8]. Using these matrices the frequency response function (*FRF*) is calculated by assuming as input a unitary, lumped, harmonic excitation at frequency ω applied at $x=L\cdot\xi_f$, and as output the transverse displacement at $x=L\cdot\xi_w$,

$$FRF(\xi_w,\xi_f,j\omega)=\left[\mathbf{0}\quad \mathbf{Z}_w(\xi_w)\quad \mathbf{0}\right]\cdot\mathbf{G}(j\cdot\omega)\cdot\left[\mathbf{0}\quad \mathbf{Z}_w(\xi_f)\quad \mathbf{0}\right]^T \tag{12}$$

$$\begin{aligned}
&\mathbf{H}(j\cdot\omega)=-\omega^2\cdot\mathrm{Re}(\mathbf{M})+j\cdot\omega\cdot\mathrm{Re}(\mathbf{C})+\mathrm{Re}(\mathbf{K}+\boldsymbol{\Delta}\mathbf{K})\\
&\boldsymbol{\Delta}\mathbf{H}(j\cdot\omega)=-\omega^2\cdot j\cdot\mathrm{Im}(\mathbf{M})-\omega\cdot\mathrm{Im}(\mathbf{C})+j\cdot\mathrm{Im}(\mathbf{K}+\boldsymbol{\Delta}\mathbf{K})\\
&\mathbf{G}(j\cdot\omega)=\left[\mathbf{H}(j\cdot\omega)+\boldsymbol{\Delta}\mathbf{H}(j\cdot\omega)\right]^{-1}\ ,\quad \mathbf{G}=\left(\mathbf{I}+\mathbf{H}^{-1}\cdot\boldsymbol{\Delta}\mathbf{H}\right)^{-1}\cdot\mathbf{H}^{-1}
\end{aligned} \tag{13}$$

where $\mathbf{H}^{-1}$ can be expressed in closed form by means of modal decomposition.The normalized damping estimator z is employed to estimate the damping behaviour of a model beam.

$$z(\xi_w,\xi_f,j\omega)=\frac{\left|\mathrm{Im}\left(FRF(\xi_w,\xi_f,j\omega)\right)\right|}{\left|FRF(\xi_w,\xi_f,j\omega)\right|}\quad ,\quad z\in\Re,\ z\in[0,1] \tag{14}$$

Table 1. Model beam data.

Layer data					
	N° of layers	h_k [mm]	E_k [GPa]	G_k [10^9 Pa]	ρ_k (10^3 kg/m^3)
1L	1	{40}	{62}	{28}	{2.68}
5L	5	{0.2, 0.2, 40, 0.2, 0.2}	{62, 0.05, 62, 0.05, 62}	{28, 0.018, 28, 0.018, 28}	{2.68, 1, 2.68, 1, 2.68}
9L	9	{0.2, 0.2, 0.2, 0.2, 40, 0.2, 0.2, 0.2, 0.2}	{62, 0.05, 62, 0.05, 62, 0.05, 62, 0.05, 632}	{28, 0.018, 28, 0.018, 28, 0.018, 28, 0.018, 28}	{2.68, 1, 2.68, 1, 2.68, 1, 2.68, 1, 2.68}

Interface parameters			Constraint parameters						
	s_i [10^9 N/m^3]	φ_i [10^9 N/m^3]		k_x	k_y	c_{x1}	c_{y1}	c_{x2}	c_{y2}
1L	No interface dissipation			[10^{15} N/m^4]		[N·s/m^4]			
5L	{1.7, 1.7, 1.7, 1.7}	{3, 3, 3, 3}	1L, 5L, 9L	10	1	10	10	30	30
9L	{1.7, 1.7, 1.7, 1.7, 1.7, 1.7, 1.7, 1.7}	{3, 3, 3, 3, 3, 3, 3, 3, 3}							

Table 2. Natural frequencies and damping ratios.

Model Beam	$f1$ [Hz]	$\zeta1$ [%]	$f2$ [Hz]	$\zeta2$ [%]	$f3$ [Hz]	$\zeta3$ [%]
1L	33	0.677	206	0.11	574	0.038
5L	32	0.62	204	0.9	573	0.9
9L	33	0.63	205	2.1	573	2.07

3. MODEL APPLICATION EXAMPLES

Three different model beam solutions (1L, 5L, 9L with 1, 5 and 9 layers respectively) are presented as application examples of the proposed model. For all the three examples presented the beam length is L=1.1 m, and the beam width b=0.1 m. Distributed viscoelastic clamped-free boundary conditions, applied at $0 \le \xi \le 0.09$, with viscoelatic parameters k_x, k_y, c_{x1}, c_{y1} are assumed. It is also assumed that the whole beam is coupled to ground by distributed viscous actions, parameters c_{x2}, c_{y2} ($0 \le \xi \le 1$) to simulate the aerodynamic drag. Data for the three model beam application examples are reported in Tab.1.Comparison of the real and the imaginary part of the inertance $In = -\omega^2 \cdot FRF\left(\xi_w, \xi_f, j\omega\right)$ and of the damping estimator z values for the reported examples are shown in Figs.2-4. System natural frequencies and damping ratios (Tab. 2) can be also used to compare the damping effectiveness of the modelled solution, estimated by means of the SDOF (single degree of freedom) circle fit method. By comparing the results shown in Figs. 2-4 and in Tab.2, it can be found that by increasing the number of coating layers the effectiveness of this technology is increased as well.

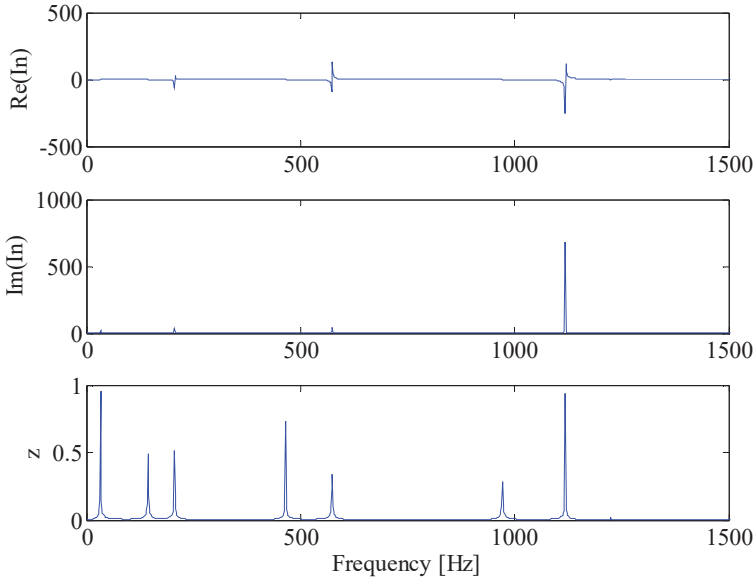

Figure 2. 1L estimated inertance (In) and *z*.

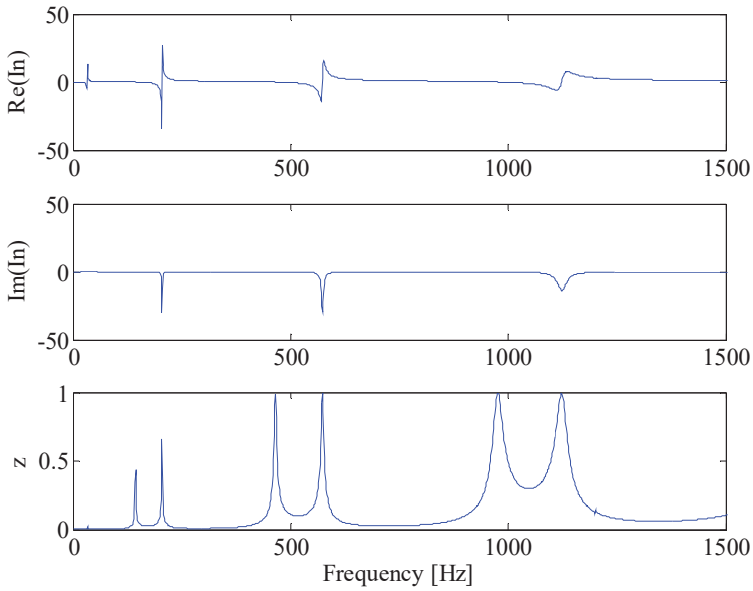

Figure 3. 5L estimated inertance (In) and *z*.

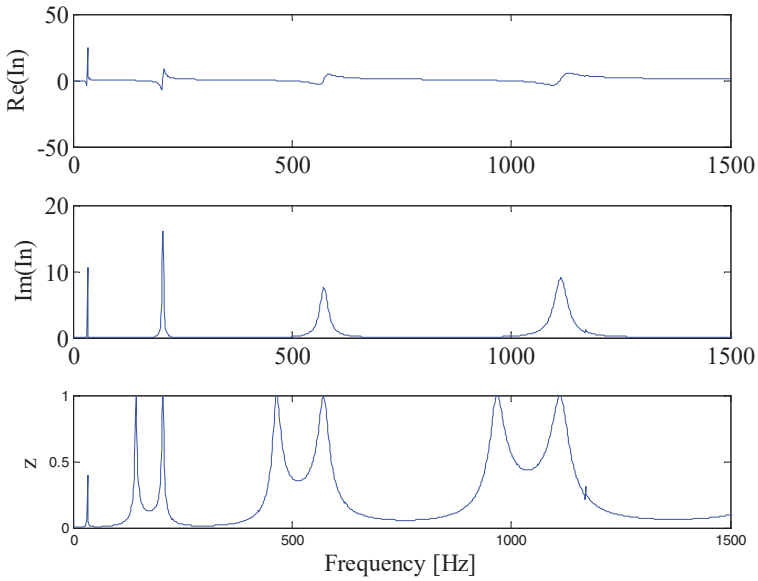

Figure 4. 9L estimated inertance (In) and *z*.

4. EXPERIMENTAL RESULTS

In this section different coating materials are taken into account, i.e. various cyanoacrylate organic polymer and bi-component organic polymer (epoxy putty) based solutions. The various specimens, in the form of a slender beam, rectangular cross uniform section, with coatings applied on the opposite faces of the beam, are tested in flexural vibration in a clamped-sliding boundary condition experimental set-up, isothermal conditions (35°C), 0.01% maximum imposed flexural strain, by means of a Dynamic Mechanical Analyzer apparatus. Experimental results are compared by means of the normalized damping estimator *z*, calculated by means of the experimentally evaluated FRF:

$$FRF(j\omega) = \overline{w}(j\omega)/F(j\omega) \tag{15}$$

Transverse displacement $\overline{w}$ and applied force F are measured at the sliding beam end in the [0.01-200] Hz frequency range. For all of the coated beams the substrate is an uniform beam (beam A), material Al1000 alloy, length $(1.1\pm0.001)\cdot10^{-2}$ m, thickness (0.5±0.01) mm, section area $(1.5\pm0.01)\cdot10^{-4}$ m^2, density (2680±5) kg/m^3. The different coating composition and thickness values are reported in Tab. 3. In B-I beams the coating material is a general purpose cyanoacrylate polymer (Loxeal® 47, high viscosity gel) from Loxeal S.r.l. In C-G beams metal and ceramic powders are mixed with the cyanoacrylate polymer in different volume fraction ratios, the average powder grain size is ~25 μm for Fe and ceramic powders, and ~50 μm for the granite powder. In beams H, I the coating is made of alternate laminated Al1000 (thickness $50\cdot10^{-5}$ m) and cyanoacrylate layers (thickness $50\cdot10^{-5}$ m). The coating solutions of the L-O beams are obtained from different bi-component epoxy solution, Milliput® for L,N beam and Loxeal Epostik for M,O beams, 1:1 volume fraction mix of the two epoxy components; Fe powder is added in the N, O solutions.

Table 3. Coating solutions

Beam	Layer numbers	Coating composition	Coating thickness (m)
A	1	Uncoated Al1000 beam	Beam thickness $0.5 \cdot 10^{-3}$
B	3	Cyanoacrylate	$1.0 \cdot 10^{-4}$
C	3	Cyanoacrylate Fe 15% powder mix	$1.0 \cdot 10^{-4}$
D	3	Cyanoacrylate Fe 30% powder mix	$1.0 \cdot 10^{-4}$
E	3	Cyanoacrylate Ceramic 15% powder mix	$1.0 \cdot 10^{-4}$
F	3	Cyanoacrylate Ceramic 30% powder mix	$1.0 \cdot 10^{-4}$
G	3	Cyanoacrylate Granite 30% powder mix	$1.0 \cdot 10^{-4}$
H	5	Alternated laminate Al1000 and Cyanoacrylate layers	$1.0 \cdot 10^{-4}$
I	9	Alternated laminate Al1000 and Cyanoacrylate layers	$2.0 \cdot 10^{-4}$
L	3	Bi-component epoxy putty, Milliput®	$1.0 \cdot 10^{-4}$
M	3	Bi-component epoxy putty, Loxeal Epostik	$1.0 \cdot 10^{-4}$
N	3	Bi-component epoxy putty, Milliput®, Fe 15% powder mix	$1.0 \cdot 10^{-4}$
O	3	Bi-component epoxy putty, Loxeal Epostik, Fe 15% powder mix	$1.0 \cdot 10^{-4}$

Both the cyanoacrylate-powder mix coatings related to C, D, E, F, G solutions and the epoxy-powder mix coatings related to L, M solutions are investigated in order to improve the damping capabilities. H, I solutions are tested in order to evaluate the constrained layer damping effect [1]. From Figs. (5-6) it can be observed that the cyanoacrylate coating significantly improves the damping capabilities of the beam specimen at low frequencies ([0÷60] Hz) and that only limited changes in the damping behaviour are obtained by adding Fe and ceramic powders with respect to B case, except for D and G in the high frequency range ([150÷200] Hz). Fig.6 shows that the Al-cyanoacrylate multilayer coating interface is associated to a z increase with respect to the uncoated solution (A), and that such effect strongly depends on the number of coating layers adopted. The z increase is observed over all of the frequency range [0÷200] Hz. Results from epoxy based coatings are reported in Fig. (7) and it can be observed that (L, N) Milliput coating architectures, with and without the addition of metallic powders, show higher *z* values at all of the measured frequencies ([0÷200] Hz) with respect to the other epoxy based coating solutions (M, O).

5. INDUSTRIAL APPLICATIONS

The proposed L coating solution is also tested in a real industrial application, i.e. the casing of a mechanical gear pump, Fig. (8). Since the vibrations of the pump casing forced by the internal oil pressure oscillations are expected to contribute to the pump acoustic noise emission in working conditions, the effect of the application of the coating layer technology can be relevant. Sound pressure measurements made in a semi-anechoic chamber, Fig. (8b), are used to compare the acoustic emissions of the uncoated and coated pump in operating conditions at different revolution speed *n* and output oil pressure *p* values.

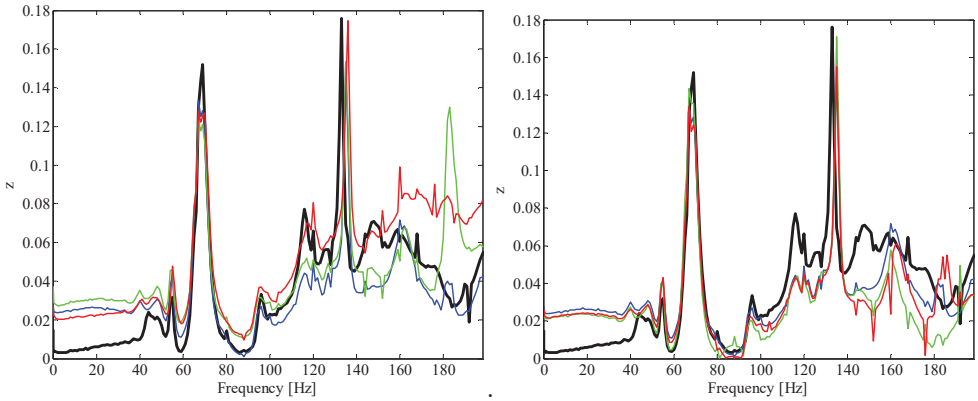

(a) (b)

Figure 5. *z* estimated values: a) A (black), B (blue), C (green),D (red), b) A (black), B (blue), E (green), F (red).

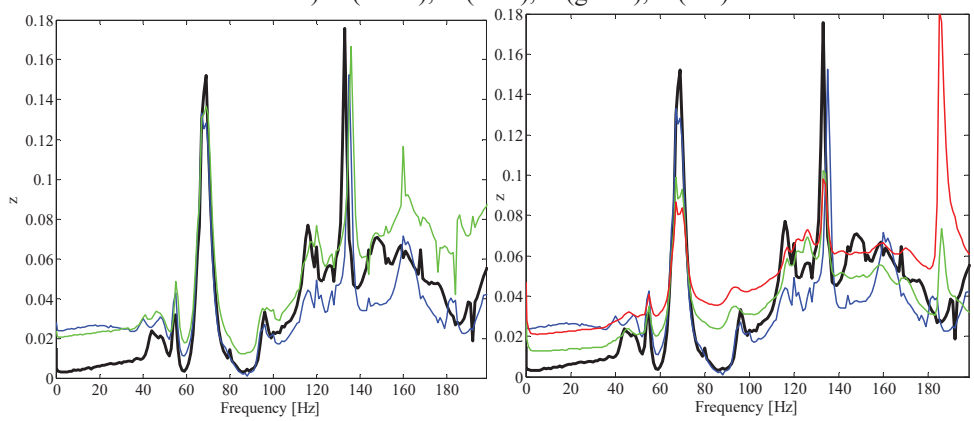

(a) (b)

Figure 6. *z* estimated values: a) A (black), B (blue), G (green), b) A (black), B (blue), H (green), I (red).

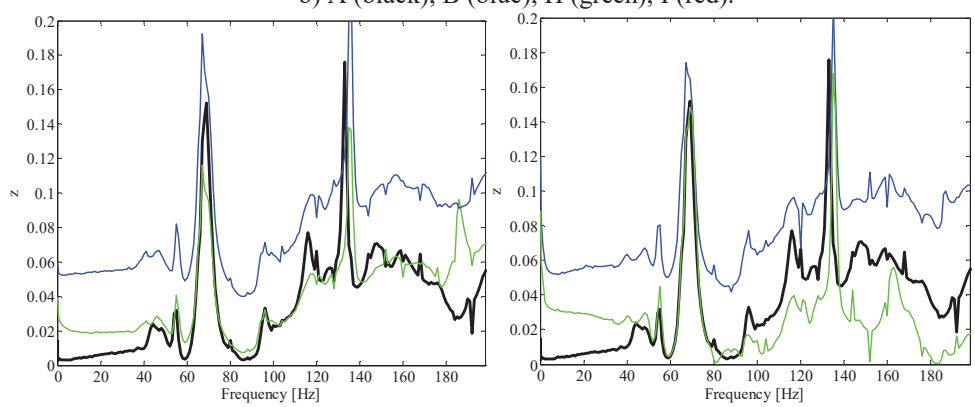

(a) (b)

Figure 7. *z* estimated values: a) A (black), L (blue), M (green); b) A (black), N (blue), O (green).

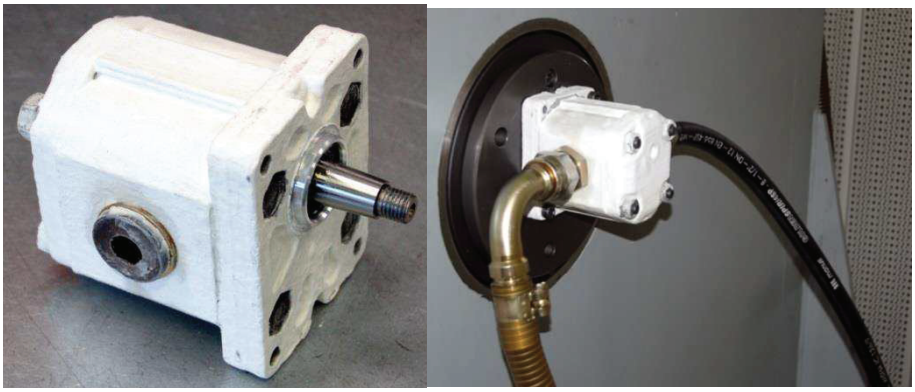

(a) (b)

Figure 8. a) coated pump, b) coated pump during sound pressure test .

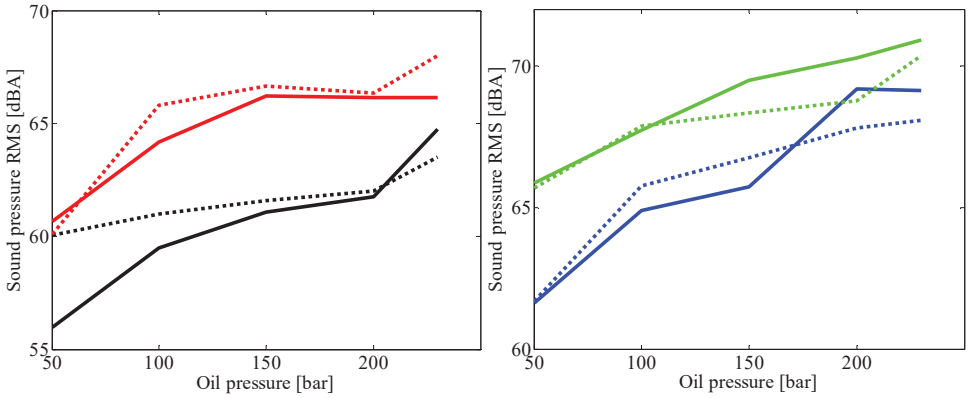

(a) (b)

Figure 9. Total RMS sound pressure v/s fluid pressure, uncoated pump (dotted line), coated pump (solid line) : a) 1000 rpm (black), 1500 rpm (red); b) 2000 rpm (blue), 3000 rpm (green)

The dBA total root mean square (RMS) values, evaluated from[0÷20000] Hz measured freqency range, for the uncoated and coated pump are compared. Fig. (9) shows that the acoustic emission of the coated pump is reduced with respect to the uncoated solution in a limited range of operating conditions, so that this coating architecture cannot be considered effective with respect to the operating pump noise reduction. Nevertheless, multilayer architectures are expected to be more effective if a constrained layer damping contribution is properly designed, and will be investigated in future works.

6. CONCLUSIONS AND FUTURE DEVELOPMENT

An extended multilayer beam modeling tool is proposed, with the aim to find optimal coating solutions maximizing dissipative action at the interface between the layers. Three

model beam application examples (1L, 5L, 9L) are shown and it can be observed that as the number of coating layers increases, the system damping behaviour increases as well.

Some different innovative coating solutions are experimentally investigated and evaluated by means of a normalized damping estimator $z(j\omega)$. A z increase, with respect to uncoated specimens, is observed for specimens coated with single-layer, cyanoacrylate based solutions in the [0÷60] Hz frequency range and with multi-layer, Al-Cyanoacrylate based solutions in the [0÷200] Hz frequency range. The single-layer epoxy based coating solutions gave different results, but the specific L case was associated to effective results in the [0÷200] Hz frequency range.

An industrial application case is presented, consisting on the measurement of an industrial gear pump whose casing was coated by means of the L coating solution L, but no meaningful results were obtained to justify the application of this technology in this industrial field. Multilayer coating architectures, optimized to maximize dissipative actions at the interface between different layers, will be experimentally investigated in future applications of this technology, and new applications in the oleodynamic pump, gearing, industrial automation, automotive and aerospace industrial sectors will be taken into account.

Acknowledgements

This study was developed within the CIRI-MAM with the contribution of the Regione Emilia Romagna, progetto POR Fesr Tecnopoli. Support from Andrea Zucchini, Dr.Danilo Persici from Marzocchi Pompe S.p.A., Casalecchio di Reno, Italy, and from Dr.Massimo Penatti from Loxeal S.r.l. is also kindly acknowledged.

REFERENCES

[1] J. A. Rongong, A. A. Goruppa, V. R. Buravalla, G. R. Tomlinson, F. R. Jones, 2004,"Plasma deposition of constrained layer damping coating". Proc. Instn Mech. Engrs Vol. 218 Part C: J. Mechanical Engineering Science 218 pp. 669-680

[2] C. Blackwell, A. Palazzotto, T. J. George, C. J. Cross, 2007 ,"The evaluation of the damping characteristics of hard coating on titanium". *Shock and Vibrations* **14** pp. 37-51

[3] L. Yu, Y. Ma, C. Zhou, H. Xu, 2005, "Damping capacity and dynamic mechanical characteristics of the plasma sprayed coatings". *Material Science and Engineering A* **407** pp. 174-179

[4] V. R. Buravalla, C. Remillat, J. A. Rongong, G. R. Tomlinson, 2001, "Advances in damping materials and technology". *Smart Materials Bulletin* **2001**(8) pp. 10-13

[5] X. Wang, Y. Pei, Y. Ma, 2013, "The effect of microstructure at interface between coating and substrate on damping capacity of coating systems". *Applied Surface Science* **282** pp. 60-66

[6] S. Amadori, G. Catania, 2017, "Robust identification of the mechanical properties of viscoelastic non-standard materials by means of frequency domain experimental measurements". Composite Structures **169** pp. 79 – 89

[7] S. Amadori and G. Catania, 2018, "An effective coating material solution and modeling technique for damping oriented design of thin walled mechanical components ". *Composite Structures* 191, pp.251-267

[8] In Proceedings, S. Amadori, G. Catania, "Multi-layer composite coating technology for high damping mechanical structural applications". Engineering Dynamics and life sciences, Proceedings of the 14th International Conference on Dynamical Systems Theory and

Applications, Lodz, 11-14 December 2017 edited by J. Awrejcewicz, M. Kazmierczak, J. Mrozowski, P. Olejnik, 2017, vol.3, pp. 97-108

[9] M. Di Sciuva, 1992, "Multilayered anisotropic plate models with continuous interlaminar stresses". *Composite Structures* **22** pp.149-167

[10] J. N. Reddy, 1990 , "On refined theories of composite laminates". *Meccanica* **25** pp. 230-238

[11] D. Liu, X. Li, 1996, "An overall view of laminate theories based on the displacement hypothesis". *Journal of Composite Materials* **30**(14) pp. 1539-1561

[12] L. Iurlaro, M. Gherlone, M. Di Sciuva, A. Tessler, 2015, "Refined Zigzag Theory for laminated composite and sandwich plated derived from Reissner's Mixed Variational Theorem". *Composites Structures* **133** pp. 809-817

AN OLD MECHANISM TO IMPROVE WIND ENERGY HARVESTNG

Alessandro Zanarini
Department of Industrial Engineering, University of Bologna, Italy
E-mail: a.zanarini@unibo.it

Abstract. *Not only the well known and spread horizontal axis machines are present in the wind turbine scenario, but other architectures have found their niche. Among them, the Darrieus solution is known for its relatively compact design and small size, but, even more, for its vertical axis, as well as for the vertical blades distributed on the side of a rotating cylinder, even when twisted with special 3D helical shapes. Contrary to the horizontal axis solution mostly as 3-bladed version, the Darrieus design can not take advantage of the axis orientation control of the blade plane, because it accepts wind from any direction. But in order to maximise the efficiency in harvesting energy from the wind, the Darrieus turbine searches for the best attack angle between each blade and the wind flow at a specific speed, optimised along the complete rotation of the blade around the central axis. Together with a simple self-control towards the wind flow direction, a solution to improve the energy conversion into torque comes from the design of a controlled guidance of the attack angle of the vertical blades towards the flow.*
In this work the common use of an old mechanism, the four-bar linkage, is analysed to generate the passive control of each of the 3 blades in a simple Darrieus turbine design to improve the efficiency. This activity was made to understand, with relatively simple models, the advantages and drawbacks of such mechanism architecture for the optimal guidance of each blade, as a preliminary and feasibility methodological study for a potential research path in wind energy harvesting alternative solutions. The work therefore deals with the selection of a common wing profile and a 3-bladed machine scheme, together with the adoption of four-bar linkage for each passively controlled blade. The aerodynamic force distribution and torque simulation follow, as functions of the angular position, at two different wind speeds in a complete turbine rotation. The assumptions, the formulation and results for the simple Darrieus machine with an attack angle guidance mechanism are discussed in detail.

Keywords: *Wind turbines, Darrieus turbine, vertical axis wind turbine, VAWT, wind energy harvesting, four-bar linkage, mechanisms in wind energy, attack angle control.*

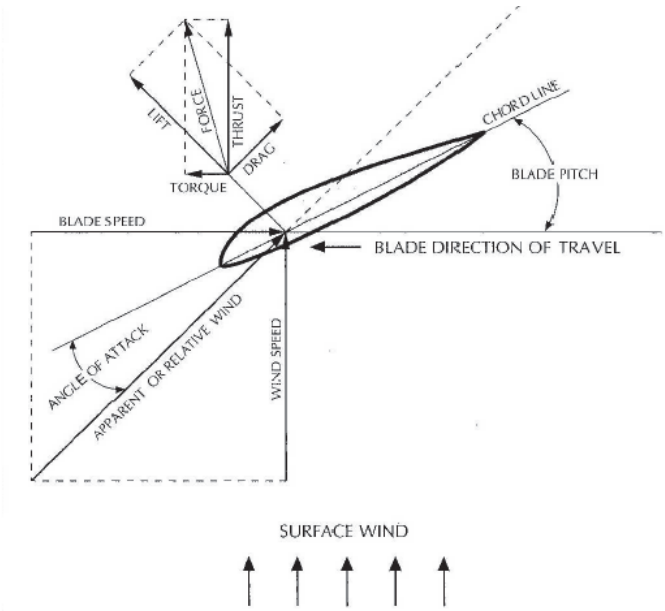

Figure 1. Wind forces on the blade.

1. INTRODUCTION

The correct angle of attack and blade shape are the key-points in harvesting the maximal energy from the wind flow. Furthermore, the output torque and power generation can be unsteady quantities also in a single revolution of the turbine. This works addresses the regulation of the attack angle in Vertical Axis Wind Turbines (VAWTs) by means of a four-bar linkage, which drives the position of each blade towards the flow direction.

The basic concepts about the aerodynamic forces at the ground of wind energy harvesting are introduced in section 2.. After briefly presenting in section 3. the main architectures of the VAWTs against the Horizontal Axis Wind Turbines (HAWTs), in section 4. the passive control solution to guide the attack angle in VAWTs is explained. In section 5. the inertial contributions are taken into account to write the motion equations of the whole machine. The latter are used to simulate the forces and torques available at specific wind speeds with the aim of being able to simulate the energy harvesting of the passively controlled HAWT. Conclusions are drawn in section 6..

2. SOME AERODYNAMIC BASIC CONCEPTS

In this preliminary study it is important to track the generation of distributed forces on the machine, as the real engine of the wind energy harvester of any architecture.

Origin of aerodynamic pressure on a wing profile

As can be depicted in Figure 1, the wind on a wing generates forces depending on the actual position of the wing towards the flow direction, which is considered as uniformly distributed

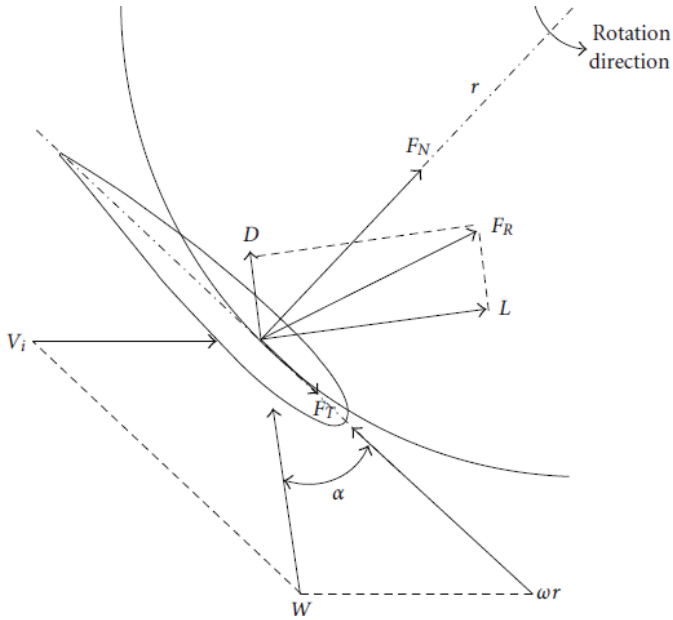

Figure 2. Wind forces on the blade. Angles and vectors of relevance.

on a plane orthogonal to the wind direction. The blade itself is moving on a travel direction orthogonal to the absolute wind surface with a certain speed, therefore the wind impacts the blade with a relative velocity direction, as vectorial sum of the wind speed and of the blade speed. The blade faces the relative wind direction with an attack angle from the chord line. The latter has a pitch angle regarding the blade direction of travel. The pitch angle will be addressed as the controlled angle to optimise the attack angle for a specific wind relative speed.

The wind flows around the blade with different speeds depending on the shape and on the attack angle: the Bernoulli principle tells us that where the flow is faster the pressure is lower, whereas on the side of slower flow there is an increase of the pressure field. The pressure difference is the origin of the forces on the blade, which push the blade toward the lower pressure zone. The aerodynamic force can be seen as the vectorial sum of a *lift* and *drag* components, where *lift* force is orthogonal to the relative wind direction, whereas *drag* force has the same direction of the apparent wind. In Figure 1 also another decomposition is shown, calling *torque* or *tangent* component that on the blade travel direction and *thrust* or *normal* the one orthogonal to it, thus along the absolute wind speed. It is actually the *tangent* component that can harvest energy from the wind to a power generator for a guided blade in a wind turbine.

As an example more focused on the VAWTs [1], in Figure 2 a turbine blade is rotating at rotational speed ω on a circular trajectory of ray r, therefore with a tangential speed ωr. The wind absolute velocity is directed as $\mathbf{V_i}$, thus the wind relative velocity becomes the vector $\mathbf{W}$. From the latter the attack angle $\alpha(\lambda)$ can be measured, where λ is the tip speed ratio defined as $\lambda = \frac{\omega r}{V_i}$. In this configuration, the forces are clearly depicted as drag force $\mathbf{D}$, lift force $\mathbf{L}$, normal force $\mathbf{F_N}$, tangential force $\mathbf{F_T}$ and resultant force $\mathbf{F_R}$.

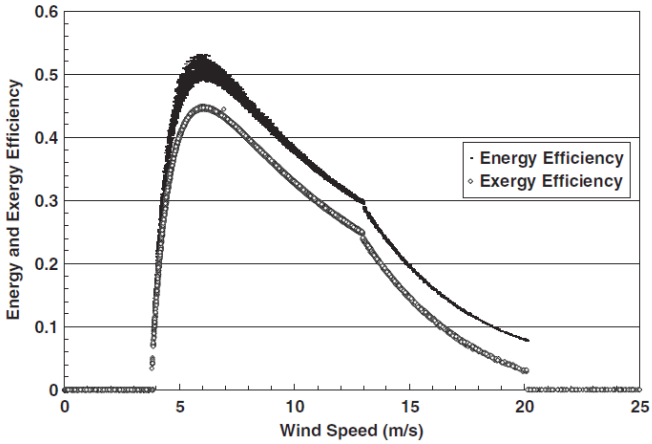

Figure 3. Efficiency as function of wind speed.

Dependence of forces on wing angles

Among the many references available in literature, [2] might be useful to deeply understand the behaviour of the air around a wing blade. In brief, the shape of the section, together with the tip speed ratio and the attack angle, have a strong influence on the evaluation of the forces that can be extracted from the wind flow. By defining the drag coefficient C_d and the lift coefficient C_l, a tangential force coefficient C_t can be formulated as $C_t = C_l sin\alpha - C_d cos\alpha$. Given the blade height s and air density ρ, the *instant* tangential force $F_T = \frac{1}{2} C_t \rho s V_i^2$ on a single blade can be evaluated at a specific configuration. But, as in the case of Figure 2, the blade is tracing a circular trajectory, therefore continuously changing the relative angles and parameters. Thus an average tangential force $F_{T_{mean}}$ needs to be estimated: $F_{T_{mean}} = \frac{1}{2\pi} \int_0^{2\pi} F_T(\theta) d\theta$. When thinking to a VAWT composed of N blades, each with chord length c, the solidity $\sigma = \frac{Nc}{2\pi r}$ can define the fraction of the perimeter, which is occupied by the blades; from such a machine with N blades, an average torque τ can be calculated: $\tau = F_{T_{average}} N r$; this leads to an average extracted power $P_{turbine} = \tau\omega$.

Efficiency considerations

Independently from the architecture, the harvesting has to understand its limits of efficiency. Being the wind power $P_{wind} = 1/2 \rho d s V_i^3$, according to Betz the extractable wind power $P_{Betz} = 1/2 \rho d s V_i^3 4\beta(1-\beta)^2$, with interference factor $\beta = \frac{V_i - V_{out}}{V_i}$, is only a fraction of the wind power P_{wind}; therefore a theoretical efficiency $\eta = \frac{P_{Betz}}{P_{wind}}$ can be defined and evaluated as 0.59.

In reality each turbine can not reach the theoretical efficiency, which works as the upper bound, but it is constrained by the losses to a lower performance, which can be evaluated by the Coefficient of Performance C_P as $C_P = \frac{P_{turbine}}{P_{wind}} = \frac{\tau\omega}{1/2 \rho d s V_i^3}$. It is interesting to note

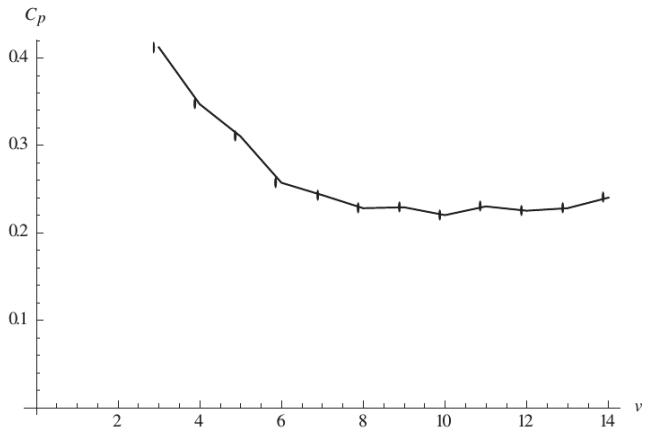

Figure 4. Coefficient of performance as function of wind speed in a Darrieus VAWT.

that for the HAWTs the $C_{P_{max}}$ is in the range [0.4,0.5], whereas for the VAWTs is around 0.4, therefore lower than in HAWTs, far from the theoretical efficiency η, but that there is a strong relationship with the wind speed. In [3, 4] it was suggested to use the *exergy* as a measure of turbine performance, as in Figure 3, because of the more parameters involved in wind harvesting, such as air pressure and temperature: again the dependence on the wind speed is relevant, as confirmed in Figure 4.

Self-starting in Darrieus turbines

As noted in [5], the starting of VAWTs can be problematic (and costly to be solved), as in Darrieus wind turbine the efficiency is very low for low tip speed ratios λ, due to the cyclic dependence of the attack angle α on the azimuthal angle θ, as can be seen in Figure 5, where for low tip speed ratio λ the variation in the attack angle is relevant. The Darrieus VAWT has a so-called "dead zone" where it needs external aid to start rotating: as can be seen in Figure 6, when $\lambda \in [0.75, 2.70]$ the produced torque is negative, meaning that the turbine can not start autonomously and can not reach any higher speed. A solution to the self-starting issue in network-isolated systems can be the change in the machine geometry, by means of convex blades, flexible blades, or variable pitch, as later discussed in section 4..

3. WIND TURBINE ARCHITECTURES WITH VERTICAL AXIS

Most of the wind energy harvesting, in terms of power production, is covered by the HAWTs, mainly as 3-bladed turbines. But the HAWTs are not the best solution for all the issues, as the following comparison highlights from [6, 7]:

- tower oscillations: HAWTs have stronger deflections than VAWTs.
- rotor direction control: HAWTs are strongly dependant on following the wind direction, which must be orthogonal to the blades' plane; for VAWTs it might only be a matter of optimising the harvesting.

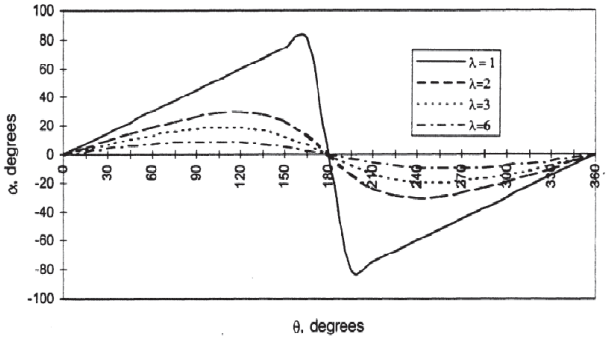

Figure 5. Variations in a Darrieus turbine of the attack angle α on the azimuthal angle θ as function of the tip speed ratios λ.

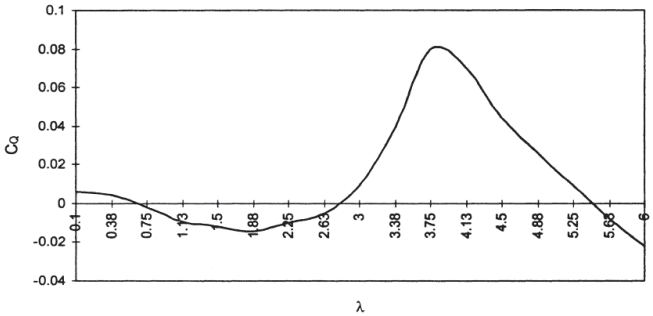

Figure 6. Torque in a Darrieus turbine versus the tip speed ratio.

- self-starting: only HAWTs start autonomously, while VAWTs need a motor or other solutions.
- generator location: in HAWTs the generator is located at the top of the tower, with great costs in mounting and in maintenance; for VAWTs the generator can lay on the lowest position, with relevant savings.
- blade area: VAWTs generally have blade with larger areas to increase the energy harvesting, though with cost increases than in HAWTs.
- noise emission: VAWTs generally have a lower blade speed and less flow, with less noise than HAWTs, also for the more compact architecture.
- efficiency: for HAWTs the efficiency is about 40-50%, while for VAWTs is only around 40%.
- blades: the shape and dimension of the blades can increase significantly the costs related to the specific architecture; for HAWTs the blades are connected to the central

Table 1. Summary of the Darrieus-type solutions for VAWTs

Type / Characteristics	Type / Characteristics	Type / Characteristics	Type / Characteristics	Type / Characteristics
Darrieus Egg-beater	Darrieus Giromill	Darrieus Masgrowe [8]	Darrieus Crossflex [9]	Darrieus Twisted Blades
		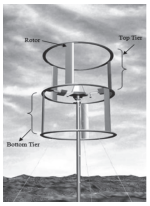	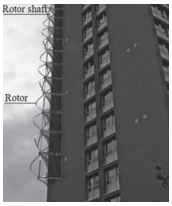	
Low starting torque	Rectilinear blades	Dual-level blades 90° phased	Many Egg-beater turbines	Smooth detachment of air flow
High efficiency	2-5 simpler blades	Easier starting	Reduced inertia	Positive lift for easier start
High costs of wings	Fix or variable pitch	Efficiency	Flexible wings	High blade costs
	for an easier start		Efficient for high wind speeds	Lower efficiency

Table 2. Summary of other architecture solutions for VAWTs

Type / Characteristics	Type / Characteristics	Type / Characteristics
Savonious Turbine [10]	Sistan Turbine [11]	Zephir Turbine
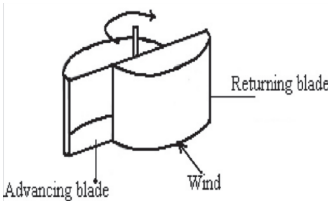	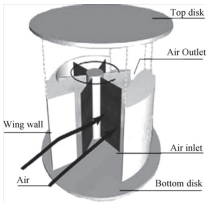	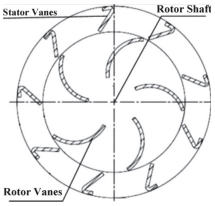
Only drag forces	Only drag forces	Stator vanes for lower turbulence
Lower efficiency	Buildings integration	Low efficiency
Low use	Higher drag with end disks	Low diffusion

axis on the top of the tower, while for VAWTs linkages build the structure around the vertical axis.

- blade flexibility: typical problem of the HAWTs due to the bending of the blades that can cause interference with the tower, especially in *upwind* conditions, when the rotor is positioned before the tower in the direction of the flow; in *downwind* conditions the deflection can alter the relative wind velocities and cause noise or efficiency losses.

- height: HAWTs are less influenced by the ground profile, reaching relevant altitude above the base; to be in the same conditions the VAWTs should be also positioned on a tower.

This paper aims at inquiring the feasibility of VAWT architecture in wind energy harvesting, thanks to its lower costs and usability in complementary situations to those where the HAWTs are dominant.

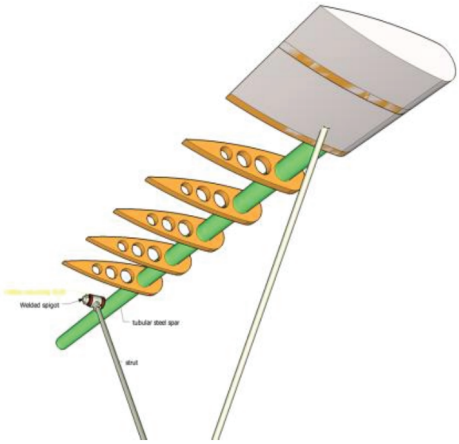

Figure 7. Example of blade skeleton.

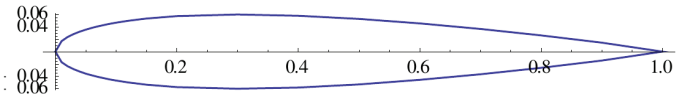

Figure 8. NACA 0012 parametric profile.

Darrieus-type solutions

Some of the Darrieus-type architectures are summarised in Table 1, together with the main characteristics and specific references.

Other solutions

In Table 2 different solutions of VAWTs rather than the Darrieus-type ones are sketched, also with their main characteristics and specific references.

4. PASSIVE GUIDANCE BY MEANS OF A FOUR-BAR LINKAGE

As already hinted in section 2., the variability of the attack angle is a source of lower performances and of the potential ”dead-zone” issue in VAWTs. It follows that there is the need to control the incidence of each blade towards the wind speed. Among the many possible actuating solutions that can be found in literature, the adoption of a passive four-bar linkage is analysed in the present contribution, which aims at assessing the feasibility of this old mechanism as passive controller. For this purpose, the aerodynamic forces will be evaluated as function of the wind speed and azimuthal angle θ for each blade and for the whole machine, by means of equilibrium conditions on a constrained mechanism.

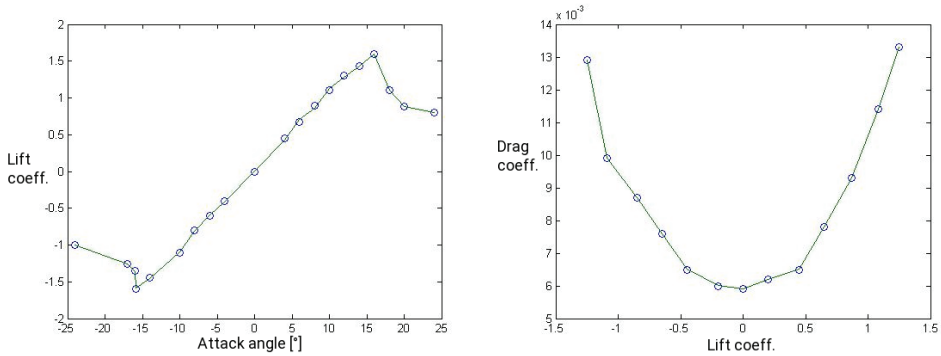

Figure 9. Lift coefficient as function of the attack angle (left) and drag coefficient as function of lift coefficient (right), with polynomial approximation.

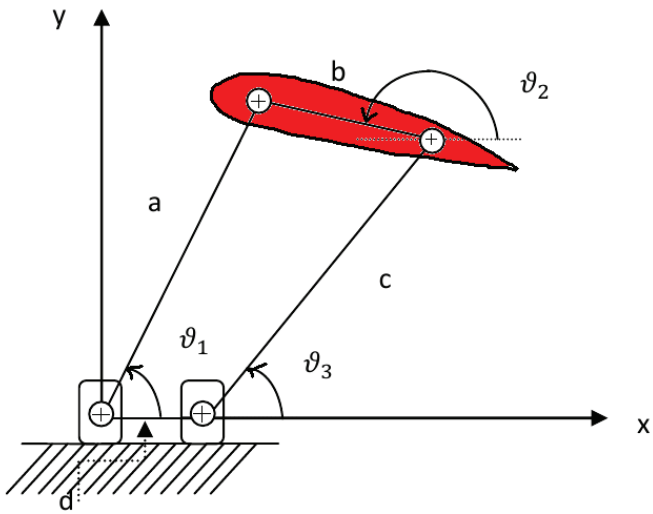

Figure 10. Four-bar linkage scheme for the passive control of the blade b.

Blade selection

Starting from the basic Giromill solution of Table 1, the skeleton of each strait blade can be exemplified as in Figure 7. The shape can have multiple profiles with their specific aerodynamic properties (see section 2.), therefore one NACA 0012 shape in Figure 8 was selected to have the lift and drag variability of Figure 9 from Reference [2].

Single blade configuration

Considering the control of a single blade, the four-bar linkage of Figure 10 presents the blade as member b, whereas two linkages a and c are connected to b and to the central shaft at eccentricity d, being the shaft the local reference for the one degree of freedom system.

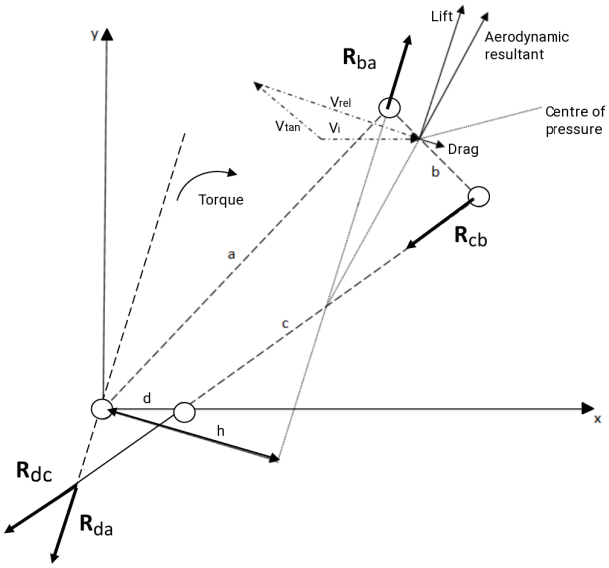

Figure 11. Aerodynamic forces, reactions and torque on the guided blade.

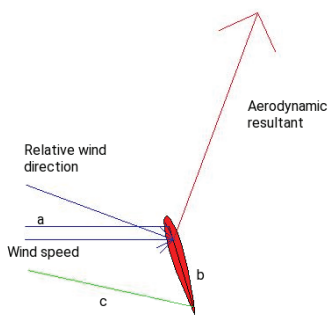

Figure 12. Example of the calculated aerodynamic force on a single blade (red=aerodynamic force [mainly lift, with minimal drag], blue=wind relative direction).

The length of each member of the mechanism describes the passive driving function of the blade, which might be optimised for specific wind speeds and blade shapes. For the presented case study, the following data were taken into account:

- a=0.373 m; b=0.085 m; c=0.380 m; d=0.026 m
- V_i=2 m/s on the x direction; ω_1= 2 rad/s

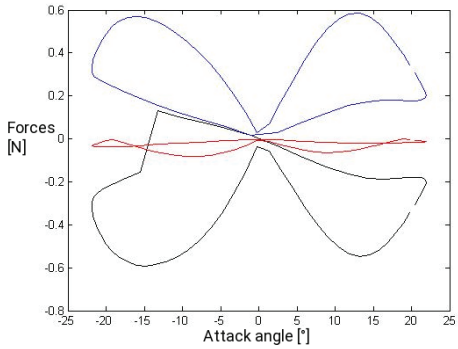

Figure 13. Force on a single blade as function of the attack angle (blue=aerodynamic; red=reaction from c; black=reaction from a).

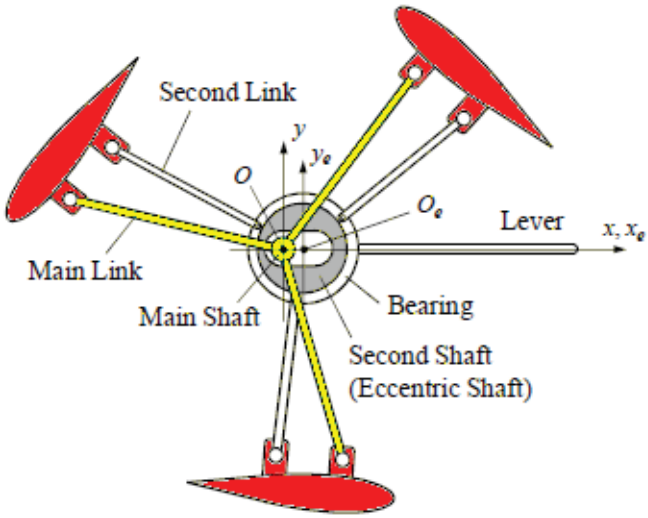

Figure 14. Possible planar scheme from [13].

As can be followed on Figure 11, at each θ_1 position follows a force pattern located on the pressure centre of the blade, therefore a torque deployment can be evaluated by means of the mechanism equilibrium [12]. Taking into account the above data of wind speed and mechanism rotational speed ω_1, the aerodynamic forces can be evaluated as in Figure 12 at position $\theta_1 = 0$. The same aerodynamic force, together with the reactions on link a and c, can be analysed as function of the variable attack angle as in Figure 13, where, though, sign discrepancies are present in this prototype study.

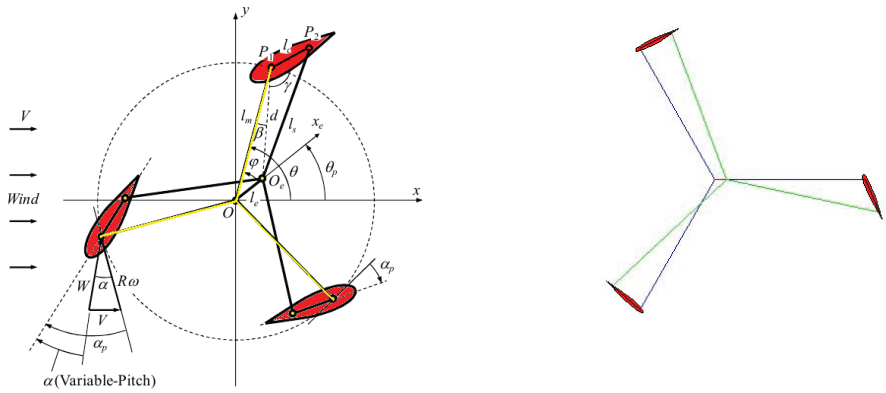

Figure 15. Scheme of the machine on the left, custom software representation on the right.

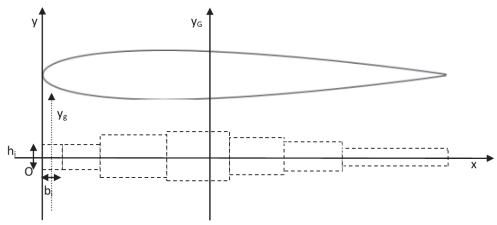

Figure 16. Simplified blade for inertia calculation.

3-bladed turbine

When working on a whole turbine each vectorial contribution of the blades must be taken into account. As in most of the architectures in Table 1, a 3-bladed VAWT with passive four-bar control mechanism was here modelled. The main link system of Figure 14 is composed of each a link in the single blade mechanism, fixed together on an eccentric shaft, whereas the secondary link system is the fusion of each c link. The lever works as optimizer of the turbine performances and might be self-actuated by a wind flap, maintaining it in the wind direction: on the left of Figure 15 this degree of freedom is called θ_P, as pitch-related; on the right side the whole turbine representation in the graphical environment of the present simulation, with $\theta_P = 0$ as mentioned above.

5. DYNAMICS OF A PASSIVE MECHANISM FOR PITCH CONTROL

The simulation of the whole machine can be done by considering all the force sources with their generalised contribution. In this specific test, however, the inertial generalised forces mainly resulted of limited impact in comparison with that of the aerodynamic forces.

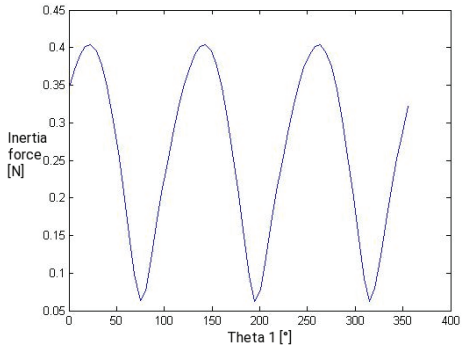

Figure 17. Inertia force of the whole system: $\omega_1 = 2rad/s \quad \dot{\omega_1} = 0rad/s^2$

Inertia contributions

Before ending with the aerodynamic force simulation of the whole mechanism, the generalised inertia forces have to be taken into account. Starting from each blade contribution, together with the related passive driving mechanism dynamics, it is possible to build the inertia generalised forces acting on the whole machine. To evaluate the mass, centroidal location and inertia moment of a blade, a simplification can be made as in Figure 16 by finding an equivalence between the original NACA 0012 shape and a sum of 7 rectangular contribution, instead of evaluating the integrals, for sake of simplicity in the calculations. The following data were used in the inertia simulations: $m_a = 0.44[kg]$, $m_{blade} = 0.10[kg]$, $m_c = 0.45[kg]$, $J_a = 4/3m_a a^2[kgm^2]$, $J_c = 4/3m_c c^2[kgm^2]$, $J_{blade} = \sum_i \rho/12(h_i b_i^3 + b_i h_i^3) + m_i(x_i - x_G)^2[kgm^2]$. The inertia force of the whole system was simulated in a complete revolution of the passively guided VAWT, with the different conditions on the main link in terms of constant angular velocities and accelerations, as reported in the captions of Figures 17-22. Only in the latter conditions the inertia contributions appeared as relevant in comparison to the aerodynamic forces, with potential issues when counter-acting the wind energy harvesting. From what simulated, it appears that the inertia force are more sensible to angular velocity changes, rather than angular accelerations.

Aerodynamic force simulations

The aerodynamic forces can now be simulated with different conditions on the constant angular speed of the main link. The first case assumes the angular velocity of $2rad/s$, the second sees an increment to $5rad/s$, while the third test is again with angular speed of $2rad/s$, but with the optimiser lever raised of $60°$. Figures 23, 25 amd 27 present the aerodynamic resultant as mapped in its horizontal and vertical components during a whole turbine revolution. Figures 24, 26, 28 instead show the aerodynamic resultant force modulus as function of the angular position of the reference principal link. The angular speed affects the aerodynamic forces with lower magnitude than for the inertial ones, though the distribution in a revolution is changing significantly, raising some concerns about counter acting contributions. Especially at higher speeds ($\omega = 5rad/s$), the magnitude of the aerodynamic forces is comparable to that of the inertia ones, while the distribution is less regular. The actuation of

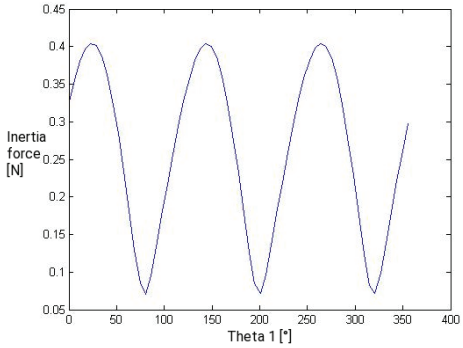

Figure 18. Inertia force of the whole system: $\omega_1 = 2rad/s \quad \dot{\omega_1} = 1rad/s^2$

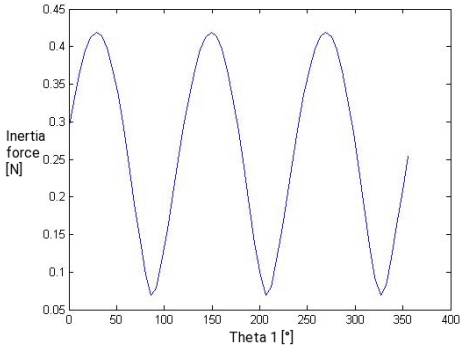

Figure 19. Inertia force of the whole system: $\omega_1 = 2rad/s \quad \dot{\omega_1} = 3rad/s^2$

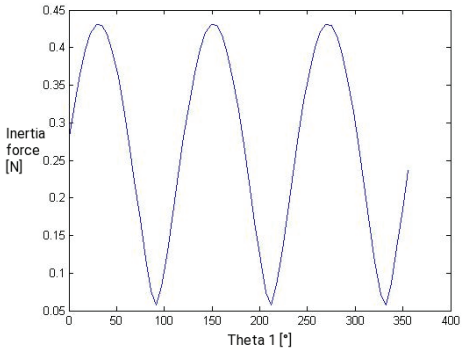

Figure 20. Inertia force of the whole system: $\omega_1 = 2rad/s \quad \dot{\omega_1} = 4rad/s^2$

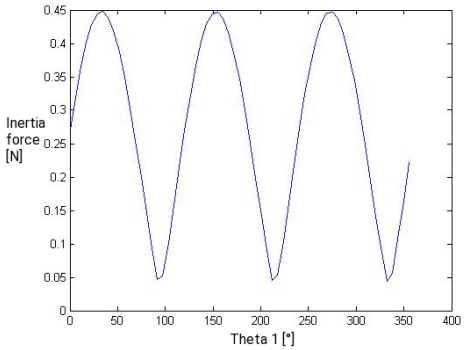

Figure 21. Inertia force of the whole system: $\omega_1 = 2rad/s \quad \dot{\omega_1} = 5rad/s^2$

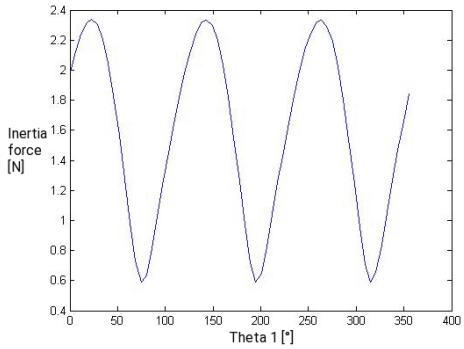

Figure 22. Inertia force of the whole system: $\omega_1 = 5rad/s \quad \dot{\omega_1} = 5rad/s^2$

the optimiser lever indeed plays a negative effect on the aerodynamic forces, again showing that the best pitch angle compromise is obtained with the lever in the same direction of the main flow of the undisturbed wind. Figures 27 and 28 show substantial changes in shape and amplitude.

Aerodynamic torque simulations

With the same test cases above, the aerodynamic torques are elaborated along a whole revolution of the turbine. Figures 29, 30 and 31 show the aerodynamic torque contributions and their resultant. While in Figure 29 the contributions of each blade seem to be regularly out-phased, and none is counter-acting as negative, in Figure 30, with higher constant angular speed ω_1, the aerodynamic contributions seem more irregular and, more relevant, have partial counter-acting effect in the negative zones. The resultant of Figure 30 has therefore many positions with negative value, acting therefore has a brake on the revolution of the system; in such situations the inertia torque should also be taken into consideration, clearly highlighting the impossibility for the VAWT to reach higher speeds. In Figure 31, the actuation of the

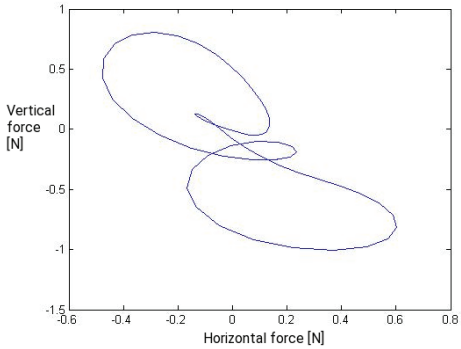

Figure 23. Resultant of the 3 aerodynamic forces in a whole revolution (horiz. vs vert.) V_i=2 m/s; ω= 2 rad/s.

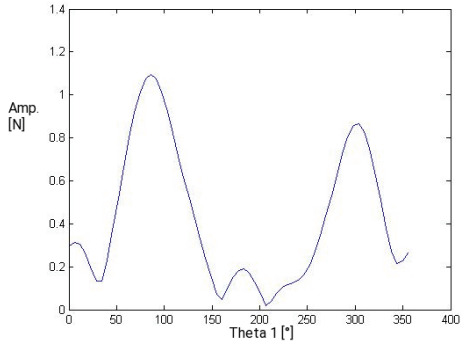

Figure 24. Resultant of the 3 aerodynamic forces in a whole revolution (modulus vs θ_1) V_i=2 m/s; ω= 2 rad/s.

pitch-optimizer lever brings the three aerodynamic torque contributions partly, but regularly, in the negative range, with a resultant that is lowered, sometime to close-to-null values, much lower than the inertial contributions seen above.

Recall to system equations

In this simplified modelling, the whole system dynamics is governed by the aerodynamic and inertia forces. To be able to describe it, a Lagrangian approach can be followed by means of the kinetic energy and external force work. For each blade, knowing the inertia moments of the blade and the driving linkages, the kinetic energy can be expressed as:

$$T_i = \frac{1}{2}\left[J_{a_i}\dot{\theta}_{1_i}^2 + J_{c_i}\dot{\theta}_{3_i}^2 + J_{blade_i}\dot{\theta}_{2_i}^2\right] = \frac{1}{2}\left[J_{a_i} + J_{c_i}\tau_{31_i}^2 + J_{blade_i}\tau_{21_i}^2\right]\dot{\theta}_{1_i}^2 = \tag{1}$$
$$= \frac{1}{2}\left[J_{R_i}\left(\theta_{1_i}, \dot{\theta}_{1_i}\right)\right]\dot{\theta}_{1_i}^2,$$

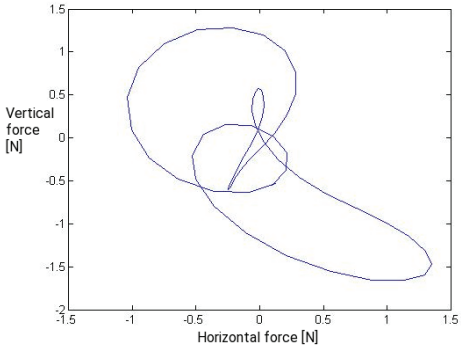

Figure 25. Resultant of the 3 aerodynamic forces in a whole revolution (horiz. vs vert.) V_i=2 m/s; ω= 5 rad/s.

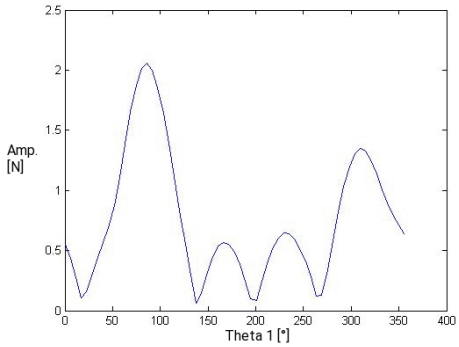

Figure 26. Resultant of the 3 aerodynamic forces in a whole revolution (modulus vs θ_1) V_i=2 m/s; ω= 5 rad/s.

keeping in mind that the blades are phased by $120°$, therefore the main link of reference is angled of θ_{11}, the one of the second blade of $\theta_{12} = \theta_{11} + 2\pi/3$, the one of the third of $\theta_{13} = \theta_{11} + 4\pi/3$. It can be clearly seen, also in the above formulation that reduces the multibody inertia contributions to a one degree of freedom system, how the turbine has a variable reduced inertia, therefore showing different dynamic properties along the whole revolution. The problem might also be approached by multibody modelling as done by the author in other studies [14–18].

From the expression of the aerodynamic torque contributions, the total work of the aerodynamic forces follows as:

$$W = M_{aero_1}\theta_{11} + M_{aero_2}\theta_{12} + M_{aero_3}\theta_{13}. \tag{2}$$

Finally, the motion equations can be obtained in the Lagrange formulation by proper derivation of the Lagrangian function $L = T_1 + T_2 + T_3$, made of the kinetic energies of the 3 blades:

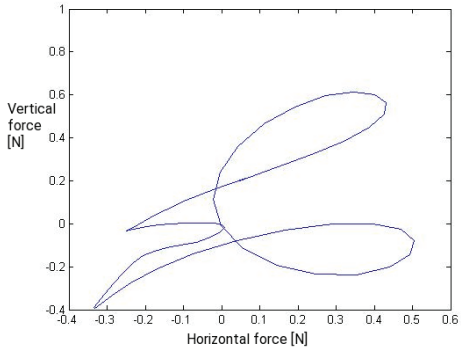

Figure 27. Resultant of the 3 aerodynamic forces in a whole revolution (horiz. vs vert.) V_i=2 m/s; ω= 2 rad/s; lever at 60°.

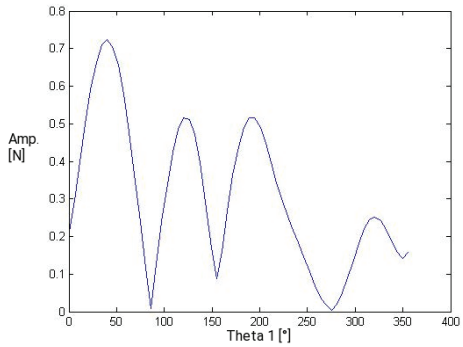

Figure 28. Resultant of the 3 aerodynamic forces in a whole revolution (modulus vs θ_1) V_i=2 m/s; ω= 2 rad/s; lever at 60°.

$$\frac{d}{dt} \quad \frac{\partial L}{\partial \dot{\theta}_{11}}\Bigg) - \frac{\partial L}{\partial \theta_{11}} = \frac{\partial W}{\partial \theta_{11}}. \tag{3}$$

The motion equation are valuable for simulating the transients of the turbine, when both aerodynamic and inertia forces can affect the stability of the rotational speed, not inquired in this early work. It must be recalled how this approach does not take into account any damping effect of the wind on the turbine structure. Though, the *nervous* nature of the forces seen above opens questions about evolving the modelling towards the introduction of flexible degrees of freedom, as done in [19–21], to forecast with better insight dangerous instabilities, durability issues due to flexural or torsional vibrations, and forbidden speeds for the system.

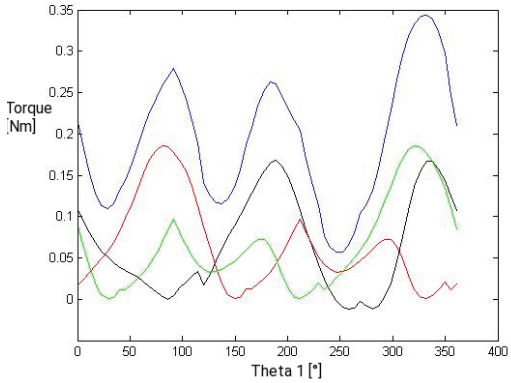

Figure 29. Resultant (blue) and single contributions (red, green, black) of the aerodynamic torques in a whole revolution (modulus vs θ_1) V_i=2 m/s; ω= 2 rad/s.

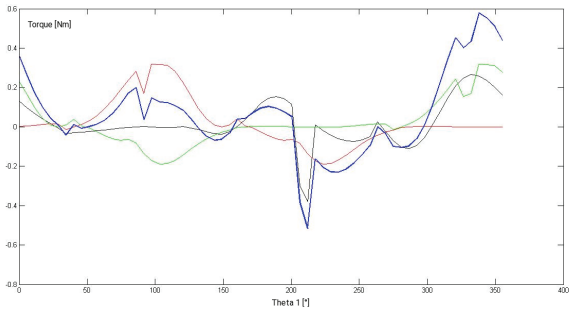

Figure 30. Resultant (blue) and single contributions (red, green, black) of the aerodynamic torques in a whole revolution (modulus vs θ_1) V_i=2 m/s; ω= 5 rad/s.

6. CONCLUSIONS

The present contribution has briefly outlined how the modelling of aerodynamic forces can be joined with mechanical system dynamics in the application of a four-bar linkage as passive regulator of the attack angle in VAWTs. In particular, detailed kinematics & aerodynamic model based quantities were achieved with simple assumptions, with a better understanding of basic phenomena, in agreement with literature evidences, than an average energy based assumptions. Section 5. has strongly highlighted how the harvested torque, and therefore also the output power, is other than constant at each revolution, surely posing issues in network frequency. Furthermore, there is a relevant limitation in the speed range achievable due to the counter-acting force from aerodynamic and inertia sources.

These methodological results are transferable to other investigations: design, selection, optimisation of different turbines and architectures. Enhancements can be easily foreseen in the selection of the wing profile, when not a morphing one, in the assessment of the reachable

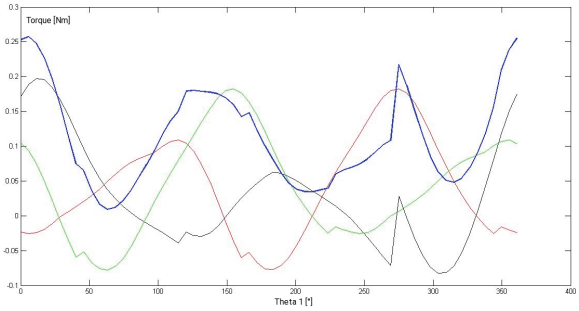

Figure 31. Resultant (blue) and single contributions (red, green, black) of the aerodynamic torques in a whole revolution (modulus vs θ_1) V_i=2 m/s; ω= 2 rad/s; lever at 60°.

speed ranges and sustainable transients, o in the optimisation of the architecture for specific critical speeds. Furthermore, a marked improvement of the understanding of critical working conditions was proposed, able to be applied to a wider set of real industrial aero-generators, thanks to the improvements in the calculation efficiency that might be shortly implemented.

Also the modeling of wind turbines can take advantage of the flexible multibody approach seen in [19–21], as well as in the advanced modelling of the gear stiffness in [22] for the gearbox, because of the discontinuity of the output torque that, with all its fluctuations, can easily excite the structural dynamics of the machine, especially with torsional vibrations.

Acknowledgements

This contribution saw its beginning with the precious aid of Ugo Gorini, who followed my directions and suggestions in implementing the code to obtain the shown results during his bachelor thesis works.

REFERENCES

[1] Carrigan, T. J., Dennis, B. H., Han, Z. X., and Wang, B. P., 2012. "Aerodynamic Shape Optimization of a Vertical-Axis Wind Turbine Using Differential Evolution". *ISRN Renewable Energy,* **2012**, pp. 1–16. Article ID 528418, doi:10.5402/2012/528418.

[2] Abbott, I., and Von Doenhoff, A., 1959. *Theory of wing sections, including a summary of airfoil data.* Dover books on physics and chemistry. Dover Publications. https://aeroknowledge77.files.wordpress.com/2011/09/58986488-theory-of-wing-sections-including-a-summary-of-airfoil-data.pdf.

[3] Pope, K., Dincer, I., and Naterer, G., 2010. "Energy and exergy efficiency comparison of horizontal and vertical axis wind turbines". *Renewable Energy,* **35**(9), pp. 2102 – 2113. doi:10.1016/j.renene.2010.02.013.

[4] Sahin, A. D., Dincer, I., and Rosen, M. A., 2006. "Thermodynamic analysis of wind energy". *International Journal of Energy Research,* **30**(8), pp. 553–566. doi:10.1002/er.1163.

[5] Kirke, B. K., 1998. "Evaluation of self-starting vertical axis wind turbines for stand-alone applications". PhD thesis, Griffith University, Brisbane (Queensland), Australia. https://www120.secure.griffith.edu.au/rch/items/d1a0b579-7560-8462-75da-f75671e8cce2/1/.

[6] DeCoste, J., McKay, D., Robinson, B., Whitehead, S., Wright, S., Koksal, M., and Hughes, L., 2005. Vertical axis wind turbine. Tech. rep., Department of Mechanical Engineering, Dalhousie University. MECH 4010 Design Project, http://citeseerx.ist.psu.edu/viewdoc/download?doi=10.1.1.452.6381&rep=rep1&type=pdf.

[7] Bhutta, M. M. A., Hayat, N., Farooq, A. U., Ali, Z., Jamil, S. R., and Hussain, Z., 2012. "Vertical axis wind turbine a review of various configurations and design techniques". *Renewable and Sustainable Energy Reviews,* **16**(4), pp. 1926 – 1939. doi:10.1016/j.rser.2011.12.004.

[8] Gorelov, D. N., and Krivospitsky, V. P., 2008. "Prospects for development of wind turbines with orthogonal rotor". *Thermophysics and Aeromechanics,* **15**(1), Mar, pp. 153–157. doi:10.1134/S0869864308010149.

[9] Sharpe, T., and Proven, G., 2010. "Crossflex: Concept and early development of a true building integrated wind turbine". *Energy and Buildings,* **42**(12), pp. 2365 – 2375. doi:10.1016/j.enbuild.2010.07.032.

[10] Mohamed, M., Janiga, G., Pap, E., and Thevenin, D., 2011. "Optimal blade shape of a modified savonius turbine using an obstacle shielding the returning blade". *Energy Conversion and Management,* **52**(1), pp. 236 – 242. doi:10.1016/j.enconman.2010.06.070.

[11] Mueller, G., Jentsch, M. F., and Stoddart, E., 2009. "Vertical axis resistance type wind turbines for use in buildings". *Renewable Energy,* **34**(5), pp. 1407 – 1412. doi:10.1016/j.renene.2008.10.008.

[12] Zanarini, A., 2012. *Analisi cinetostatica grafica di meccanismi piani. Applicazioni per la Meccanica delle Macchine*. Societá Editrice Esculapio, Bologna, Italy. ISBN - 978-88-7488-545-9.

[13] Kiwata, T., Kita, T., Yamada, T., Takata, S., Komatsu, N., and Kimura, S., 2008. "Performance of vertical axis wind turbine with variable-pitch straight blades by a linkage mechanism". *Transactions of the Japan Society of Mechanical Engineers Series B,* **74**(748), pp. 2543–2551. doi:10.1299/kikaib.74.2543.

[14] Catania, G., and Zanarini, A., 2003. "Dynamic contribution of tires in vehicle suspension modeling: An experimental approach". In Proceedings of the ASME International Mechanical Engineering Congress and Exposition, Washington, DC, USA, November 1521, 2003, Design Engineering, Volumes 1 and 2, ASME, pp. 1–8. doi:10.1115/IMECE2003-41255.

[15] Zanarini, A., and Catania, G., 2004. "Evaluation of spatial mechanism eigenproperties with respect to kinematical configuration". In Proceedings of the 5éme Conférence Internationale Méthodes de Surveillance et Techniques de Diagnostic Acoustiques et Vibratoires, October 11-13 2004, Senlis (France), CETIM, pp. 1–10. https://www.researchgate.net/publication/266896167_-Evaluation_of_spatial_mechanism_eigenproperties_with_respect_to_kinematical_configuration.

[16] Zanarini, A., 2008. "Kinematics-based variability of the dynamic behaviour in spatial mechanisms". In Proceedings of the ISMA2008 Conference, September 15-17, Leuven (Belgium), P. Sas, ed., KUL, pp. 2175–2190. Multi-body dynamics and control, Paper 327, doi:10.13140/RG.2.1.2666.5048.

[17] Zanarini, A., and Brugnoni, E., 2012. "Frequency analysis of a motorbike under motion conditions". In Proceedings of the ISMA2012-USD2012 Conferences, Leuven, Belgium, 2012 September, Sas and Moens, eds., Vol. Multy-body dynamics and control, KUL, pp. 2291–2306. doi:10.13140/RG.2.1.2404.3608, https://www.isma-isaac.be/past/conf/isma2012/proceedings/papers/isma2012_0456.pdf.

[18] Zanarini, A., and Brugnoni, E., 2013. "A time-varying dynamic problem for the frequency analysis of an off-road motorcycle". In Proceedings of the Sesta giornata di studio Ettore Funaioli, July 2012, Bologna (Italy), pp. 351–376. doi:10.6092/unibo/amsacta/3715.

[19] Catania, G., and Zanarini, A., July 2017. "A meshless approach in flexible multibody system modelling". In Proceedings of the Decima giornata di studio Ettore Funaioli, July 15th 2016, Bologna (Italy), pp. 175–196. doi:10.6092/unibo/amsacta/5600.

[20] Catania, G., and Zanarini, A., July 2018. "On the effects of flexibility in a quick return planar mechanism". In Proceedings of the Undicesima giornata di studio Ettore Funaioli 21 luglio 2017 - Bologna, Italy. doi:10.6092/unibo/amsacta/5963.

[21] Catania, G., and Zanarini, A., 2019. "Flexible multibody system dynamics by means of a spectral based meshless approach". *Advances in Applied Mathematics and Mechanics*. Accepted in November 2018, in press for August 2019, doi:10.4208/aamm.OA-2018-0053.

[22] Zanarini, A., July 2018. "About the modelling of teeth mesh flexibility in planetary gears". In Proceedings of the Undicesima giornata di studio Ettore Funaioli 21 luglio 2017, Bologna, Italy. doi:10.6092/unibo/amsacta/5963.

SOMMARI

SLM OF EXTRUSION DIES WITH LIQUID NITROGEN COOLING

Riccardo Pelaccia[1], Barbara Reggiani[1], Ivan Todaro[2], Giuseppe Valli[2], Lorenzo Donati[2], Rosario Squatrito[2], Alessandro Fortunato[2], Luca Tomesani[2]

[1] *DISMI Department of Sciences and Methods for Engineering, University of Modena and Reggio Emilia, Via Amendola 2, 42122, Reggio Emilia, Italy.*

[2] *DIN Department of Industrial Engineering – University of Bologna, Viale Risorgimento 2, 40136, Bologna, Italy.*

Keywords: *additive manufacturing, extrusion, cooling, conformal, nitrogen*

EXTENDED ABSTRACT

Temperature control during aluminium extrusion is a mandatory activity in order to produce defect-free profiles and to optimize process productivity [1]. During the extrusion process, the profile exit temperature increases due to amount of work spent to overcome friction and to plastically deform the workpiece that is converted to heat. In addition, if the ram speed or the extrusion ratio increase, the temperature further raises leading to detrimental surface defects such as hot cracks [1]. The main advantages of dissipate the excessive generated heat in the die and at the end of the forming zone are related to the possibility of increasing only slightly the extrusion force and to reduce the conduction path from the forming zone to the cooling source. In addition, it is possible to cool critical die areas directly by sizing and positioning cooling channels or cooling nozzles adequately to prevent hot cracking [1]. However, the manufacturing of conformal cooling channels close to the main forming zone by means of conventional machining is a difficult task for profiles and dies with highly complex geometries. Thus, the use of additive manufacturing technologies is a promising approach to allow a conformal cooling [1-2]. The chromium hot-work tool steels are the most widely selected materials for forging, die-casting and extrusion dies applications because of their high thermo-mechanical strength, fatigue strength, toughness and relative low cost [2]. Nowadays, thanks to the selective laser melting (SLM) technology, it is possible to produce structures with 99% density [2]. Since, to date, the additive manufacturing processes are often accompanied with higher manufacturing time and costs than conventional subtractive methods, a new concept for a hybrid extrusion die is presented [1-2].

In the present work, a multi-die is proposed in which the expensive AM part, the insert with conformal cooling channels, is integrated into a conventional machined steel housing. A profile produced with a short die lifetime and critical issues on thermal field has been identified and selected consisting in a round bar of 10mm diameter made by AA6060. A helicoidally channel has been designed to obtain a localized cooling with liquid nitrogen in the bearings, where the most critical temperatures are reached. Helix pitch and channel diameter had to be the best trade-off among liquid nitrogen flow capability, nitrogen inlet and outlet channels position, thermocouple hole position, mechanical stability of the insert and actual production possibility via additive manufacturing process. To this aim, as preliminary phase of the work, several insert designs have been investigated. The final design was provided with a toroidal channel and eight radial nitrogen outlets in the profile exit zone.

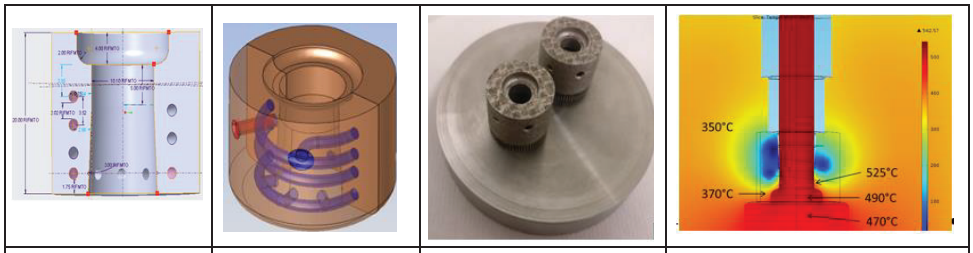

a)	b)	c)	d)

Figure 1. a-c) SLM Insert: from designs to manufacturing;
d) temperatures in extrusion with nitrogen cooling.

This allowed to obtain an inert gas covered zone where the profile flowing from the die reaches the highest temperature, thus avoiding profile oxidation. Finally, two AM inserts in H13 steel have been manufactured with SLM technology with different cooling channels diameters, 1.5 and 3 mm.

In addition to the experimental SLM manufacturing of the inserts, numerical investigation of extrusion with and without nitrogen liquid cooling have been performed [2-3]. An Eulerian approach to the extrusion problem (already deformed billet) and 1D cooling channel modeling were used. An extrusion speed of 5 mm/s was set in the FE model with a 200 mm long billet pre-heated at 480 °C. The ram, the container and the die initial temperatures were fixed equal to 480 °C, 400 °C and 490 °C respectively. As results, a peak extrusion load of 2.15 MN was obtained, fully in line with the typical values of an extrusion process, with an exit profile temperature of 550 °C. Without cooling, values in the insert were very close to those reached in the aluminium part. The numerical analysis of the cooled die was carried out with a liquid nitrogen flow rate of 1 l/min. The cooling efficiency in terms of heat removal was investigated by monitoring the temperature map and the extrusion load and by comparing the achieve results with the uncooled condition. The peak exit profile temperature dropped of a 7% with respect to the uncooled condition, thus limiting the risk of defects caused by excessive process temperatures, in addition without a significant increase in the extrusion load. Near the bearings, good results were achieved with a 26% decrease of insert temperatures.

In conclusion, the manufacturing of an extrusion dies by means of additive manufacturing technologies has been proved to allow the integration of conformal cooling channels. The benefits of cooling by liquid nitrogen have been further observed with an innovative developed numerical model, thus offering a powerful tool to optimize the process efficiency.

REFERENCES

[1] Hölker R, Jäger A, Ben Khalifa N, Tekkaya AE, 2013. “Controlling heat balance in hot aluminum extrusion by additive manufactured extrusion dies with conformal cooling channels”. Int J Precis Eng Manuf Vol. **14–8**, pp 1487–1493

[2] Klocke F., Arntz K. et al, 2017 “State-of-the-art Laser Additive Manufacturing for Hot-work Tool Steels”, Procedia CIRP **63**, pp 58–63

[3] Mazur M., Brincat P., Leary M., Brandt M., 2017 “Numerical an d experimental evaluation of a conformally cooled H13 steel injection mould manufactured with selective laser melting”, Springer-Verlag, Int J Adv Manuf Technol Vol. **93**, pp 881–900

VERIFICA SPERIMENTALE DI METODOLOGIE DI TEST TAILORING CON ECCITAZIONE STOCASTICA MONOASSIALE E MULTIASSIALE

Andrea Tosini[1], Emiliano Mucchi[1], Giorgio Dalpiaz[1]

[1]*Dipartimento di Ingegneria, Università di Ferrara, Italia*
E-mail: andrea.tosini@unife.it, emiliano.mucchi@unife.it, giorgio.dalpiaz@unife.it

Keywords: *qualifica a vibrazioni, test monoassiali, test multiassiali*

SOMMARIO ESTESO

Molte strutture e componenti meccanici durante la loro vita sono esposti a forti sollecitazioni dinamiche che possono portare a guasti dovuti, principalmente, a danneggiamento a fatica. Rientrano in questa categoria, ad esempio, i telai delle autovetture, sollecitati dalle asperità del fondo stradale, e le strutture off-shore, soggette all'azione delle onde oceaniche.

Nella pratica industriale è necessario prevedere un ragionevole time-to-failure già durante la fase di progettazione mediante, generalmente, criteri di fatica multiassiale e testare poi su prototipi la reale durata. I test dinamici eseguiti sono spesso test accelerati. Infatti, per ragioni pratiche, la durata del test deve essere più breve rispetto alla vita reale del componente; ciò si ottiene amplificando opportunamente le eccitazioni rispetto a quelle misurate in condizioni di esercizio per procurare al componente in test lo stesso danneggiamento che subirebbe durante l'intero ciclo di vita [1].

Gli standard di test attuali sono comunemente pensati per essere applicati a tavole vibranti monoassiali: la multiassialità delle eccitazioni, tipicamente sempre presente nel reale ambiente operativo, viene simulata ripetendo il test accelerato in modo sequenziale per ogni direzione cartesiana. Studi reperibili in letteratura [2] hanno messo in luce come questa procedura non solo sia dispendiosa in termini di tempo (il componente deve essere smontato e rimontato in una orientazione diversa ad ogni test) ma possa potenzialmente portare a guasti non osservabili nella reale vita operativa.

Partendo da queste considerazioni è stata messa a punto una campagna sperimentale su provini di acciaio intagliati utilizzando lo shaker triassiale presente nel laboratorio di Ingegneria dell'Università di Ferrara (Fig.1a). L'utilizzo di provini creati ad-hoc è una strategia ampiamente utilizzata nell'ambito della ricerca sperimentale, fondamentale per avere il controllo dello stato tensionale nel punto più sollecitato responsabile della propagazione del danneggiamento a fatica.

I test realizzati sono stati di due tipi: monoassiali e biassiali, con differenti livelli di eccitazione; per i test biassiali si sono considerati diversi gradi di correlazione. I test hanno permesso di verificare l'attendibilità della cosiddetta *inverse power law*, la legge di riduzione

temporale alla base di tutte le principali metodologie di test accelerati. Dal momento che tale legge deriva da considerazioni teoriche relative alla fatica monoassiale stazionaria, risulta interessante valutarne l'effettiva applicabilità anche al caso multiassiale, soprattutto in vista di un possibile sviluppo che potrebbero avere tali tecniche di test in futuro.

I test monoassiali, i più simili alle condizioni ideali per l'applicazione dell'inverse power law, hanno permesso di evidenziarne un aspetto critico legato alla non stazionarietà della tensione nel punto più sollecitato, che si verifica a seguito della propagazione della cricca. Ciò può portare a previsioni di durata sbagliate della vita effettiva del componente. Nei test effettuati l'errore fra test con tensione stazionaria e test non stazionari si è attestato attorno il 13%.

Nei test multiassiali invece, gli stessi profili di eccitazione usati per i test su singolo asse sono stati applicati simultaneamente a due direzioni ortogonali, utilizzando alto e basso livello di correlazione. I risultati ottenuti mostrano come il fattore di accelerazione dell'inverse power law (corrispondente alla pendenza della retta di Fig.1b) debba essere sostanzialmente diminuito rispetto ai corrispettivi test monoassiali. La correzione da applicare è funzione del grado di correlazione impiegato: a parità di danneggiamento, eccitazioni con bassa coerenza mostrano un fattore di accelerazione inferiore del 47% rispetto gli analoghi test con alta coerenza. La possibile spiegazione è da ricercarsi nel diverso meccanismo di propagazione della cricca, influenzato dalla variazione casuale della direzione della risultante di accelerazione.

Infine, è stato condotto anche uno studio sull'influenza dei valori RMS di accelerazione da adottare per la stima del coefficiente di accelerazione quando si progetta una campagna sperimentale su un nuovo componente. Le osservazioni hanno permesso di concludere che la migliore scelta debba ricadere su valori RMS ben separati e che la loro scelta è tanto più rilevante quanto più la correlazione fra gli assi è bassa.

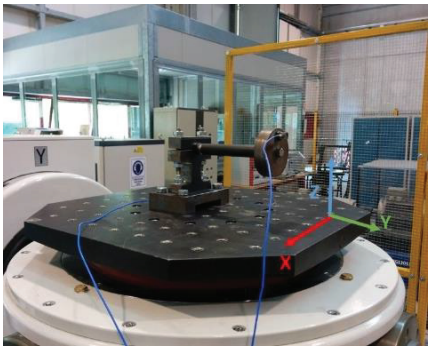

(a)

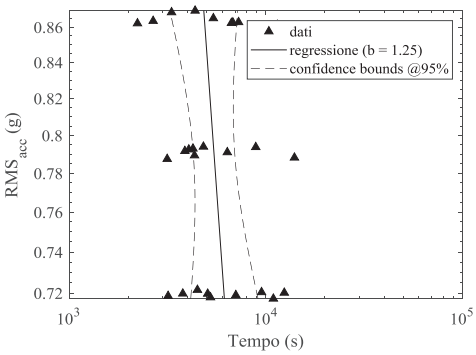

(b)

Figura 1. (a) sistema di test; (b) misure ottenute per i test multiassiali con bassa coerenza

BIBLIOGRAFIA

[1] Lalanne, C., 2014. "Mechanical vibration and shock analysis - Specification Development". *Wiley-ISTE*.

[2] Whiteman, W. E. and Berman, M. S., 2001. "Inadequacies in uniaxial stress screen vibration testing". *Journal of the IEST,* **44**(4), pp. 20–23.

TEST ACCELERATI DI QUALIFICA A VIBRAZIONE: SVILUPPO DI NUOVI SOFTWARE DI MISSION SYNTHESIS

Emanuele Pesaresi, Marco Troncossi

Dipartimento di Ingegneria Industriale, Università di Bologna, Italia
E-mail: emanuele.pesaresi2@unibo.it, marco.troncossi@unibo.it

Keywords: *Test di qualifica a vibrazione, Test Tailoring, Mission Synthesis, Fatigue Damage Spectrum, Kurtosis*

SOMMARIO ESTESO

I test di qualifica a vibrazione sono utilizzati in ambito industriale (e.g. settore automobilistico, manifatturiero, aerospaziale) per verificare, mediante l'utilizzo di tavole vibranti o shaker, l'idoneità di un componente alle sollecitazioni a cui sarà soggetto durante la sua vita attesa. In particolare per la verifica della vita a fatica di sistemi soggetti a vibrazioni meccaniche, le Norme (e.g. MIL-STD810, NATO, RTCA DO160) suggeriscono procedure che non considerano le effettive condizioni di sollecitazione dei componenti e che risultano generalmente eccessivamente severe. E' quindi comune tendenza quella di personalizzare i test in funzione delle reali vibrazioni misurate sul campo (*Test Tailoring*) anziché ricorrere agli Standard.

Nei test volti a valutare il comportamento a fatica, a fronte delle ore di vita del componente (diverse decine o centinaia), gli algoritmi implementati in alcuni software commerciali [1] permettono di eseguire prove accelerate di fatica che mirano a produrre lo stesso danno ascrivibile all'applicazione pratica ma in un tempo minore. Il danno viene solitamente stimato mediante la funzione spettrale Fatigue Damage Spectrum (*FDS*) [2], da cui viene sintetizzata la specifica del test (*Mission Synthesis*), nella forma di una Power Spectral Density (*PSD*). A partire dalla *PSD*, il controller dello shaker genera il segnale temporale del test accelerato, il quale è sempre caratterizzato da una distribuzione dei suoi valori tendente a quella Gaussiana [3, 4]. Questo tipo di distribuzione potrebbe non corrispondere a quella della vibrazione reale a cui è soggetto il componente; in tal caso, dal momento che la natura dell'eccitazione non viene preservata, risulta lecito dubitare dell'affidabilità dei test, nonostante il danno indotto dal test accelerato e dalle sollecitazioni dell'applicazione reale (stimato in termini di *FDS*) sia teoricamente lo stesso [5].

Allo scopo di rendere i test maggiormente realistici, si è diffusa in letteratura la tendenza a controllare durante i test vibratori un parametro statistico denominato kurtosis [3, 4], il quale rappresenta una efficace e sintetica metrica che descrive globalmente il contenuto di picchi di un segnale. Per segnali Gaussiani questo parametro ha il valore teorico di 3.0, per segnali in cui compaiono componenti deterministiche (segnali Sine On Random o Platicurtici) ha un valore minore, mentre per segnali in cui compaiono picchi di elevata

ampiezza (segnali Leptocurtici) dovuti ad esempio a micro-urti ha un valore maggiore. In letteratura, esistono diversi algoritmi [4-9] che permettono la sintesi di segnali aventi una *PSD* ed un kurtosis desiderati. Allo stato dell'arte, le formulazioni analitiche o procedure numeriche implementate negli algoritmi di controllo del kurtosis non considerano però la *FDS* del segnale sintetizzato, che perciò risulterà in generale diversa da quella a cui è soggetto il componente. Il lavoro di ricerca di cui si occupano gli autori è quindi volto a proporre algoritmi innovativi che riescano ad accelerare i test tramite l'equivalenza del danno (*FDS*) tra la prova accelerata e le vibrazioni reali, riuscendo contemporaneamente anche a preservare la natura del segnale per mezzo del parametro kurtosis, oltre al contenuto in frequenza (*PSD*).

Oltre al lavoro di ricerca, la collaborazione con Aziende interessate al progetto ha portato (e porterà) alla produzione di interfacce grafiche (GUI) che implementano gli algoritmi innovativi, facilmente utilizzabili dall'utente tramite settaggio di un numero relativamente ridotto di parametri. Una prima GUI prodotta ha riguardato la implementazione degli algoritmi già presenti in alcuni software commerciali, con aggiunta di migliorie dal punto di vista sia di velocità che precisione computazionale. Una seconda GUI prodotta ha reso fruibili gli algoritmi sviluppati in [6] grazie ai quali è possibile sintetizzare un segnale vibratorio controllandone il kurtosis e la *PSD*. La collaborazione con Aziende ha permesso di ottimizzare "l'usabilità" del software grazie ai feedback ricevuti dagli utilizzatori.

Altre due interfacce grafiche sono attualmente in produzione, le quali implementano algoritmi non ancora ottimizzati ma già funzionanti in ottica di aggiungere il controllo della *FDS* a quello del kurtosis per lo svolgimento di test accelerati.

BIBLIOGRAFIA

[1] Lalanne C., *Mechanical Vibration and Shock Analysis – Volume 5: Specification Development.* 2nd ed. , 2009, John Wiley & Sons, Inc – ISTE, London

[2] Lalanne C., *Mechanical Vibration and Shock Analysis – Volume 4: Fatigue Damage.* 2nd ed. , 2009, John Wiley & Sons, Inc – ISTE, London

[3] Van Baren P., "The missing knob on your random vibration controller", *Sound and Vibration*, 2005, **39**:2-7

[4] Steinwolf A., "Vibration testing of vehicle components by random excitations with increased kurtosis", *International Journal of Vehicle Noise and Vibration*, 2015, **11**(1):39-66

[5] Cornelis, A. Steinwolf, M. Troncossi, A. Rivola, Shaker testing simulation of non-Gaussian random excitations with the fatigue damage spectrum as a criterion of mission signal synthesis, *Proceedings of the 2015 International Conference on Engineering*, Liubljana, Slovenia (2015)

[6] Pesaresi E., *Leptokurtic signals in random control vibration testing*, MSc Thesis in Mechanical Engineering, University of Bologna, 2017

[7] J. Zhang,B. Cornelis,B. Peeters,K. Janssens,P. Guillaume, *A new practical and intuitive method for kurtosis control in random vibration testing,* ISMA 2016 Conference, Leuven, Belgium (2016)

[8] D.O. Smallwood, *Generating non-Gaussian vibration for testing purposes,* Sound and Vibrations, Vol.39, No. 10 (2005)

[9] J. J. Van Baren, P. Van Baren, *Kurtosion*^{tm}*-getting the kurtosis into the resonances,* SAVIAC (2007)

UNCERTAINTIES ON FATIGUE DAMAGE UNDER RANDOM LOADINGS THROUGH SPECTRAL METHODS

Julian Marcell Enzveiler Marques, Denis Benasciutti and Roberto Tovo

Department of Engineering, University of Ferrara, Italy
E-mail: nzvjnm@unife.it, bnsdns@unife.it, tvr@unife.it

Keywords: *fatigue damage, frequency-domain approach, Power Spectral Density, single-moment method*

EXTENDED ABSTRACT

Engineering components are usually subjected, in service, to random stress time-histories over time. Noteworthy examples are vehicles excited by road irregularity or engine vibrations, structures subjected to wave or wind loadings. To assess the fatigue damage and component service life, two different approaches can be used. The most commonly used one is based on time-domain analysis of random stress time-histories (Rainflow counting method and Palmgren-Miner rule). This method is based on well-established procedures and does not require too complex theories, however it usually needs long time-history records to achieve a reasonable confidence in the estimated statistical distribution of rainflow cycle and fatigue damage. In view of these requirements, we can adopt a so-called frequency-domain (spectral) approach, which characterizes a random loading by its Power Spectral Density (PSD) function. One of the greatest advantages of the spectral approach, compared with the time-domain analysis, is the possibility to exploit the PSD to estimate all statistical parameters characterizing a random loading (e.g. variance, number of peaks and zero-crossings), and also to evaluate the expected value of fatigue damage $E(D)$ by relatively simple analytical equations. Several spectral methods are available in the literature (e.g. narrow-band approximation, TB method, single-moment method, etc.) that apply to stationary, ergodic and Gaussian random loading [1, 2].

If the PSD function is known explicitly (for example, ISO for road irregularity, Pierson–Moskowitz for waves), the estimated damage is somehow "exact". In practical situations, however, the PSD is estimated from a measured time-history record, according to some recommendations [3]; it is then affected by a statistical uncertainty quantified through a confidence interval. The uncertainty in the estimated PSD turns out an uncertainty in the expected damage estimate. Also a variance σ_D of the damage around its expected value $E(D)$ has to be taken into account [4].

The aim of this work is to investigate the effect of the above-mentioned uncertainties on the fatigue damage estimated by a frequency-domain approach. To evaluate the confidence limit on fatigue damage, numerical test cases are performed, in which the statistical parameters of simulated random loading are fully controlled by specifying a "target" PSD function, Fig. 1. To this end, the use of simulated signals proves to be more advantageous than real signals, for which the "true" PSD is not known *a priori* and it can only be estimated from measurements.

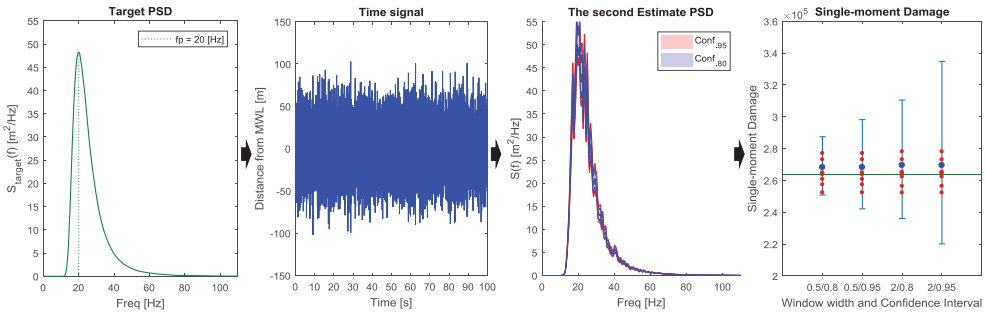

Figure 1. Analysis steps from "target" PSD to confidence band of fatigue damage.

In simulations, the "target" PSD is a Pierson–Moskowitz spectrum for sea wave loads. The target PSD is used for simulating stationary Gaussian random signals, which are then used for estimating back the PSD in two analysis steps: first using the narrowest filter to identify the relevant peaks in the spectrum, second using a broader filter in order to improve the frequency resolution in the estimated PSD. This approach is recommended by Morrow, while Lalanne suggests the threshold of statistical error and filter [4, 5]. The PSD estimation is performed by Welch's method with Hanning window and 75% overlapping, which guarantees a constant weighting on a broad part of the window [4]. Both 80% and 95% confidence levels are calculated on the estimated PSD. The single-moment method is used to estimate the fatigue damage from the average estimated PSD, as well as from upper/lower confidence limits. A confidence band for the fatigue damage is then constructed and compared to the exact value calculated from the "target" PSD.

The preliminary results show that the "target" damage always falls within the confidence band, which makes the proposed procedure very promising. It is noted that the higher is the level of confidence, the larger is the range of the damage interval. On the other hand, a longer time-history record provides more reliable results, closer to the "target" PSD. This study tries to assess the level of uncertainty associated with the damage estimate that, which comes from the uncertainty in the PSD estimate. This result could be useful when designing structures undergoing random loading. As a future perspective, this study will prove useful in processing measured signals, for which the "target" PSD is not known in advance and only its estimate is available.

REFERENCES

[1] Benasciutti, D., and Tovo, R., 2018. "Frequency-based analysis of random fatigue loads Models, hypotheses, reality". *Materialwiss. Werkstofftech.,* **49**(3), March, pp. 345–367.

[2] Larsen, C.E., and Lutes, L.D., 1991. "Predicting the fatigue life of offshore structures by the single-moment spectral method", *Probab. Eng. Mech.,* 6, June, pp. 96–108

[3] Lalanne, C., 2014. Random Vibrations Mechanical Vibration and Shock Analysis Random Vibration, 3rd ed., Vol. 3, John Wiley & Sons Inc.

[4] Crandall, S., and Mark, W., 1963. Random Vibrations in Mechanical Systems, Massachusetts Institute of Technology, Academic Press Inc.

[5] Morrow, C., 1958. "Averaging time and data-reduction time for random vibration spectra". *The Journal of Acoustical Society of America*; I - 30(5), pp. 456–461, II – 30(6), pp. 572–578.

MODELLO DI UN SEGNALE DI GUASTO SU CUSCINETTI IN AZIONAMENTI A CARRELLI INDIPENDENTI

Jacopo Cavalaglio Camargo Molano[1], Marco Cocconcelli[1], Riccardo Rubini[1], Massimo Gibertini[1]

[1]Dipartimento di Scienze e Metodi dell'Ingegneria, Università di Modena e Reggio Emilia, Italia
E-mail: jacopo.cavalagliocamargomolano@unimore.it, marco.cocconcelli@unimore.it, riccardo.rubini@unimore.it, massimo.gibertini@gmail.com

Keywords: *modello di segnale, diagnostica, cuscinetti volventi, carrelli indipendenti*

SOMMARIO ESTESO

Una delle tecnologie più promettenti nell'industria è senza dubbio il sistema di trasporto a carrelli indipendenti, che può sostituire i motori a induzione e le catene cinematiche in diverse applicazioni, soprattutto nel campo delle macchine per il confezionamento automatico [1]. Il sistema di trasporto a carrelli indipendenti è costituito da diverse unità mobili in moto su di un circuito chiuso, e ognuno delle unità può muoversi liberamente rispetto alle altre. Ogni carrello è costituito da un motore lineare a induzione, in cui i magneti si trovano sui carrelli mobili insieme a un dispositivo per la retroazione (ad esempio un sensore Hall per tenere traccia della posizione), mentre gli avvolgimenti e gli azionamenti sono posti sul telaio. Il sistema di controllo aziona ciascun carrello in modo indipendente in base al profilo di movimento caricato. I carrelli sono collegati al telaio attraverso una serie di rulli, i cui cuscinetti sono soggetti ad usura. In questo articolo si è sviluppato un algoritmo per la simulazione del segnale di vibrazione atteso in condizioni di danneggiamento dei carrelli indipendenti. In particolare, in presenza di diversi tipi di danni sui cuscinetti volventi presenti.

Il modello prende in considerazione il profilo di movimento, la progettazione meccanica del carrello, la geometria del percorso, i carichi previsti e il tipo di guasto sul cuscinetto a rulli. Il modello proposto è un'estensione di precedenti lavori degli autori [2, 3], fornendone in questa sede una validazione numerica e sperimentale. In particolare, dopo una prima verifica numerica della corretta simulazione in condizioni stazionarie di funzionamento, si è svolta una validazione sperimentale del modello in condizioni non stazionarie, dimostrando la validità del modello e del segnale di vibrazione restituito. In Fig. 1 si mostra il confronto tra gli spettri calcolati sperimentalmente e simulati nel caso di danno sull'anello esterno ed in presenza di slittamenti random all'interno del cuscinetto volvente. I risultati ottenuti dimostrano la validità dell'algoritmo proposto.

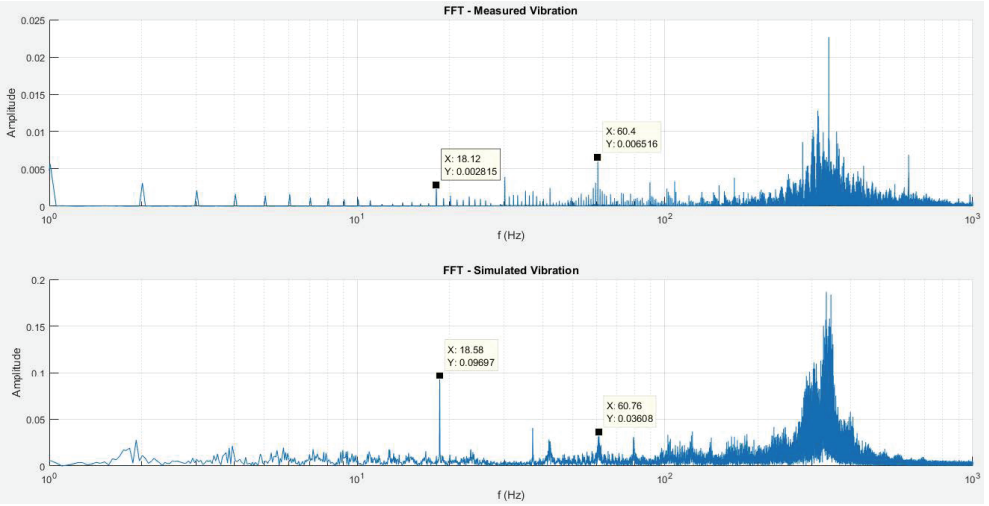

Figura 1. Spettro del segnale sperimentale e simulato, danno anello esterno, v=1500 mm/s, slittamenti random abilitati.

BIBLIOGRAFIA

[1] Cavalaglio Camargo Molano, J., Rossi, S., Cocconcelli, M., Rubini, R., 2017. "Dynamic model of an independent carts system", Adv. Ita. Mech. Sc. Mech. and Machines Sc., **47**, Springer, pp. 379-387.

[2] Cocconcelli, M., Cavalaglio Camargo Molano, J., Rubini, R., Capelli, L., and Borghi, D., 2018, "Bearing fault model for an independent cart conveyor", in Proceedings of the 6th International Conference on Condition Monitoring of Machinery in Non-Stationary Conditions, Santander, Spain, 20-22 June.

[3] D'Elia, G., Cocconcelli, M., and Mucchi, E., 2018, "An algorithm for the simulation of faulted bearings in nonstationary conditions", *Meccanica*, **53**(45), Springer, pp. 1147-1166.

ON THE DIAGNOSTICS OF TWO DEGREES OF FREEDOM PLANETARY GEARBOXES

Gianluca D'Elia[1], Giorgio Dalpiaz[1], Emiliano Mucchi[1]

[1]*Engineering Department, University of Ferrara, Italy*
E-mail: gianluca.delia@unife.it, giorgio.dalpiaz@unife.it, emiliano.mucchi@unife.it

Keywords: *planetary gearboxes, differential, diagnostics, vibrations*

EXTENDED ABSTRACT

Gearboxes are commonly used in many automotive, aerospace and industrial applications. As rotating machines, they suffer fatigue cycles in working conditions, often aggravated by non-stationary loads. Even a small failure could lead to catastrophic results, ergo condition monitoring and diagnostics procedures should be adopted in order to avoid accidents and generate cost savings. Over more than two decade, researchers focus the attention on the development of vibration based fault diagnosis methodologies that are applied on gearbox signals [1]. A plethora of advanced vibration signal processing techniques can be applied in order to extract diagnostic information in complex geared transmission [2]. Among them the class of planetary gearboxes is probably the most challenging [3]. Independently from the analysed transmission, the usual diagnostics procedure has some common points, such as: i) extraction of the specific signature of all gears and bearings, ii) evaluation of peculiar parameters on the extracted signals. Usually, the extraction of the specific gear signatures is performed by means of the well kwon time synchronous average (TSA) technique, proposed by Braun in the mid 70s [4]. However, such TSA techniques relate to gears with fixed vibration transfer paths from the source of the vibration to the transducer. With planetary gears the vibration transfer path is not fixed but it is subjected to variation. A technique for the evaluation of the TSA vibration signals associated with the sun and planet gears of a planetary gear arrangement was proposed by McFadden in the early 90s [5]. However, this technique has a main drawback related to the high signal length needed for the extraction of the planet/sun gear TSAs. An alternative method, which overcome this drawback, was proposed by Forrester in [6]. This method is based on the inclusion of a selective time filter into the signal averaging process. This filter accounts for the separation of the contribution of each planet/sun signature by time-waiting the global vibration signal.

Differential are planetary gear arrangement with two degrees of freedom, therefore the Forrester method could by adopted after angular resampling the vibration signal with the bevel drive gear which is fixed to the planet carrier. In this work, in order to reduce the analysing time of a complete geared transmission, the planetary TSA is not applied to the differential gear arrangement, but an "ordinary" TSA is used, Figure 1.

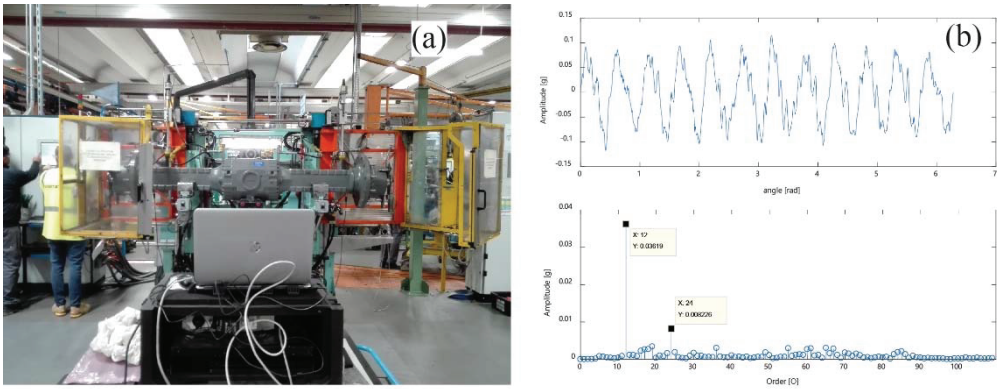

Figure 1. (a) test-rig, (b) planet TSA with corresponding spectrum

Firstly, the vibration signal is angular resampled with the relative rotation frequency of the differential planet/sun gears and then the TSA operation is performed. Via this approach, the signature of each individual differential planet gears can not be extracted, but a main signature of all the planet contribution is obtained. This global planet vibration can not answer to the question: "What is the faulted planet?". However, this global vibration conveys pivotal information of the presence of a possible fault inside one differential planet at the very least. This clue is enough for a fault diagnostics of the differential gear arrangement.

REFERENCES

[1] Lebold M., McClintic K., Campbell R., Byington C., Maynard K., 2000, "Review of Vibration Analysis Methods for Gearbox Diagnostics and Prognostics", Proceeding of the 54th Meeting of the Society for Machinery Failure Prevention Technology, Virginia Beach, VA, pp. 623-634, May 1-4.

[2] M. Buzzoni, E. Mucchi, G. D'Elia, G. Dalpiaz, 2017, "Diagnosis of Localized Faults in Multistage Gearboxes: A Vibrational Approach by Means of Automatic EMD-Based Algorithm", Shock and Vibration 2017, pp. 1-22.

[3] G. D'Elia, E. Mucchi, M. Cocconcelli, 2017, "On the identification of the angular position of gears for the diagnostics of planetary gearboxes", Mechanical Systems and Signal Processing 83, pp. 305-320.

[4] S. Braun, 1975, "The extraction of periodic waveform by time domain averaging", Acustica, Vol. 32, No. 2, pp. 69-77.

[5] P. D. McFadden, 1991, "A technique for calculating the time domain averages of the vibration of the individual planet gears and sun gear in an epicyclic gearbox", Journal of Sound and Vibration, Vol. 144, No. 1, pp. 163-172.

[6] D. Forrester, 1998, "A method for the separation of epicyclic planet gear vibration signatures", Acoustical and Vibratory Surveillance Methods and Diagnostic Techniques, Senlis, France, October.

RICONOSCIMENTO DI INFESTAZIONE DA SITOPHILUS ORYZAE TRAMITE L'ANALISI DEI SUONI RILEVATI

Luca Capelli[1], Marco Cocconcelli[1], Riccardo Rubini[1]

[1]*Dipartimento di Scienze e Metodi dell'Ingegneria, Università di Modena e Reggio Emilia, Italia*
E-mail: 31445@studenti.unimore.it, marco.cocconcelli@unimore.it, riccardo.rubini@unimore.it

Keywords: *analisi del segnale, pattern recognition, sitophilus oryzae*

SOMMARIO ESTESO

Le perdite di grano causate da infestazioni di insetti non sono trascurabili e il conseguente danno economico non può essere ignorato dalle aziende che lavorano derrate alimentari. I costi considerevoli per il contrasto di simili infestazioni possono essere ridotti solo grazie a una loro precoce identificazione. Lo *Sitophilus Oryzae* è l'insetto che viene preso in considerazione in questo lavoro in quanto rappresenta uno dei principali insetti infestanti del grano.

Gli insetti adulti sono identificabili abbastanza agevolmente setacciando il grano mentre fino a poco tempo fa è stato più difficile e più costoso identificare le larve: la femmina di *S. oryzae* depone una larva all'interno di una cariosside dopo avervi praticato un foro e si premura di richiuderlo a processo terminato, rendendo così difficile la loro identificazione [1]. Alcune aziende hanno pensato di produrre uno strumento che permette di ascoltare in cuffia anche i suoni emessi dalle larve all'interno delle cariossidi, così da poterle identificare prima che siano diventate insetti adulti e abbiano nel frattempo mangiato gran parte della cariosside che le ospitava [2].

Partendo dall'uso di questo strumento si è sviluppato un metodo di rilevamento automatizzato della presenza delle larve e degli adulti di *S. oryzae* che non richiedesse più la presenza di un operatore addetto all'ascolto dei rumori provenienti dai campioni di grano analizzati mediante l'utilizzo di cuffie e microfono.

L'algoritmo sviluppato, interpretando le registrazioni audio di segnali acquisiti da un apposito microfono, riesce a identificare la presenza di *S. oryzae* in un campione di grano e a stimare la maggiore o minore presenza di adulti rispetto alle larve.

È stata condotta una campagna sperimentale di registrazione dei suoni provenienti da un set di campioni di grano specifici, in collaborazione e presso il Laboratorio di Entomologia del Dipartimento di Scienze della Vita dell'Università di Modena e Reggio Emilia.

L'algoritmo proposto filtra il segnale in una specifica banda di frequenza determinata sperimentalmente, calcola la potenza media istantanea del segnale e la variazione del suo

valore nel tempo (Fig. 1). Per identificare la variazione di potenza del segnale causata da un morso piuttosto che da un movimento dell'insetto si è fatto riferimento a una finestra temporale mobile della durata paragonabile a quella di un morso. Per ciascuna finestratura si è valutato il valore massimo e minimo della potenza istantanea al suo interno. Variazioni superiori a 10 volte il valore minimo misurato sono state associate alla presenza di un masticamento, mentre variazioni di almeno 2.5 volte il valore minimo sono state associate al movimento dell'insetto tra un chicco di grano e l'altro, identificando la presenza di adulti.

Il software realizzato si è dimostrato capace di riconoscere l'infestazione in atto di *S. oryzae* evidenziando la contemporanea presenza insetti adulti e larve o dei soli adulti.

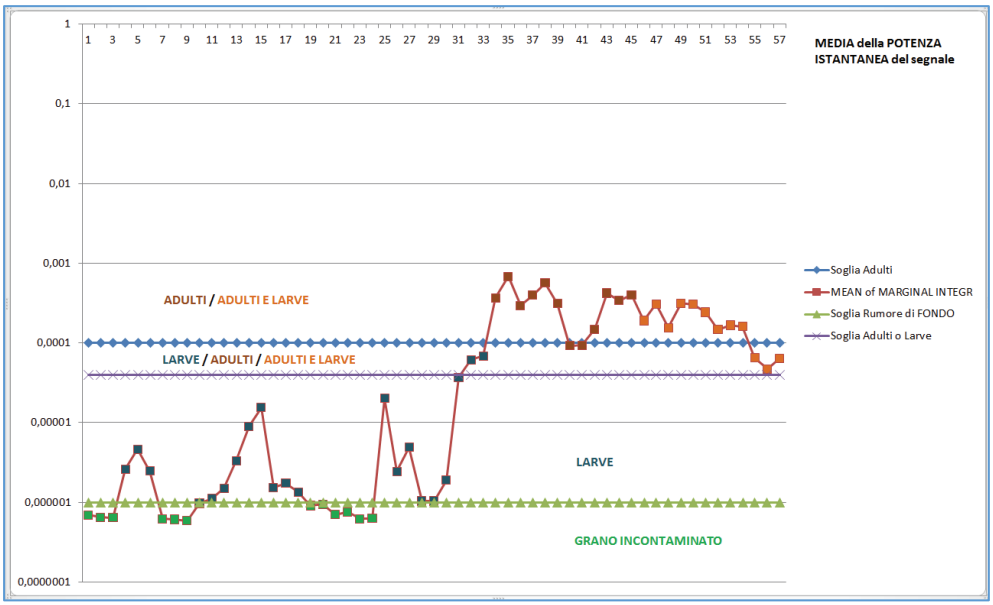

Figura 1. Soglie di potenza e potenze medie caratteristiche delle 57 registrazioni analizzate

BIBLIOGRAFIA

[1] Rees, D. P., 2007. "Insects of stored grain: a pocket reference", Collingwood: CSIRO Publishing (2 ed.).
[2] Liu, H., Lee, S.H. and Chahl, J.S., 2016. "A review of recent sensing technologies to detect invertebrates on crops". *Precision agriculture*, **18**(4), pp. 635-666.

USE OF THE PRINCIPLE OF VIRTUAL WORK TO EXPLAIN THE HUMAN JOINT MOTION: APPLICATION TO THE KNEE

Michele Conconi[1], Nicola Sancisi[1], Vincenzo Parenti-Castelli[1]

[1]*Department of Mechanical Engineering, University of Bologna, Italy*
E-mail: michele.conconi@unibo.it

Keywords: *Principle of virtual work; Reciprocity; Natural Motion; Knee*

EXTENDED ABSTRACT

The study of natural motion of human joints, i.e. the unresisted motion that the articulations exhibits in the absence of external loads, provides insights into their physiology. The natural motion represents the baseline condition upon which deformations of passive structures (i.e., ligaments and cartilage) take place when loads are applied. During natural motion, the strain energy density stored within ligaments and cartilage is minimized, reducing the chance of microdamage occurrences and the corresponding metabolic cost for tissue repairing. The study of the natural motion is thus fundamental to understand the joint physiology. In this work, the geometrical arrangement of the constraints necessary for the joint natural motion is theoretically derived from the application of the principle of virtual work. The implication of this general approach will be derived and experimentally verified for the knee.

The relative motion of the tibia and femur is constrained by knee passive structures, particularly by the anterior and posterior cruciate and the medial and lateral collateral ligaments (ACL, PCL, MCL, LCL), together with the medial and lateral articular contacts (MAC and LAC). In general, six constraints are not compatible with an unresisted motion. Despite that, it was experimentally proven that the tibio-femoral motion describes a well-defined one degree-of-freedom three-dimensional unresisted trajectory compatible with the constraints imposed by the knee passive structures [1]. For this to be possible, some specific properties must hold. A first requirement is ligament isometry. If ligament would elongate, an unresisted motion would necessary imply a perfectly statically balanced system [2]: however, this condition could be obtained only by non-physiological zero-free-length elastic elements [3]. It follows that no or negligible ligament elongation may occur during natural motion, confirming the experimentally noted isometric behaviour [4]. In the absence of variation of the elastic potential energy and considering negligible friction, the principle of virtual work (PVW) implies the reciprocity between the twist, representing the knee instantaneous helical axis (IHA) of motion, and all the resultant wrenches of passive constraints, independently from their number or type. In this condition, the wrench-to-IHA distance d_i can be expressed as:

$$d_i = \left(h_t + h_i\right)\frac{\left\|\mathbf{u}_t \cdot \mathbf{u}_i\right\|}{\sin(\beta_i)} = \frac{\left(h_t + h_i\right)}{\tan(\beta_i)}, \quad i = 1,\mathrm{K}\ ,n \tag{1}$$

where h and $\mathbf{u}$ denote the screw pitch and direction, respectively, subscripts t and i denote the IHA and the i-th wrench, and β_i the angle between the directions of the two. We hypothesized that the wrenches corresponding to the resultants of each ligament and contact constraints are pure forces, i.e. that the pitches of the screws representing these wrenches are zero. This hypothesis is supported by many studies [5-7], where parallel mechanisms capable to replicate the knee natural motion were defined by substituting ligament and contact constraints with rigid links. We also hypothesized that the work produced by the passive constraints against the translation along the IHA is negligible. This second hypothesis agrees with experimental analyses [8] and with the representation of the knee as a spherical mechanism [9]. Finally, we consider the effect of knee internal fiction negligible.

Under these hypotheses, Eq. (1) tends to zero, i.e. the line of action of all the constraint forces must intersect the knee IHA over the whole natural motion range. To verify this property, we analized 4 in-vitro and 1 in-vivo legs, computing the mean wrench to IHA distance for each of the six constraints (Tab. 1). Results can be considered as a validation of the property.

Table 1. Mean wrench-to-IHA distance over the entire range of flexion. Star denotes in-vivo exo

	Leg 1	**Leg 2**	**Leg 3**	**Leg 4**	**Leg 5***
ACL-to-IHA [mm]	1.41 ± 1.79	0.80 ± 0.68	2.02 ± 1.13	1.72 ± 1.40	4.47 ± 2.89
PCL-to-IHA [mm]	2.06 ± 1.62	1.71 ± 1.33	2.74 ± 1.82	1.41 ± 1.08	4.29 ± 2.86
MCL-to-IHA [mm]	2.85 ± 2.31	3.37 ± 2.14	2.26 ± 1.23	1.41 ± 0.08	3.62 ± 2.76
LCL-to-IHA [mm]	1.35 ± 1.26	2.15 ± 2.70	1.44 ± 0.71	1.36 ± 0.96	4.44 ± 3.31
MAC-to-IHA [mm]	1.21 ± 1.19	1.24 ± 0.79	2.02 ± 0.88	1.14 ± 0.94	3.31 ± 2.17
LAC-to-IHA [mm]	1.78 ± 1.60	1.52 ± 1.23	1.30 ± 0.91	1.37 ± 0.93	2.96 ± 1.80

REFERENCES

[1] Wilson, D., et. al., 2000, "The components of passive knee movement are coupled to flexion angle," Journal of Biomechanics, 33(4), pp.465-473.

[2] Herder, J., 2001, "Energy-free Systems. Theory, conception and design of statically balanced spring mechanisms,". PhD thesis, Delft University of Technology, Delft, The Netherlands.

[3] Deepak, S., and Ananthasuresh, G., 2012, "Perfect static balance of linkages by addition of springs but not auxiliary bodies," Journal of Mechanisms and Robotics, 4(2) DOI: 10.1115/1.4006521.

[4] Wilson, D. R., Feikes, J. D., and O'Connor, J. J., 1998, "Ligaments and articular contact guide passive knee flexion," J Biomech, 31(12), pp.1127-1136.

[5] Parenti-Castelli, V., Di Gregorio, R., 2000, "Parallel mechanisms applied to the human knee passive motion simulation". In: ARK 2000, Lenarcic, J., Stanisic, M. (Eds.), 333-344.

[6] Ottoboni, A., et al., 2010, "Articular surface approximation in equivalent spatial parallel mechanism models of the human knee joint: An experiment-based assessment," IMECHE, Part H, 224(9), pp.1121-1132.

[7] Nardini F., et al., 2016, "Definition of a subject-specific model of the knee in vivo," Gait & Posture, 49, pp.S6.

[8] Blankevoort, L., Huiskes, R., and de Lange, A., 1990, "Helical axes of passive knee joint motions," J Biomech, 23(12), pp.1219-1229.

[9] Sancisi, N., and Parenti-Castelli, V., 2010, "A 1-Dof parallel spherical wrist for the modelling of the knee passive motion," Mechanism and Machine Theory, 45(4), pp.658-665.

HIERARCHICAL MULTISCALE RESORBABLE NANOFIBROUS SCAFFOLDS FOR TENDON TISSUE REGENERATION

Alberto Sensini[1], Maria Letizia Focarete[2, 3], Chiara Gualandi[2, 3], Juri Belcari[1], Andrea Zucchelli[1], Alexander Kao[4], Gianluca Tozzi[4], Liam Boyle[5], Gwendolen Reilly[5], Luca Cristofolini[1, 3]

[1]*Department of Industrial Engineering, University of Bologna, Italy*
E-mail: luca.cristofolini@unibo.it, alberto.sensini@unibo.it

[2]*Department of Chemistry "G. Ciamician", University of Bologna, Italy*
E-mail: marialetizia.focarete@unibo.it

[3]*Health Sciences & Technologies Interdep. Center for Industrial Res., University of Bologna*

[4]*Zeiss Global Centre, School of Engineering, University of Portsmouth, UK*
E-mail: gianluca.tozzi@port.ac.uk

[5]*INSIGNEO Institute for in silico Medicine, University of Sheffield, UK*
E-mail: g.reilly@sheffield.ac.uk

Keywords: *Electrospinning, tendon tissue engineering, high-resolution x-ray tomography, cell viability.*

EXTENDED ABSTRACT

Regeneration of tendons represents nowadays an unsolved clinical problem worldwide. Resorbable electrospun nanofibrous scaffolds mimicking the morphology and mechanical properties of tendon fascicles were developed in a previous study [1].

The aims of the study were: (i) to develop a hierarchical multiscale nanofibrous electrospun scaffolds mimicking the morphology and the biomechanical properties of tendons; (ii) to characterize their structure from the morphological and mechanical point of view; (iii) to evaluate its cell viability.

Electrospun bundles of aligned nanofibers of poly-L-lactic acid (PLLA) were produced by wrapping electrospun mats on a drum collector [1]. To produce the hierarchical multiscale tendon-like scaffold 100 bundles of 100 mm length were aligned together. An "epitenon-like" sheath of PLLA was electrospun on the bundles to group and compact them together. The morphology of the multiscale scaffolds was evaluated with scanning electron microscopy (SEM) and high-resolution x-rays computed tomography (XCT). The orientation of the nanofibers was assessed following a validated XCT-based protocol [2]. Different voxel sizes of the XCT scans were chosen to permit a multiscale approach to the

investigation (0.4 micrometers for the bundles, and 8.5-20 micrometers for the multiscale scaffolds). The mechanical properties of both single bundles and hierarchical multiscale scaffolds were tested with a monotonic ramp to failure. In order to reproduce physiological scenarios of failure, physiological strain rates were used (33%/sec. for the single bundles and 100%/sec. for the hierarchical multiscale scaffolds). Cell infiltration was evaluated with human fibroblasts and the scaffolds evaluated with a histological investigation.

The nanofibers and the bundles showed diameters in the range of the collagen fibrils and fascicles in the human tendon [3]. The SEM and XCT images showed that the nanofibers were aligned within the bundles in a physiological way. The sheath was homogeneous, and the bundles were compactly assembled. The XCT and SEM investigation confirmed also a morphology and hierarchical structure of both the single bundles and the hierarchical multiscale scaffolds similar to the human fascicles and tendons [3]. The single bundles and the hierarchical multiscale scaffolds showed a ductile behaviour with mechanical properties in the range of human tendons [3, 4]. Cells successfully infiltrated into the scaffolds and proliferated inside them in a physiological way.

The promising results for the produced hierarchical multiscale electrospun scaffold of PLLA confirm the potential of the production process developed in this study, able to produce high-fidelity scaffolds for regeneration and replacement of tendon tissue.

REFERENCES

[1] Sensini A., Gualandi C., Cristofolini L., Tozzi G., Dicarlo M., Teti G., Mattioli-Belmonte M. and Focarete M. L., 2017, ”Biofabrication of bundles of poly(lactic acid)-collagen blends mimicking the fascicles of the human Achille tendon”, *Biofabrication:* ***9***(1), pp. 1–13.

[2] Sensini A., Cristofolini L., Focarete M. L., Belcari J., Zucchelli A., Kao A. and Tozzi G., 2018, “High-resolution x-ray tomographic morphological characterisation of electrospun nanofibrous bundles for tendon and ligament regeneration and replacement”, *Journal of Microscopy*: 00(0), pp. 1-11

[3] Goh K. L., Bechet D. M.," Hierarchical Mechanics of Connective Tissues: Integrating Insights from Nano to Macroscopic Studies", 2014, *Journal Biomedical Nanotechnology*:**10**(10), pp. 2464–2507

[4] Murphy W., Black J., 2016, "Handbook of Biomaterial Properties", *Springer*, New York.

BODY ANTHROPOMETRY AND LOCAL BONE MICROARCHITECTURE MAY IMPROVE DETERMINING HIP FRACTURE RISK BEYOND DXA

Marco Palanca[1], Saulo Martelli[2], Egon Perilli[2], Luca Cristofolini[1]

[1]*Dept of Industrial Engineering, Alma Mater Studiorum - University of Bologna, Italy*
E-mail: marco.palanca2@unibo.it, luca.cristofolini@unibo.it

[2]*Medical Device Research Institute, Flinders University, SA, Australia*
E-mail: saulo.martelli@flinders.edu.au, egon.perilli@flinders.edu.au

Keywords: *fracture mechanics, femur, microCT, sideways fall, drop tower*

EXTENDED ABSTRACT

The common clinical method for predicting the hip fracture risk is based on Dual-energy X-Ray Absorptiometry (DXA) planar measurements of Bone Mineral Density (BMD, T-score) averaged over large femoral regions (neck, trochanteric, inter-trochanteric and Ward's triangle) and has poor sensitivity and specificity. However, fracture onset is determined by the local tissue properties and the dynamic load caused by the fall, which in turn is determined by the body mass, the speed at touchdown and the energy absorbed by the tissues surrounding the femur [1]. Aims: to reproduce a sideways fall scenario *in vitro* and to compare 1) femoral fracture outcomes with fracture risk predictions using the T-score 2) and a combination of clinical-level Computed-Tomography (CT) measurements of BMD and body anthropometric (BA) parameters.

Seven femurs (T-score range: -3.59, 0.77) were collected (Table 1). Micro-computed tomography (micro-CT) images (29 µm voxel size) were acquired at the Australian Synchrotron (Clayton VIC, Australia) [2] and clinical-CT (0.7 mm pixel size) were performed. To reproduce a realistic sideways fall, a drop-tower was used: femurs were placed with 10° of abduction and 15° of internal rotation and loaded on the greater-trochanter. Patient-specific energy loading conditions, based on donor BA (weight, height and soft-tissue thickness) were defined for each specimen [3].

Table 1. Comparison of fracture risk estimate based on DXA (if T-score < 2.5 indicated as "Y", otherwise "N"), CT BMD and BA, and experimentally observed fractures (N: non-fractured; Y: fractured).

Specimen	#1	#2	#3	#4	#5	#6	#7
DXA T-score prediction	N	N	N	Y	Y	Y	Y
CT BMD+BA prediction	N	Y	N	Y	Y	Y	N
Fracture experiment	Y	Y	N	Y	Y	Y	N

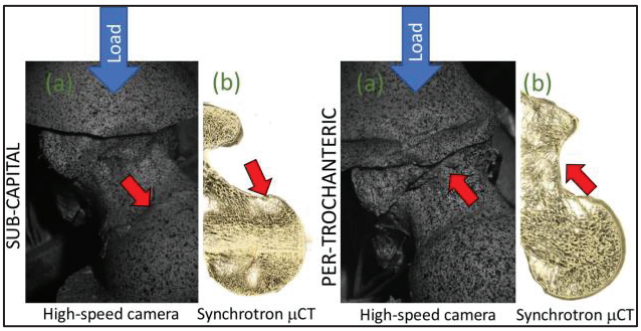

Figure 1. Different failure patterns: sub-capital (left) and per-trochanteric (right). Images of the specimens acquired with high-speed camera during the tests ((a) for both specimens) and synchrotron micro-CT images of the intact bone (b). Red arrows: failure point; blue arrow: direction of applied load.

During the impact, images of the femoral neck were video-recorded with two high-speed cameras (15,000 Hz, Vision research, Phantom UHS-12). Specimens were categorized in high- and low-risk of fracture, based on: 1) DXA-based diagnosis of osteoporosis (T-score < -2.5 meaning high risk); and 2) fracture predictions based on clinical-CT estimates of BMD through an established finite-element procedure [4] and impact loads determined by:

$$F = M*v/t; \tag{1}$$

where M is the body mass, v is the speed at touchdown and t is the impact duration [3]. Predictions and fracture test outcomes were compared. Fracture onset location, determined from the high-speed images, was compared with the local internal bone micro-architecture in the micro-CT images.

Four out of 7 specimens (#3, #4, #5, #6) showed either a fracture or no-fracture, in agreement with the DXA-based predictions. However, two specimens identified as non-osteoporotic (#1, #2) did actually fracture, whereas one osteoporotic specimen (#7) did not fracture (Table 1). CT-based BMD and BA correctly predicted six out of 7 specimens.

The femurs showed two different failure patterns: sub-capital and per-trochanteric (Fig. 1). The observed microstructure of the trabecular bone suggested that failure onset might be linked to the local trabecular bone architecture.

The clinical classification of osteoporosis (DXA T-score <-2.5) only partially predicted the actual femoral fracture observed in a simulated sideways fall (4 out of 7). Predictions based on CT BMD combined with body anthropometry gave a better prediction (6 correct out of 7). Body anthropometry and bone microstructure may play a fundamental role [4] in identifying the risk of femoral fracture while falling on a side.

REFERENCES

[1] Robinovitch et al., JOR, 13: 956-962, 1995.
[2] Martelli, Perilli, *JMBBM*, 84: 265-272, 2018.
[3] Van der Kroonenberg, *JBE*, 117(3): 309-19, 1995.
[4] Schileo et al., *J Biomech*, 47: 3531-38, 2014

LABORATORIO DI FORMAZIONE E RICERCA *TAILOR*: TECHNOLOGY AND AUTOMATION FOR INDUSTRY LABORATORY

Ivo Campione, Jessica Rossi, Augusto Bianchini, Giangiacomo Minak, Marco Troncossi

Dipartimento di Ingegneria Industriale, Università di Bologna
E-mail: ivo.campione@unibo.it, jessica.rossi12@unibo.it, giangiacomo.minak@unibo.it, augusto.bianchini@unibo.it, marco.troncossi@unibo.it

Keywords: *Industria 4.0, Automazione, Robotica, Manutenzione predittiva, Additive manufacturing*

SOMMARIO ESTESO

Nel quadro industriale attuale, la spinta verso sistemi altamente automatizzati, flessibili e modulari è sempre più pervasiva e tesa a garantire lo sviluppo tecnologico e la competitività industriale delle Imprese. In questo scenario, caratterizzato da una forte dinamicità e ricerca dell'innovazione, si riporta la recente attivazione del laboratorio *TAILOR* (Technology and Automation for Industry LabORatory), risultato della collaborazione pluriennale tra il Dipartimento *DIN* dell'*Università di Bologna* e l'Azienda *Siropack Italia* (Cesenatico, FC). Per sostenere la sinergia tra Università e Impresa, Siropack Italia ha riservato al *DIN* uno spazio di 300 m^2 all'interno del proprio stabilimento, in cui svolgere attività di ricerca congiunta, percorsi di alta formazione e avviare partnership a livello nazionale e internazionale. Il laboratorio *TAILOR* offre gli strumenti necessari per supportare ed accelerare l'innovazione, quali: (i) coinvolgimento di docenti e giovani ricercatori dell'Università di Bologna a supporto della ricerca avanzata di tecnologie innovative; (ii) immediato trasferimento tecnologico, produzione ed applicazione di soluzioni ad alto livello nell'ambito aziendale tramite il coinvolgimento diretto delle Imprese. Obiettivo primario e fondamentale di *TAILOR* è il supporto alla formazione di figure professionali su diversi livelli: studenti di Ingegneria attraverso l'esperienza pratica in laboratorio; inserimento di tirocinanti e tesisti nel contesto industriale; attività di ricerca di alta qualificazione per dottorandi; sviluppo di competenze avanzate per lavoratori. L'esperienza attiva in un laboratorio integra la formazione universitaria e facilita l'acquisizione di competenze mirate all'inserimento nel mondo industriale. Da questa vocazione deriva il nome *TAILOR*, che richiama l'idea di laboratorio come luogo in cui l'esperienza pratica consente l'insegnamento di un mestiere, valorizzandone consapevolezza e responsabilità. La collaborazione, definita da un accordo quadro siglato a Settembre 2017, include attività di ricerca multidisciplinare, attualmente svolte da 2 dottorandi e 3 docenti attivi nei settori di Meccanica Applicata alle Macchine, Impianti Industriali Meccanici, e Progettazione Meccanica e Costruzione di Macchine.

Nel breve termine, la ricerca è focalizzata sullo sviluppo dell'automazione in ambito meccanico. Una delle tematiche trattate comprende la definizione di strategie di controllo

per robot industriali e collaborativi, ovvero robot progettati per poter operare in collaborazione con l'uomo. Essi permettono di combinare la forza, la precisione e la ripetibilità dei robot tradizionali con le capacità cognitive proprie degli esseri umani [1]. Queste strategie saranno testate su un'isola robotizzata appositamente progettata e dotata di due robot, un antropomorfo ed uno SCARA, messi a disposizione a titolo gratuito (assieme ad altri componenti elettrici) da *Mitsubishi Electric*. La cella, attualmente in fase di allestimento, sarà dotata anche di vari dispositivi di visione, sia fissi che solidali ai robot, e che saranno utilizzati per l'implementazione di sistemi di controllo *vision-based* [2]. L'utilizzo di sistemi di visione ha una serie di vantaggi, tra cui la possibilità di definire strategie operative nel caso di situazioni in cui si debba garantire il riconoscimento e tracciabilità dei prodotti, esigenza industriale piuttosto sentita.

Un'altra attività di ricerca riguarderà l'allungamento del ciclo di vita dei prodotti attraverso manutenzione su condizione e predittiva. Queste strategie di manutenzione si basano sul monitoraggio continuo di parametri significativi dello stato del sistema, attraverso l'applicazione di sensori innovativi ed interconnessi. Conoscere la condizione dei componenti consente di identificare in tempo reale i danneggiamenti, intervenendo solo quando necessario e poco prima della rottura. Inoltre, un'approfondita analisi dei segnali acquisiti permette di determinare le cause del problema e stimare la vita residua dei componenti [3]. Una corretta manutenzione, oltre a preservare sicurezza ed evitare ritardi e perdite di produzione, consente l'ottimizzazione e l'estensione della vita dei prodotti, e fornisce supporto per la decisione di sostituire vecchie attrezzature con nuove tipologie più sostenibili. Ciò è alla base dell'*economia circolare*, che si propone come nuovo modello di business capace di portare benefici ambientali, economici e sociali [4].

Altre attività di ricerca, svolte all'interno di *TAILOR*, riguarderanno la progettazione e la prototipazione di meccanismi e servoazionamenti ad elevate prestazioni, cui seguirà la sperimentazione sui banchi prova forniti (a titolo gratuito) da *SMC*, *FESTO* e *Pneumax*. Inoltre il laboratorio sarà fornito di una stampante 3D, per valutare l'inserimento nel processo produttivo di tecniche e di sistemi di prototipazione rapida, che permettono una serie di vantaggi nello sviluppo di nuovi componenti. La gestione ed il controllo di componenti, macchine ed impianti sarà effettuata con software MES (Manufacturing Execution System) di ultima generazione, fornito da *Mitsubishi Electric*.

BIBLIOGRAFIA

[1] Colgate J., Wannasuphoprasit W., Peshkin M.A., 1996. "Cobots: robots for collaboration with human Operators". *Proceedings of the international mechanical engineering congress and exhibition,* 58, pp.433–439.

[2] Malis E., 2002. "Survey of vision-based robot control", INRIA, Sophia Antipolis, France.

[3] Shin J.H., Jun H.B., 2015. "On condition based maintenance policy", *Journal of Computational Design and Engineering*, 2, pp. 119-127.

[4] Chilamkurti N., Torabi T. and Elhdad R., 2014. "Ontology-based framework for maintenance activity analysis". *International Journal Systems Assurance Engineering Management*, 5(1), pp. 84-98.

TRIANGOLI E QUADRILATERI PIEGHEVOLI

Alessandro Rivola[1], Nicola Golfari[2]

[1]*Dipartimento di Ingegneria Industriale, Università di Bologna*
E-mail: alessandro.rivola@unibo.it

[2]*Architetto, via Vigna 3, Milano, Italia*
E-mail: ngolfari@gmail.com

Keywords: quadrilatero articolato, *Grashof*, *folding linkages*.

SOMMARIO ESTESO

La presente nota riguarda la possibilità di realizzare dei quadrilateri articolati piani pieghevoli (*folding*) a partire da una catena cinematica chiusa *RRR*, ossia da una catena cinematica senza mobilità formata da tre membri binari e tre coppie rotoidali.

Seguendo la formulazione di *Grashof* [1], in [2] si dimostra che un quadrilatero articolato può assumere una configurazione in cui tutti i membri sono allineati (cioè è *folding*) se e solo se è soddisfatta la condizione limite del criterio di *Grashof*, ossia se vale la:

$$s + l = p + q \tag{1}$$

in cui s indica la lunghezza del membro più corto, l quella del membro più lungo e p e q le lunghezze intermedie. La configurazione in cui tutti i membri del mecca-nismo si allineano viene denominata *change point* e il meccanismo è definito *change-point mechanism* [1–3], o appartenente alla categoria dei *folding linkages* (meccanismi "pieghevoli") [4, 5].

Si consideri ora una catena cinematica chiusa costituita da tre membri binari e tre coppie rotoidali, ossia una catena cinematica triangolare, e si voglia determinare in quale punto di ogni lato del triangolo si debba collocare l'asse di una quarta coppia rotoidale in modo da ottenere un quadrilatero articolato *folding*.

Si può dimostrare che una soluzione del problema è costituita dai tre punti di tangenza (T_a, T_b, T_c) dei tre lati con la circonferenza inscritta nel triangolo, vedi Figura 1(a). In altri termini, se si colloca l'asse della quarta coppia rotoidale in uno qualunque dei punti di tangenza T e si assume come telaio del quadrilatero ar-ticolato un'asta qualsiasi, si ottiene sempre un quadrilatero *folding*. Nel quadrilatero ottenuto il lato più corto è sempre opposto al lato più lungo e al *change point* si avrà sovrapposizione, secondo la terminologia di *Grashof*, nelle due coppie di aste adiacenti (s, p) e (l, q).

Una ulteriore soluzione è inoltre costituita dai tre punti (P_a, P_b, P_c) di Figura 1(b), che non sono altro che i punti di tangenza dei lati del triangolo con le rispettive

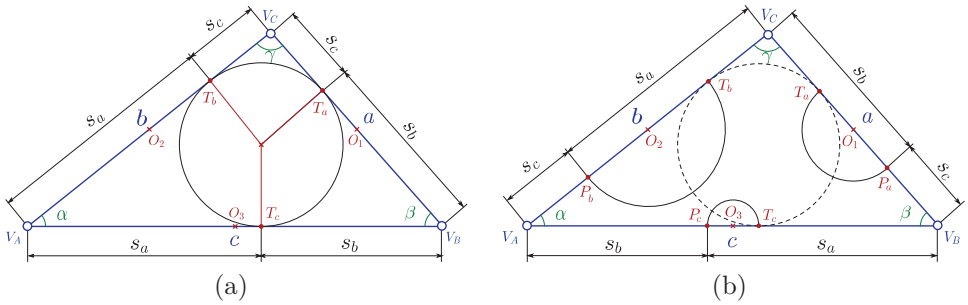

Figura 1. Catena RRR: le posizioni in cui collocare la quarta coppia rotoidale per ottenere un quadrilatero *folding* sono i tre punti di tangenza (T_a, T_b, T_c) dei tre lati con la circonferenza inscritta nel triangolo, oppure i tre punti (P_a, P_b, P_c) di tangenza dei lati del triangolo con le rispettive circonferenze exscritte.

circonferenze exscritte. In altre parole, se si colloca l'asse della quarta coppia rotoidale in uno qualunque dei punti P e si assume come telaio del quadrilatero articolato un'asta qualsiasi, si ottiene sempre un quadrilatero *folding*. In tale quadrilatero il lato più corto è sempre adiacente al lato più lungo, e al *change point* si avrà distensione nelle due coppie di aste adiacenti (s, l) e (p, q).

Se si esaminano tutti i casi in cui si può collocare la quarta coppia rotoidale in uno dei punti di tangenza T o P , a seconda del membro che viene assunto a telaio si distingueranno 24 situazioni (4 per ciascuno dei 6 punti di tangenza).

Nel caso più generale in cui il triangolo di partenza non sia né isoscele né equilatero, se tra i 24 casi si eliminano quelli ripetuti restano 12 diversi quadrilateri *folding*, ciascuno dei quali può assumere una sola configurazione *change point*. Si può facilmente verificare che si tratta di 12 casi tra i 19 menzionati in [5], cioè dei 12 quadrilateri *folding* in grado di assumere una sola configurazione *change point*, cioè quelli che differiscono dai 7 che comprendono il parallelogramma articolato (con 2 casi), il *Kite* (con 4 casi) o il rombo (un solo caso), tutti e 7 in grado di assumere più di una configurazione *change point*.

BIBLIOGRAFIA

[1] Grashof, F., 1890. *Theoretische maschinenlehre*, Vol. 3. Verlag Von Leopold Voss, Hamburg und Leipzig.

[2] Paul, B., 1979. "A reassessment of Grashof's criterion". *Journal of Mechanical Design,* **101**(3), pp. 515–518.

[3] Hartenberg, R. S., and Denavit, J., 1964. *Kinematic synthesis of linkages*. McGraw-Hill, New York, pp. 75–78.

[4] Murray, A., and Larochelle, P., 1998. "A classification scheme for planar 4R, spherical 4R, and spatial RCCC linkages to facilitate computer animation". *ASME Paper No. DETC98/MECH-5887*.

[5] McCarthy, J. M., and Soh, G. S., 2010. *Geometric design of linkages*, 2nd ed., Vol. 11. Springer Science & Business Media.

DYNAMICALLY FEASIBLE TRAJECTORIES FOR A DELTA-LIKE CABLE-SUSPENDED ROBOT

Giovanni Mottola, Marco Carricato

Department of Industrial Engineering, University of Bologna, Italy
E-mail: giovanni.mottola3@unibo.it, marco.carricato@unibo.it

Keywords: *Dynamics of cable-suspended robots, singularity analysis, cable interfer-ence, translational motion, parallelograms*

EXTENDED ABSTRACT

Cable-driven parallel robots (CDPRs) have an end-effector (EE) connected to a fixed frame by cables whose lengths can be controlled by coiling and uncoiling them on cable winches. Cable-suspended parallel robots (CSPRs) are a subgroup of CDPRs where cables are kept in tension mainly by gravity, which pulls the EE downwards. CSPRs that use as many cables n as the number m of degrees of freedom (DOF) of the EE are called *fully-constrained*: in particular, we consider a robot of this category.

Cable actuation offers interesting advantages, such as potentially very large workspaces, but has a fundamental drawback: cable tensions τ_i must be positive at all times. If inertia forces are small enough that they can be neglected, this condition requires the EE to remain within the *Static Equilibrium Workspace* (SEW), which is the set of poses where static equilibrium is possible with $\tau_i > 0$ [1]. Researchers have now shown that inertia forces can help in keeping cables in tension, even as the robot moves beyond its SEW [2–4]: this can provide new applications for such robots, as the usable workspace becomes much larger.

Often, it is not necessary to fully control the EE pose: in a purely-translational robot, the orientation remains constant while only the EE position is controlled. This kind of motion may be obtained with a robot having 6 cables that are kept pairwise parallel and at the same length, so that they form three parallelograms.

Some of the first CSPRs with an architecture based on this concept are in [5] (for rescue operations in disaster-struck areas), [6] (for the construction sector), [7] (for large-scale 3D printing) and [8] (to help disabled people overcome architectural barriers, such as pedestrian bridges). Often, the robots include more than 6 cables, to guarantee that cable tensions remain positive, by having the cables pull on each other; in other works, antagonistic jacks pushing on the EE are employed for the same goal.

In our work, instead, we only use 6 cables, the minimum number for a fully-constrained robot with a finite-size EE, with no external tensioning devices. Furthermore, this robot can be controlled by only 3 actuators, where each motor acts upon two cables in the same parallelogram (which must remain at the same length), which further simplifies design and reduces the total cost. For this robot, we aim to define dynamic trajectories that take advantage of the inertia force on the EE to maintain the cables under tension (and thus to guarantee proper robot control).

Since we consider the most general three-parallelogram architecture, some of the CSPRs introduced in previous works [5,7] are also covered as special cases: in this sense, our present work unites and further develops previous research on both 3-DOF spatial cable robots and dynamically feasible motions for CSPRs.

Having defined the geometry of the robot and assuming that no external forces are exerted on the EE besides gravity and inertia, we derive the conditions that guarantee positive tensions in all cables, for the most general robot architecture. Then, we introduce a special geometry, such that the robot's dynamic equations are equivalent to those of a *virtual* 3-cable robot with point-mass EE: this allows the equations of motion to be greatly simplified. With this architecture, the results on the feasibility of dynamic motions of 3-cable point-mass robots that we obtained in our previous work [2] can be reused. Furthermore, for this simpler geometry, the SEW of the robot can be described analytically and has a simple geometric shape; see for instance [5,6], where the SEW had to be found numerically.

To provide a full analysis of our robot, we also derive the singularity locus: here, we can distinguish between *actuation singularities* and *constraint singularities*, where in the latter the robot gains an additional DOF [9]. Also, we analytically define the zones of possible cable interference; it is found that, under some conditions on the placement of the cable attachment points, both the singularity locus and the cable interference zones can be easily defined and avoided. Finally, we describe the *reachable workspace* as the set of points where the EE can be brought when taking into account the limits on the cable lengths.

Finally, experimental results from tests on a prototype are presented.

Our work is currently submitted to a peer-reviewed scientific journal.

REFERENCES

[1] Stump, E., and Kumar, V., 2006. "Workspaces of cable-actuated parallel manipulators". *ASME J. Mech. Des.,* **128**(1), pp. 159–167.

[2] Mottola, G., Gosselin, C., and Carricato, M., 2018. "Dynamically feasible periodic trajectories for generic spatial three-degree-of-freedom cable-suspended parallel robots". *ASME J. Mech. Rob.,* **10**(3), p. 031004.

[3] Jiang, X., Barnett, E., and Gosselin, C., 2018. "Dynamic point-to-point trajectory planning beyond the static workspace for six-DOF cable-suspended parallel robots". *IEEE Trans. Robot.,* **34**(3), pp. 1–13.

[4] Jiang, X., Barnett, E., and Gosselin, C., 2018. "Periodic trajectory planning beyond the static workspace for 6-DOF cable-suspended parallel robots". *IEEE Trans. Robot.,* **34**(3), pp. 1–13.

[5] Bosscher, P., Williams, R., and Tummino, M., 2005. "A concept for rapidly-deployable cable robot search and rescue systems". In Proc. of the ASME 2005 IDETC/CIE, pp. 589–598.

[6] Bosscher, P., Williams, R., Bryson, L., and Castro-Lacouture, D., 2007. "Cable-suspended robotic contour crafting system". *Automation in construction,* **17**(1), pp. 45–55.

[7] Barnett, E., and Gosselin, C., 2015. "Large-scale 3D printing with a cable-suspended robot". *Additive Manufacturing,* **7**, pp. 27–44.

[8] Castelli, G., Ottaviano, E., and Rea, P., 2014. "A Cartesian cable-suspended robot for improving end-users' mobility in an urban environment". *Robotics and Computer-Integrated Manufacturing,* **30**(3), pp. 335–343.

[9] Conconi, M., and Carricato, M., 2009. "A new assessment of singularities of parallel kinematic chains". *IEEE Trans. Robot.,* **25**(4), pp. 757–770.

LIGHTWEIGHT VOLUME FILLING WITH TRABECULAR STRUCTURES EVOLVED FROM REGULAR TESSELLATION OF 3D SPACE

Eugenio Dragoni[1], Valerio Armando Ciace[1]

[1]*Dept of Engng Sciences and Methods, University of Modena and Reggio Emilia, Italy*
E-mail: eugenio.dragoni@unimore.it, valerioarmando.ciace@unimore.it

Keywords: *additive manufacturing, volume filling, trabecular structures, 3d tessellation*

EXTENDED ABSTRACT

Additive manufacturing is a technology that produces three-dimensional parts layer by layer from a variety of materials [1]. It has been rapidly gaining popularity as a true manufacturing process in recent years. In the additive manufacturing process, a digital data file is transmitted to a production machine, which ultimately translates an engineering design into a 3D-printed part with virtually any conceivable shape. The majority of parts produced by additive technologies are not printed solid. Printing solid parts requires high amounts of material and long print time resulting in high costs and structural inefficiency. To optimise the printing process most parts are printed with solid shells and filled with a lightweight cellular structure. The infill behaves basically as the core material in a sandwich construction with the main aim of providing distributed support to the load-carrying outer shells (Figure 1). This paper proposes a simple two-step method to design periodic filling materials based on the combination of two well-established sciences. In the first step, the 3D volume to be filled is divided into regular solids by following the rules of tessellated spaces. In the second step, each unit volume is replaced by an isostatic lattice structures obtained by placing one-dimensional beams along the edges and across the faces of the original solid [2, 3]. This simple procedure gives rise to entire classes of easily manufactured porous metamaterials that are intrinsically lightweight, strong and stiff. Examples are supplied for the tessellation of regular volumes (using triangular, square and hexagonal prisms, Figure 2) and for the mapping of irregular shapes (using rhombic dodecahedra, truncated octahedra and Weaire–Phelan grids, Figure 3). Figure 4 shows sandwich-like structures manufactured with ABS polymer by Fused Deposition Modelling technology using the unit cells of Figure 2.

REFERENCES

[1] Gibson, I., Rosen, D.W., and Stucker, B., 2009. *Additive manufacturing technologies*, Springer.
[2] Wadley, H.N.G., 2006. "*Multifunctional periodic cellular metals*". Phil Trans R Soc A, 364, 31–68.
[3] Dragoni E., 2013. "*Optimal mechanical design of tetrahedral truss cores for sandwich constructions*". J. Sandwich Structures and Materials, 15, 464–484.

(a) (b)

Figure 1. Sandwich-like parts with (a) regular shape and (b) irregular shape.

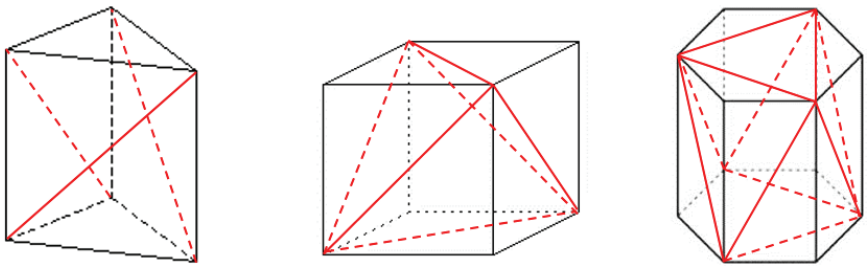

(a) (b) (c)

Figure 2. Unit cells for tessellation of regular volumes: (a) pentahedron, (b) hexahedron, (c) hexagonal prism (red lines show added beams needed to achieve self-rigidity).

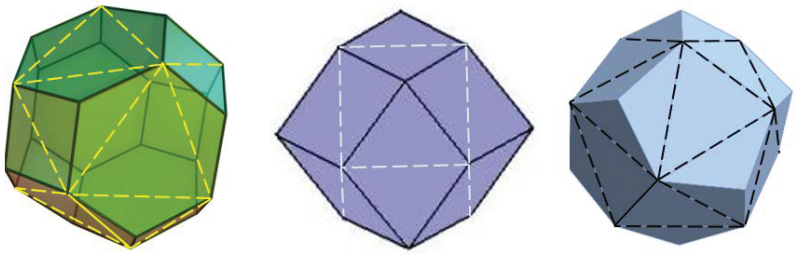

(a) (b) (c)

Figure 3. Examples of elemental cells suitable for tessellation of irregular volumes: (a) truncated octahedron, (b) rhombic dodecahedron, (c) Weaire-Phelan cell (dashed lines across faces show added beams needed to achieve self-rigidity.

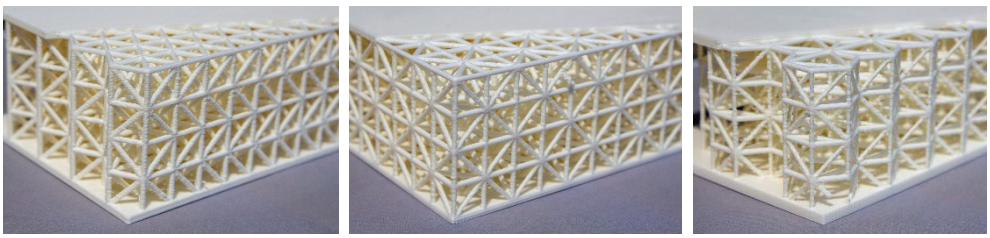

(a) (b) (c)

Figure 4. Examples of sandwich-like prototype manufactured by FDM: (a) pentahedron, (b) hexahedron, (c) hexagonal prism.

SHAPE OPTIMIZATION OF THE FILLET UNDER A BOLT'S HEAD

Andrea Sorrentino[1], Davide Castagnetti[1], Andrea Spaggiari[1], Eugenio Dragoni[1]

[1]*Department of Science and Methods for Engineering, University of Modena and Reggio Emilia, Italy*
E-mail: andrea.sorrentino@unimore.it, davide.castagnetti@unimore.it, andrea.spaggiari@unimore.it, eugenio.dragoni@unimore.it

Keywords: *bolt, stress concentrations, optimization, Particle Swarm algorithm, finite element*

EXTENDED ABSTRACT

The aim of this work is to minimize the stress concentration factor of the fillet under a ISO M12 bolt's head, through a shape optimization procedure. Many solutions are suggested in literature. In particular, Pedersen [1] proposes the use of super elliptical shapes re-entering the head, which strongly reduces stress concentration but is difficult to be manufactured.

The present work proposes an innovative solution, which replaces the standard circular fillet with a double circular arc fillet external to the bolt head, through a completely automated solving procedure. This work optimizes this fillet geometry by connecting a commercial multipurpose optimization software (VisualDOC 8.0) and a finite element (FE) solver (Abaqus 13.0): the Particle Swarm Optimization (PSO) algorithm and a parametric FE model of the bolt were exploited to solve the problem.

The analysis involved two steps. First, we optimized the radiuses R_1 and R_2, see Fig. (1a). Second, we optimized all the four project variables: the head's diameter, D, the height, H, and the two fillet radiuses R_1 and R_2, see Fig. (1a).

The stress concentration factor relative to the gross cross-sectional area, K_{tg}, is defined in Eqn. (1):

$$K_{tg} = \sigma_{max} / \sigma_{nom} \tag{1}$$

where σ_{max} is the maximum Von Mises stress on the fillet under the bolt head and σ_{nom} is the nominal stress acting on the bolt shank.

The results in Fig. (1b) show the stress contours in the bolt head, where the red area corresponds to the peak Von Mises stress.

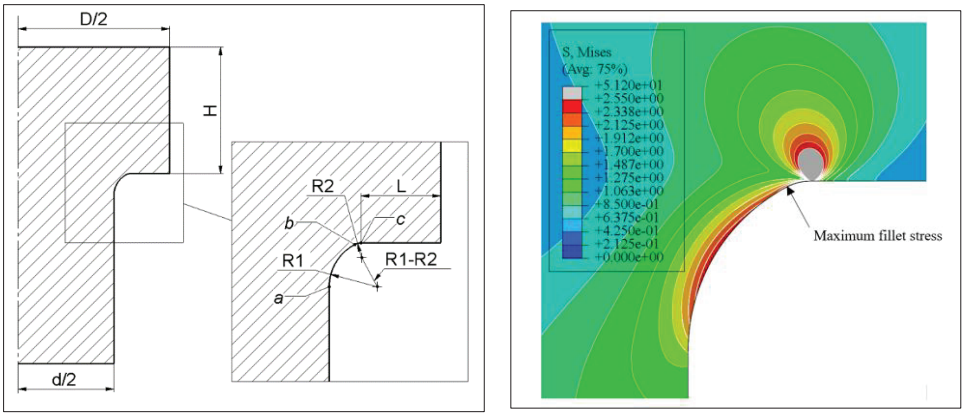

(a) (b)

Figure 1. Double arc parametrization of the head fillet considering an axisymmetric model of the bolt (a), detail of the Von Mises stress contours of the optimized geometry (b).

The results show that the optimal radiuses of this double circular arc fillet are $R_1 = 1.52$ *mm* and $R_2 = 0.42$ *mm* with a stress concentration factor, K_{tg}, equal to *2.52*. By comparison, the standard circular fillet and the elliptical shape suggested by Pedersen [1], both external to the bolt's head, have a stress concentration factor K_{tg} equal, respectively, to *2.92* and *2.67* [1, 2]. It comes that the double circular arc fillet here proposed grants a reduction of the maximum stress of *13,7%* compared with the standard circular fillet, and of *5,4%*, compared with the elliptical shape solution. Finally, the simultaneous optimization both of the two fillet radiuses R_1 and R_2, and of the head's diameter *D* and the height *H*, allows an *8%* decrease of the stress concentration factor, K_{tg}, from *2.52* down to *2.32*, with strong improvement in fatigue life resistance.

REFERENCES

[1] Niels L Pedersen, 2013, "Overall bolt stress optimization", *JSA Journal*, @IMechE (2013), pp. 155-163.
[2] In book, WD Pilkey, 1997, *Peterson's stress concentration factors*, 2nd ed., John Wiley & Sons, New York, pp. 508.

UN PARADOSSO IN TRAVI CURVE: DALLA ACCADEMIA ALLA APPLICAZIONE

Luigi Leopardi[1], Roberto Lugli[2], Antonio Strozzi[1]

[1]*DIEF – Dipartimento di Ingegneria 'Enzo Ferrari', Università di Modena e Reggio Emilia, Modena, Italia*

[2]*Libero professionista, Modena*

Parole chiave: paradosso, tensioni flessionali, linearizzazione alla Gateaux, ottimizzazione occhio

SOMMARIO ESTESO

Risulta a volte possibile ridurre le tensioni in un componente meccanico tramite rimozione di materiale, dove le gole schermo sono l'espediente maggiormente noto. Limitandoci alle travi rettilinee, sono da tempo note alcune situazioni nelle quali, rimuovendo materiale dalle zone della sezione più lontane dall'asse neutro, si ottiene una diminuzione della tensione flessionale. Viceversa, in una trave rettilinea non si riesce a ridurre le tensioni flessionali rimuovendo materiale dalle zone centrali, vicine all'asse neutro. Passando alle travi curve, si presentano alcuni esempi nei quali si consegue una riduzione tensionale rimuovendo materiale da zone prossime all'asse neutro. Questo comportamento costituisce un paradosso apparentemente sconosciuto. Per interpretare matematicamente tale risultato, si sviluppa un approccio basato sulla linearizzazione secondo Gateaux; con tale approccio risulta possibile definire analiticamente una striscia nell'intorno dell'asse neutro, la quale delimita le zone dalle quali è possibile rimuovere materiale riducendo simultaneamente le tensioni flessionali.

Anche se questo risultato paradossale risulta accademicamente interessante, la severità della richiesta di contemporanea diminuzione di tensione e di sezione trasversale comporta che la diminuzione di tensione praticamente conseguibile sia spesso troppo limitata per risultare tecnicamente vantaggiosa. Per conseguire risultati praticamente utili, si è quindi mitigato l'approccio precedente, adottando il compromesso di accettare un lieve aumento di tensione, purché la diminuzione di area risulti più rilevante. Basata su questo approccio, si è definita analiticamente una striscia, più ampia di quella precedentemente citata, rimuovendo materiale dalla quale si ottiene un limitato aumento di tensione accoppiato ad una sensibile diminuzione di area. Impiegando tale approccio, si propone una ottimizzazione di un occhio, con particolare riguardo al piede di biella, introducendo una tasca laterale di sezione rettangolare e di ingombro radiale variabile angolarmente, calibrata in modo da produrre una situazione di tensione uniforme al bordo interno dell'occhio. A causa delle varie approssimazioni introdotte nella teoria per ottenere espressioni progettuali in forma chiusa, si intende validare i risultati analitici tramite gli Elementi Finiti

VIRTUAL SIMULATION TECHNOLOGIES FOR HUMAN-CENTRED DESIGN OF TRACTORS

Margherita Peruzzini[1], Fabio Grandi[1], Luca Zanni[1], Juliana Schmidt[1], Marcello Pellicciari[2], Angelo Oreste Andrisano[1]

[1]*Dipartimento di Ingegneria "Enzo Ferrari", Università di Modena e Reggio Emilia, Italy*
E-mail: margherita.peruzzini@unimore.it, fabio.grandi@unimore.it, luca.zanni91@unimore.it, juliana.schmidt@unimore.it, angelooreste.andrisano@unimore.it

[2]*Dipartimento di Scienze e Metodi dell'Ingegneria, Università di Modena e Reggio Emilia, Italy*
E-mail: marcello.pellicciari@unimore.it

Keywords: *Human-centred design, digital manufacturing, virtual simulation, human-machine interaction*

EXTENDED ABSTRACT

Human-centred design (HCD) focuses on the inclusion of human factors in product and system design in order to respond to physical, psychological, social and cultural needs of human beings [1]. It aims at the satisfaction of the user needs related to performances, aesthetics, reliability, usability, accessibility and visibility issues, costs, and many other aspects. However, the product quality as perceived by users is usually faithfully assessed only at the end of the design process, while it is very difficult to predict on 3D CAD model. As a consequence, HCD consists of the application of human-related information to the design of tools, machines, systems, tasks, jobs, and environments for safe, comfortable, and effective human use. As far as industrial system design, the optimization of posture, physical overload, perceived effort, discomfort, and physical fatigue is fundamental to satisfy the users' needs and prevent musculoskeletal disorders [2]. In this context, the analysis of human factors has a central role in the understanding of human behaviours and performance interacting with socio-technical systems, and the application of that understanding to design of interactions [3].

Traditionally the analysis of human-related aspects of a product is based on physical prototypes, which increases product development times and cost. Nowadays, with the escalation of the computational power and the decrease of equipment size, digital technologies and simulation tools allow virtualizing and assessing the human-product interaction in advance, for preventive analyses before products or systems are physically realized. Such tools allow products and interaction tasks to be simulated on digital mock-ups, and human actions and behaviours to be reproduced by digital human models (DHMs) [4]. Also wearable instruments designed for hands-free operation can be used during the

design stages within immersive environments in order to reduce the intrusiveness and allow the wearer to stay focused on their main task and be assisted by the wearable rather than be distracted, recording continuously biometric data without additional effort [5]. Furthermore, Virtual Reality (VR) technologies can be used to create a 3D immersive simulation environment where users are immersed and user experience can be validly simulated and assessed [6].

The paper proposes a digital set-up where the interaction between products and humans interacting with them is digitalized and analysed. Such an environment is useful to predict the design criticalities and to improve the global system design. The research approached is based on the creation of a virtual environment replicating the human-system interaction and collecting data about the behavioural and cognitive responses thought a set of metrics, properly selected for the specific case study. Interaction between humans and products or systems are in this case digitalized and simulated by the DMU, using both virtual and physical items within a Mixed Reality (MR) environment. Metrics aims at measuring both physical and cognitive workload in terms of postural comfort, physical stress and fatigue, as well as visibility and accessibility, simplicity of actions, interaction support and satisfaction on the other hand. The proposed set-up includes different software and hardware tools, as follows:

- Siemens JACK for product digitalization;
- VICON tracking system for real users' tracking and manikin digitalization;
- HAPTION RTI plug-in for connection among real user movements and virtual manikin movements.
- a set of VICON Bonita cameras for motion capture;
- a set of 3D printed rigid bodies with markers for full body marking;
- a pair of Tobii Pro Glasses 2 to capture eye movements;
- a Bio Zephyr BioHarness sensor to record human physiological data;
- a GoPro camera to record the scene.

The industrial case study has been developed in collaboration with CNH Industrial, focusing on tractors, with the final aim to support the cabin human-centred design. The study is based on the virtualization of the cabin, where the tractor driver works and interacts with commands and controls, and the monitoring of the driver's physical and mental workload to understand the level of comfort, the usability of the interfaces, the level of stress, and the perceived quality.

REFERENCES

[1] ISO 9241-210, 2009. Ergonomics of human system interaction - Part 210: Human-centered design for interactive systems, International Organization for Standardization (ISO).

[2] Pheasant, S. 1999. *Body Space: Anthropometry, Ergonomics and the Design of Work*, Taylor & Francis, Philadelphia, pp. 121-123.

[3] Wilson, J.R., 2000. Fundamentals of ergonomics in theory and practice, *Applied Ergonomics,* vol. 31, 2000, pp. 557-567.

[4] Demirel, H.O. and Duffy, V.G., 2007. Applications of digital human modeling in industry, In V.G. Duffy (Ed.): *Digital human modeling,* Springer, Berlin, Heidelberg, pp. 824-832.

[5] Bauer, D. et al., 2016. Wear@Work – A new approach for data acquisition using wearables, *Procedia CIRP*, vol. 50, pp. 529–534.

[6] Honglun H. et al., 2007. Research on virtual human in ergonomic simulation, Computers & Industrial Engineering, vol. 53, pp. 350–356.

FATIGUE LIFE CHARACTERIZATION OF DIELECTRIC ELASTOMER TRANSDUCERS MADE OF STYRENIC RUBBER

Chen Yi[1], Lorenzo Agostini[2], Marco Fontana[3], Rocco Vertechy[1]

[1]*Department of Industrial Engineering, University of Bologna, Italy*
E-mail: yi.chen4@unibo.it, rocco.vertechy@unibo.it

[2]*Percro Laboratory, TECIP Institute, Scuola Superiore Sant'Anna, Italy*
E-mail: lorenzo.agostini@santannapisa.it

[3]*Department of Industrial Engineering, University of Trento, Italy*
E-mail: marco.fontana-2@unitn.it

Keywords: *Dielectric elastomer transducers, Fatigue, Reliability,*

EXTENDED ABSTRACT

Dielectric elastomer transducers (DETs) are incompressible deformable capacitors, made by highly elastic dielectric layers coated with compliant electrodes, that make it possible to convert mechanical energy into direct current electricity and vice-versa [1]. As such, they can be used to conceive solid-state electrostatic actuators, generators and sensors exhibiting the following advantageous properties: large energy and power densities; ease of manufacture and integration; good resistance to shocks and corrosion; silent operation; low cost [1].

Recently, styrenic rubber membranes demonstrated excellent electromechanical properties for the development of high power density and highly efficient dielectric elastomer transducers (DETs). In particular, in experimental applications as generators, inflated circular diaphragm DETs made it possible to consistently convert pneumatic energy into electricity at an energy density per cycle greater than 400 J/kg, with even higher numbers being expected for DETs configured so as to have the material working in uniform states of deformation.

These experimented performances can however be sustained for a limited number of cycles only, after which the DET will fail irreversibly. To date, very little information is available on the fatigue life performances of dielectric elastomer materials and of the transducers made thereof [2,3]. Having identified the electrical breakdown as the most probable mode of DET failure, this paper reports for the first time on a set of lifetime constant electric-stress tests conducted on styrenic dielectric elastomer membranes [2,3].

Specifically, the presentation starts with a description of the employed experimental set-up and procedures. Then, it reports and discusses the obtained experimental results. Finally, it introduce a model to predict DET lifetime that can be used in a design procedure to find optimal trade-offs between DET performance and lifetime/reliability.

REFERENCES

[1] Carpi F., De Rossi D., Kornbluh R. (2008). Dielectric elastomers as electromechanical transducers: Fundamentals, materials, devices, models and applications of an emerging electroactive polymer technology. Elsevier Science, Amsterdam.

[2] Dissado L.A. and Fothergill J.C. (1992). Electrical degradation and breakdown in polymers. No. 9., IET.

[3] Kornbluh R.,Wong-Foy A., Pelrine R., Prahlad H. and McCoy B. (2010). Long-lifetime all-polymer artificial muscle transducers. MRS proceedings, vol. 1271. Cambridge University Press.

SVILUPPO DI UNA TRASMISSIONE PTO IBRIDA ELETTRICA DI TRATTORE MEDIANTE MODELLAZIONE MULTIFISICA IN AMBIENTE IMAGINE.LAB AMESIM

Marco Polastri, Emiliano Mucchi, Giorgio Dalpiaz

Dipartimento di Ingegneria, Università di Ferrara, Italia
E-mail: marco.polastri@student.unife.it, emiliano.mucchi@unife.it, giorgio.dalpiaz@unife.it

Keywords: *Modellazione multifisica, trasmissione PTO, Amesim*

SOMMARIO ESTESO

Il sistema *P.T.O.* (*Power Take-Off*) è un apparato che provvede ad azionare gli organi in movimento delle macchine operatrici derivando, direttamente o indirettamente, la potenza necessaria dal motore del trattore [1]. Essa è costituita da un albero di trasmissione, un cambio di velocità e da un sistema di comando per l'innesto e il disinnesto, ed è applicata di serie posteriormente al trattore, all'altezza del suo assale posteriore. L'albero di trasmissione del dispositivo termina con un profilo scanalato, al quale vengono collegate le macchine operatrici tramite un albero cardanico, che deve ruotare a velocità il più possibile prossima ad un valore definito da normativa. Per massimizzare la potenza trasferibile, il regime motore di funzionamento del sistema è prossimo al regime di massima potenza erogata, che si trova in prossimità dei punti di lavoro a minimo consumo specifico [2]. La trasmissione tradizionale ha mantenuto fin dalla nascita lo stesso layout costruttivo e lo stesso principio di funzionamento, perché, pur trattandosi di un sistema indispensabile per permettere al trattore di essere una vera e propria centrale mobile di potenza, è realizzata in modo piuttosto semplice ed efficiente. Tuttavia la natura puramente meccanica obbliga a mantenere costante ed elevato il regime motore durante il funzionamento, anche se la potenza richiesta all'albero di uscita non è elevata. Ciò causa un aumento dei consumi e delle emissioni inquinanti ed acustiche, che al giorno d'oggi rendono necessaria la valutazione di una soluzione costruttiva differente per trattori ad elevata potenza. Si esamina quindi una nuova architettura che consente di superare tale limitazione e permette di ottenere un sistema molto versatile, mantenendo allo stesso tempo le stesse capacità dei tradizionali sistemi di trasmissione.

Il nuovo sistema proposto, di tipo ibrido-elettrico, è ottenuto inserendo un motore elettrico, che fornisce potenza in parallelo al motore termico tramite un rotismo epicicloidale a due gradi di libertà. Se la potenza richiesta all'albero di uscita non è elevata, tale sistema permette di mantenerne costante la velocità al variare del regime del motore termico, consentendo quindi di mantenere il punto di funzionamento in una zona a consumo specifico ridotto.

Lo strumento principale adottato per lo studio preliminare del concept è LMS Imagine.Lab Amesim, un ambiente di modellazione e simulazione multi-fisica. Con questo tool, partendo dal modello della trasmissione classica, viene modellato il prototipo e vengono eseguite

simulazioni di funzionamento in diverse condizioni di carico applicato e regime motore, confrontando configurazione ottenute variando alcuni parametri di layout, con lo scopo di mettere in luce se e in quali condizioni tale proposta sia in grado di soddisfare le performance richieste.

I risultati hanno messo in luce che effettivamente il sistema è in grado di funzionare correttamente, mantenendo cioè la velocità della presa di potenza prossima alla velocità di normativa, al variare del regime del motore termico. Ciò però accade entro alcuni limiti del valore del carico applicato, a seconda della configurazione in esame. Si è osservato inoltre che il rapporto tra potenza massima trasmissibile e potenza massima erogabile dal motore termico presenta un andamento decrescente-crescente con il regime motore. Per questo motivo, quando le condizioni di carico permettono una diminuzione della velocità del motore a combustione, oltre ai benefici ottenuti dallo spostamento del punto di funzionamento del motore stesso, si ha un aumento della quota di potenza inserita nel sistema trasferibile all'applicazione del trattore.

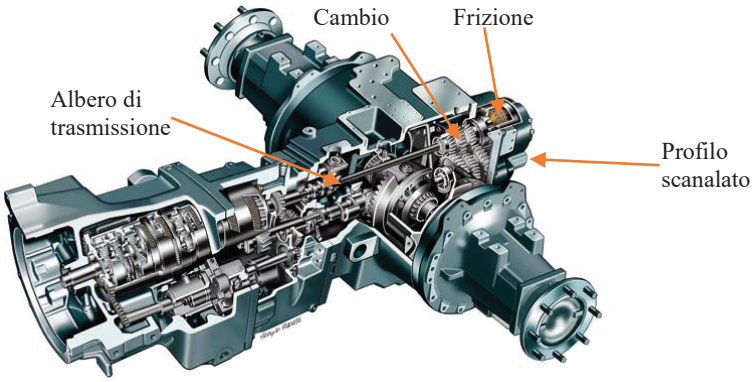

Figura 1. Il sistema PTO classico

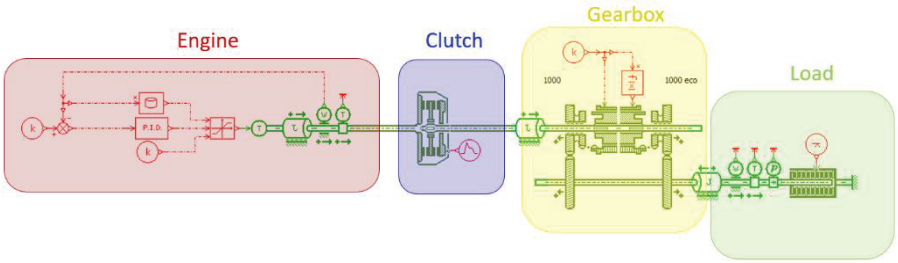

Figura 2. Modello dell'apparato PTO classico

BIBLIOGRAFIA

[1] G. Pellizzi, Macchine agricole, Edagricole, 1998
[2] E. Mehrdad, G. Yimin e E. Ali, Modern electric, hybrid electric, and fuel cell vehicles, CRC Press

A FINITE ELEMENT STUDY ON ACTUATORS MADE FROM SHAPE MEMORY ALLOY/MATRIX COMPOSITES

Luke Mizzi[1], Andrea Spaggiari[1]

[1]*Department of Sciences and Methods for Engineering, UNIMORE, Italy*
E-mail: luke.mizzi@unimore.it, andrea.spaggiari@unimore.it

Keywords: *Finite Element Method, Shape Memory Alloy, Composites, Sandwich Panels*

EXTENDED ABSTRACT

Shape memory alloys (SMAs) are materials that 'remember' their original shape after loading and return back to their undeformed shape after heating. This phenomenon arises from the phase transition that occurs upon heating from the cold martensitic phase to the hot austenitic phase and makes them ideal candidates for use in actuators.

One method of producing a compact and integrated actuator is to deform a SMA wire and then pour a matrix around it [1]. Once the matrix, typically made from epoxy resin, solidifies, it acts as the counter-balance force against the SMA wire, providing the classical agonist-antagonist way of actuation. The stroke and output force of such an actuator depends on a number of factors including the mechanical properties of the SMA wire and the matrix and the relative volumes of the two materials in the composite actuator. In this work, a combined analytical and numerical approach will be used to investigate the effect of these factors on the efficacy of the actuator as well as to find the optimum conditions required to achieve the maximal stroke and output actuation force. A Finite Element (FE) investigation on the possibility of using such an actuator to create a sandwich structure, capable of undergoing controlled bending deformation through the selective activation of actuators within the system, will also be considered.

In order to simulate the shape memory effect of the SMA wire, the Auricchio-Souza model [2,3], as implemented in the ANSYS16 FE environment, was used. The original parameters for this model were obtained by curve-fitting the model on experimental results obtained from loading tests on a Saes Getters 0.3 mm diameter Nitinol wire. A schematic of the simulation methodology used is presented in Figure 1 below. First the wire is stretched at a cold temperature (martensitic phase), then the matrix is 'formed' around the wire and the wire is released from its constraint reaching an intermediate equilibrium position, and, finally, the SMA wire is heated up performing the actuation. In order to obtain a complete picture of the effect of the aforementioned factors on the actuation potential of this composite system a number of different scenarios were simulated, including a variety of matrix/wire volume ratios and SMA and matrix mechanical properties. The results obtained indicate that all the analyzed factors are intrinsically linked to one another.

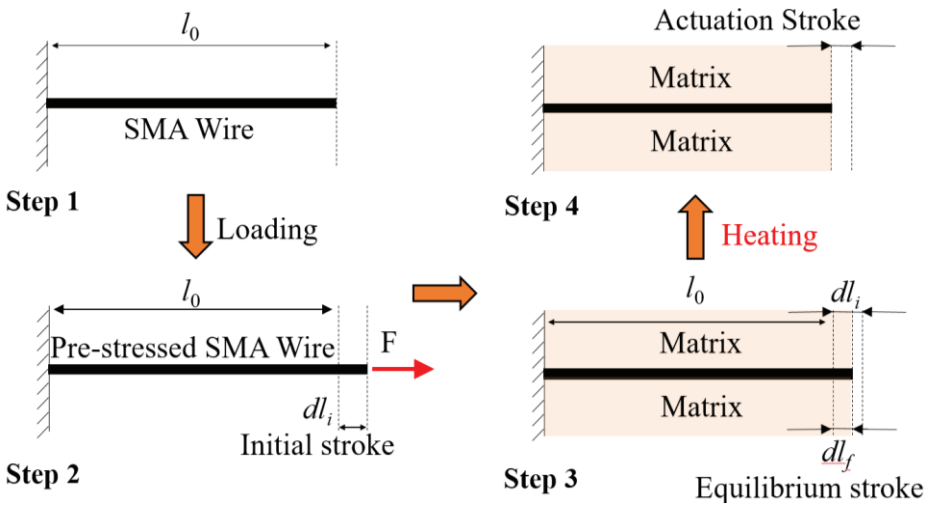

Figure 1. Schematic depicting the steps used to simulate the SMA/matrix actuators.

The relative Young's moduli of the initial and detwinned martensitic phase of the SMA wire play a vital role in determining the ideal volume of matrix required and the amount of pre-stress that must be applied to the wire in order to obtain the optimal actuation effect.

The ideal stiffness of the matrix produces a force sufficient to stop the wire from returning to its equilibrium position in detwinned martensitic state, while at the same time being compliant enough to let the wire contract as much as possible upon heating. If the threshold stiffness value is achieved then the actuation effect of the composite will be close to that of the SMA wire on its own, whilst also retaining the possibility of cyclic actuation. However, certain cases also exist where this effect can be amplified. If the detwinned martensitic phase of the SMA wire is less stiff than that of the twinned martensite and austenitic phase, as is typically the case in many SMAs, then by applying a higher prestress value one may achieve a greater actuation effect without changing the matrix stiffness. In these cases the maximum stroke of the SMA wire/matrix composite depends primarily on the maximum critical strain of the SMA wire.

The results obtained in this study are promising and following the conclusion of the analytical and numerical studies, the next step will be to attempt to realize experimentally a smart composite to validate these results, as well as implement these actuators in sandwich panel structures in order to obtain a tailored bending response.

REFERENCES

[1] Bettini, P. *et al.*, 2009. "Carbon fiber reinforced smart laminates with embedded SMA actuators – Part I: Embedding techniques and interface analysis". *J. Mater. Eng. Perform.,* **18**(5), pp. 664–671.

[2] Souza, A.C., Mamiya, E.N. & Zouain, N., 1998. "Three-dimensional model for solids undergoing stress-induced phase transformations". *Eur J Mech A Solids*, **17**, pp 789-806.

[3] Auricchio, F. & Petrini, L., 2002. "Improvements and algorithmical considerations on a recent three-dimensional model describing stress-induced solid phase transformations". *Int. J. Numer. Methods Eng*, **55**, pp 1255-1284.

DESIGN AND VIRTUAL PROTOTYPING OF A VARIABLE STIFFNESS JOINT VIA SHAPE OPTIMIZATION IN A CAD/CAE ENVIRONMENT

Angelo Oreste Andrisano[1], Giovanni Berselli[2], Pietro Bilancia[2], Marcello Pellicciari[1],

[1]*Department of Engineering "Enzo Ferrari", University of Modena and Reggio Emilia, Italy*
E-mail: angelooreste.andrisano@unimore.it, marcello.pellicciari@unimore.it

[2]*Department of Mechanical, Energy, Management and Transportation Engineering, University of Genova, Italy*
E-mail: giovanni.berselli@unige.it, pietro.bilancia@edu.unige.it

Keywords: *Safe Human-Machine interaction, Variable Stiffness Actuators, Integrated CAD/CAE Simulation, Shape Optimization, Virtual and Physical Prototype*

EXTENDED ABSTRACT

During the latest decade, collaborative robots, namely machines specifically designed for the physical interaction with humans, have been gradually making their transition from laboratories to real-world applications [1]. Naturally, whenever the envisaged task would benefit form physical human-machine interaction, safety and dependability become issues of paramount importance [2]. Nonetheless, especially when dealing with collaborative operations in the manufacturing industry, safety regulations may lead the plant designer to face opposite goals. On one hand, robots should indeed be designed so as to never cause harm to people (both during regular functioning or in case of failure). On the other hand, the wide-spread use of industrial manipulators traditionally leverages on their capabilities to carry rather high payloads, while achieving a very fast and precise positioning of the end-effector. These requirements are usually pursued by coupling powerful actuation systems with extremely rigid mechanical structures, which hardly comply with safety needs whenever the workers are supposed to enter the robot workspace. Therefore, the engineering challenge when designing collaborative robotics systems, which have to be safe and efficient at the same time, is usually tackled via the following strategies: *i)* by enhancing the robot sensory apparatus; *ii)* by adopting active control strategies; *iii)* by reducing the inertia of any moving part employing lightweight materials whenever possible. In parallel, as previously proven by several researchers [3], another way to actually implement safe machines for collaborative tasks is to increase (rather than minimize) the inherent compliance of their mechanical structure [4], simultaneously introducing the possibility to actively vary such compliance during the robot movements. This capability can be implemented, for instance, by means of Variable Stiffness Joints (VSJ), namely particular actuation systems which allow to independently control the position of an output link along with the transmission stiffness. In

light of this consideration, the present talk describes the design of a novel VSJ architecture, depicted in Fig. 1a. The VSJ can achieve stiffness modulation via the use of a pair of compliant mechanisms with distributed compliance, which act as nonlinear springs with proper torque-deflection characteristic. These elastic elements are composed of slender beams whose neutral axis is described by a spline curve with non-trivial shape. The beam geometry is determined by leveraging on a CAD/CAE framework that allows for the shape optimization of complex flexures. In particular, the design method makes use of the modeling and simulation capabilities of a parametric CAD seamlessly connected to a FEM tool. For validation purposes, proof-concept 3D printed prototypes of both elastic elements (Fig. 1a) and overall VSJ (Fig. 1b) are finally produced and tested (Fig. 1c). Experimental results fully confirm that the VSJ behaves as expected.

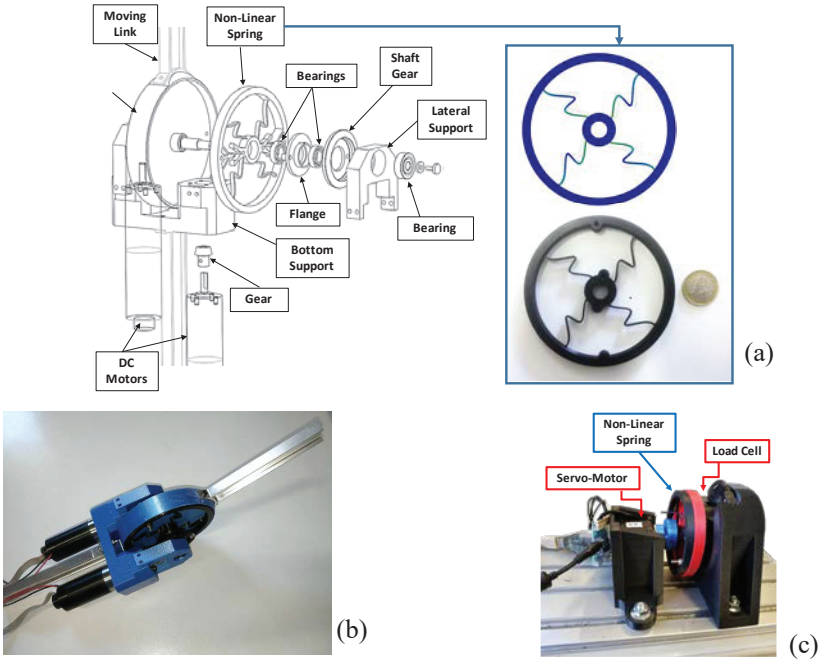

Figure 1. The novel variable stiffness joint: CAD exploded view and details of spring design (a); VSJ prototype (b); rig for spring testing (c).

REFERENCES

[1] Heyer, C., 2010. "Human-robot interaction and future industrial robotics applications". *Proceeding of the IEEE/RSJ International Conference on Intelligent Robots and Systems*, pp. 4749–4754.

[2] Fryman, J., and Matthias, B., 2012. "Safety of industrial robots: From conventional to collaborative applications". *Proceeding of ROBOTIK, 7th German Conference on Robotics*, May, pp. 1–5.

[3] Bicchi, A., and Tonietti, G., 2004. "Fast and soft arm tactics: Dealing with the safety-performance trade-off in robot arms design and control". *IEEE Robotics and Automation Magazine*, 11(2), pp. 22–33.

[4] Berselli, G., Guerra, A., Vassura, G., and Andrisano, A. O., 2014. "An engineering method for comparing selectively compliant joints in robotic structures". *IEEE/ASME Transactions on Mechatronics*, 19(6), pp. 1882–1895.

INDICE DEGLI AUTORI

Agostini Lorenzo 73
Amadori Stefano 3
Andrisano Angelo Oreste 71, 79
Belcari Juri 55
Benasciutti Denis 45
Berselli Giovanni 79
Bianchini Augusto 59
Bilancia Pietro 79
Boyle Liam 55
Camargo Molano Jacopo Cavalaglio 47
Campione Ivo 59
Capelli Luca 51
Carricato Marco 63
Castagnetti Davide 67
Catania Giuseppe 3
Ciace Valerio Armando 65
Cocconcelli Marco 47, 51
Conconi Michele 53
Cristofolini Luca 55, 57
D'Elia Gianluca 49
Dalpiaz Giorgio 41, 49, 75
Donati Lorenzo 39
Dragoni Eugenio 65, 67
Enzveiler Marques Julian Marcell 45
Focarete Maria Letizia 55
Fontana Marco 73
Fortunato Alessandro 39
Gibertini Massimo 47
Golfari Nicola 61
Grandi Fabio 71
Gualandi Chiara 55
Kao Alexander 55
Leopardi Luigi 69
Lugli Roberto 69
Martelli Saulo 57
Minak Giangiacomo 59
Mizzi Luke 77
Mottola Giovanni 63
Mucchi Emiliano 41, 49, 75
Palanca Marco 57
Parenti-Castelli Vincenzo 53
Pelaccia Riccardo 39
Pellicciari Marcello 71, 79
Perilli Egon 57

Peruzzini Margherita 71
Pesaresi Emanuele 43
Polastri Marco..... 75
Reggiani Barbara 39
Reilly Gwendolen 55
Rivola Alessandro..... 61
Rossi Jessica 59
Rubini Riccardo 47, 51
Sancisi Nicola 53
Schmidt Juliana..... 71
Sensini Alberto 55
Sorrentino Andrea..... 67
Spaggiari Andrea 67, 77
Squatrito Rosario 39
Strozzi Antonio..... 69
Todaro Ivan..... 39
Tomesani Luca 39
Tosini Andrea 41
Tovo Roberto..... 45
Tozzi Gianluca..... 55
Troncossi Marco 43, 59
Valli Giuseppe 39
Vertechy Rocco 73
Yi Chen..... 73
Zanarini Alessandro..... 15
Zanni Luca..... 71
Zucchelli Andrea 55

In questo volume sono raccolte le memorie presentate in occasione della "Dodicesima Giornata di Studio Ettore Funaioli", che si è svolta il 20 luglio 2018 presso la Scuola di Ingegneria e Architettura dell'Alma Mater Studiorum – Università di Bologna. La Giornata è stata organizzata dagli ex allievi del Prof. Ettore Funaioli con la collaborazione del DIN – Dipartimento di Ingegneria Industriale e della Scuola di Ingegneria e Architettura dell'Alma Mater Studiorum – Università di Bologna, e con il patrocinio dell'Accademia delle Scienze dell'Istituto di Bologna e del GMA – Gruppo di Meccanica Applicata.

Questo volume è stato stampato con il contributo di G.D S.p.A.

AlmaDL è la Biblioteca Digitale dell'Alma Mater Studiorum Università di Bologna. AlmaDL ospita al suo interno gli archivi Open Access che rendono pubblicamente disponibili i contributi derivanti dalle attività di ricerca, didattiche e culturali dell'Ateneo bolognese. AlmaDL attua così i principi del movimento internazionale a sostegno dell'accesso aperto alla letteratura scientifica, sottoscritti dall'Università di Bologna assieme a molte altre istituzioni accademiche, di ricerca e di cultura, italiane e straniere.

http://almadl.unibo.it

ISBN 978-88-9385-140-4

AlmaDL
University of Bologna Digital Library

ISBN 978-88-9385-140-4